Osteogenic Scaffolds for Enhanced Graft-Bone Integration in Ligament Tissue Engineering

Dina Gadalla

Dissertation submitted to the faculty of the Virginia Polytechnic Institute and State University in partial fulfillment of the requirements of the degree of

Doctor of Philosophy
in
Chemical Engineering

Aaron S. Goldstein, Chair
Richey M. Davis
Yong Woo Lee
Chang Lu
William D. Wagner

April 20, 2020

Blacksburg, VA

Keywords: tissue engineering, graft-bone integration, osteoblastic differentiation, nanoparticles, electrospinning, mesenchymal stem cells

Osteogenic Scaffolds for Enhanced Graft-Bone Integration in Ligament Tissue Engineering

Dina Gadalla

Abstract

Among the most common knee ligament injuries are those to the anterior cruciate ligament (ACL). Annually, approximately 350,000 people require surgical ACL reconstruction, accounting for more than $6 billion of health-care costs in the United States alone. An injured ACL loses its functions as it cannot heal with larger injuries and heals slowly with smaller ones. This may introduce complications, such as abnormal joint kinematics and deterioration, prior to complete rupture. Although the use of an autologous graft is the current gold standard for ACL reconstruction surgery, it is associated with donor site morbidity and a decrease in mechanical strength at the donor site. The use of allogenic grafts instead of autografts introduces the risk of disease transmission. Furthermore, integration of soft tissue grafts (e.g., hamstring tendon) to native bone is slow and risks graft pullout. To circumvent these limitations, tissue engineering seeks to fabricate suitable biomaterials that could replace the entire ACL, stimulate regeneration of the ligament tissue, and integrate with host bone tissue. Numerous efforts have led to the development of complex, multi-phased biomaterial scaffold designs that are intended to deliver an array of cell types and biological cues. Particularly, scaffolds that possess bone-regenerating biomaterials at the ends are envisioned to facilitate rapid integration with the femur and tibia. Electrospun fiber scaffolds continue to be regularly utilized for their high tensile strength, flexibility, and ability to bend. Nevertheless, fibrous scaffolds are inert and require the incorporation of trophic factors to guide tissue regeneration. Additionally, electrospun fibers are often densely packed, which can hinder cell infiltration and subsequent tissue formation. The

objective of this work was to guide bone remodeling through the incorporation of trophic factors with 1) electrospun fiber scaffolds or 2) nanoparticles that could be combined with electrospun fiber scaffolds, and 3) to develop model three-dimensional fiber-hydrogel composites that support cell viability and proliferation.

Two approaches were utilized to present the trophic factor bone morphogenic protein (BMP)-2 to stimulate bone formation. In the first approach, electrospun fibers were modified through the adsorption or covalent conjugation of BMP-2. These fibers exhibited increased BMP-2 concentrations with covalent conjugation over adsorption, and the incorporation of heparin into the fibers improved both adsorption and conjugation. Mesenchymal stem cells (MSCs) – that have the capacity to differentiate into osteoblastic cells – were able to attach and proliferate on all films yet appeared to do so to a greater extent on surfaces with higher heparin contents. Additionally, markers of osteoblastic differentiation were significantly higher on surfaces with covalently conjugated BMP-2 than on those with adsorbed BMP-2.

In the second approach, a nanoparticle system was produced to control BMP-2 delivery and release. Importantly, this flexible system can be fabricated separately, and then combined with a scaffold for tissue regeneration. In this approach, BMP-2 was combined with chitosan nanoparticles through adsorption, encapsulation, or covalent conjugation. The particular BMP-2 incorporation technique had no significant effect on BMP-2 incorporation efficiencies, but affected particle size and BMP-2 release kinetics. Specifically, covalent conjugation method caused the aggregation of particles while adsorption method allowed the most sustainable release. MSCs cultured in the presence of the different particles survived and proliferated, but only particles with adsorbed BMP-2 stimulated osteoblastic differentiation.

Finally, three-dimensional fiber-hydrogel composites of various models were fabricated to mimic the complexity of full-sized scaffolds for ACL regeneration, and to study cell infiltration, differentiation, and tissue formation. A collagen hydrogel phase was introduced to electrospun fiber scaffolds using different approaches. MSCs seeded within a thin collagen layer were able to proliferate, sense underlying substrate and spread according to fiber orientation, while those within thicker layers were not. Additionally, cells initially present in only the collagen phase infiltrated to the fiber phase. These results demonstrate that minor changes in fabrication steps to combine the two phases could significantly alter cell function during the formation of three-dimensional fiber-hydrogel composites for tissue regeneration.

Osteogenic Scaffolds for Enhanced Graft-Bone Integration in Ligament Tissue Engineering

Dina Gadalla

General Audience Abstract

The anterior cruciate ligament (ACL) is one of four ligaments that connect the thigh bone to the shin bone and stabilize the knee. Injuries to the ACL often occur during high impact sports, and ruptures can necessitate surgical intervention. ACL reconstruction surgery involves drilling tunnels through the ends of leg bones, deploying the tissue graft through the knee joint and bone tunnels, and anchoring it within the bone tunnels. The most common grafts are autografts that use tendons of the patient's own body or allografts that are obtained from cadavers. The complications associated with autografts include pain at the site of tissue harvest, while allografts risk disease transmission. Additionally, directly affixing a soft tissue graft (e.g., the hamstring tendon) to bone within the bone tunnel suffers from slow tissue integration and risk of pull-out.

Tissue engineering is a field that seeks to develop devices to direct the regeneration of damaged tissues and organs. In the context of ACL repair, it seeks to achieve a biomaterial device with the properties of ACL, that can both guide the regeneration of ligament tissue and facilitate integration with bone tunnels, eliminating the need for autografts and allografts and their associated risks. Toward the development of an engineered ACL, this work focuses on improving graft-to-bone integration. In the first project, fibrous materials are surface-modified with bone morphogenetic protein (BMP)-2 (a bone-forming protein), and then tested for their ability to stimulate formation of a bone-like tissue in cell culture. In the second project, the deployment of BMP-2 either on the surface of or within nanoparticle delivery vehicles is evaluated as an alternative strategy to stimulate bone-like tissue formation. The third project explores the inclusion

of a hydrogel phase to facilitate cell infiltration and bone-like tissue formation within fibrous materials. Together these studies provide insights into how the architecture of the engineered tissue and the deployment of bone-forming proteins can be used to enhance ACL regeneration.

Acknowledgements

I would first like to express my deep gratitude to my advisor, Dr. Aaron Goldstein for his continuous guidance throughout each stage of the process. I would like to thank him for allowing me to grow as a researcher and for his willingness and enthusiasm to always assist in anyway. I would also like to thank Dr. Richey Davis, Dr. Yong Woo Lee, Dr. Chang Lu, and Dr. William Wagner for serving as my committee members, giving their time and providing me with insightful suggestions. I would like to acknowledge the Department of Chemical Engineering and the Interdisciplinary Graduate Education Program in Regenerative Medicine for their funding sources.

I would like to thank Dr. Patrick Thayer for getting me started with learning laboratory techniques during my first few months in the lab. I am also thankful to other lab individuals that I have had the chance to directly work with including Hagar Kenawy, Allissa Jones, Mary Sage Earley, and Keshav Shah. I would like to thank Dr. Anne Nicholas for teaching me polymerase chain reaction techniques and for helping me troubleshoot when required. I would like to thank Steve McCartney at the Nanoscale Fabrication and Characterization Laboratory for training me on scanning electron microscopy. Likewise, I would like to thank Chitra Meduri, Austin Fergusson and Yow-Ren Chang for getting me trained on mechanical testing, dynamic light scattering and contact angle measurements, respectively.

I would like to thank Dr. William Ducker for the use of his contact angle goniometer, Dr. Rafael Davalos for the use of his spin coater, Dr. Vincent Wang for the use of his materials testing system, Dr. Richey Davis for the use of his Zeta-sizer instrument, and Dr. Yong Woo Lee for the use of his spectrophotometer. I would like to thank the Institute for Critical Technologies and Applied Sciences for laboratory space. Additionally, I would like to thank Diane Cannaday, Tina

Russell, Andrea Linkous and Stacy Ratcliffe in the Department of Chemical Engineering for their prompt administrative help when needed.

I would like to acknowledge my undergraduate institution, the American University of Sharjah, for providing me with an extremely valuable learning experience – whether the yearly international sports tournaments I participated in as a member of the basketball team, the complete academic involvement I was exposed to, and the semester long international exchange program I was part of – which I continue to be grateful for. I am particularly appreciative for my mentors for their genuine support, for sparking my research interest in the biomedical field, and for encouraging me to always yearn for more. I would also like to sincerely thank the life-long friends that I had made during my undergraduate study – a career shaping time in my life – who until this day continue to be significant motivators.

As a third culture child, it is often that I develop an identity that is rooted in people rather than places. I would like to thank the close friends I have been lucky to have made during my time in Blacksburg for making my experience both remarkable and one that felt like home. I am grateful for their encouragement, companionship and comfort during both my research and writing process, particularly during the earlier stages. I would finally like to express my special appreciation to my family. My parents and biggest fans, Drs. Mohamed Gadalla and Suzan El-Sayed, who continue to understand me best as PhDs themselves, have not only been reassuring in their unconditional trust and support but have also been instrumental in inspiring my career. For them, I am immensely grateful. I would also like to acknowledge my grandfather, Dr. Mohamed El-Sayed, whose own academic pursuits sixty years ago not only encouraged his children's pursuits but my own as well. Finally, I am grateful to my brothers: Omar, Adam and Akram who have always supported me, growing up with such different personalities continues to somehow shape my growth until today.

Table of Contents

List of Figures

List of Tables

Chapter 1: Introduction

1.1 Motivation

Annually, in the United States, approximately 350,000 reconstructive anterior cruciate ligament (ACL) surgeries are carried out due to its high rate of injury [1, 2]. This accounts for $6 billion in health care costs [1]. During high impact activities, the ACL is the most frequently injured ligament in the human body and its healing is slow and often incomplete due to its intraarticular location and limited vascular supply. Left untreated, ACL injuries can cause complications including abnormal joint kinematics and deterioration. Unlike other ligaments, the ACL does not heal, and surgical reconstruction with a soft autologous or allogenic tissue graft is currently the most common treatment. Nonetheless, donor site morbidity and high risk of infections are associated with autologous and allogenic grafts, respectively. Synthetic grafts are no longer used for ACL replacement due to complications, such as high rupture rates and an increased risk of osteoarthritis. While the bone-patellar tendon-bone autograft is considered the gold standard for ACL reconstruction, less invasive procedures that utilize the hamstring or quadricep tendons involve anchoring the tendon within the bone tunnel. This tendon-bone interface is slow to integrate, risking mechanical instability and graft pullout [3, 4]. In view of these significant existing drawbacks of autografts and allografts, tissue engineered ACL grafts have become a focus of significant interest. Here, the overall goal is to develop a device that mimics the biological and mechanical properties of the native ACL, serves as a temporary support to stabilize the knee, and guides ligament regeneration. An attractive strategy to achieve this device is by combining a biomaterial scaffold, the relevant cell type(s), and the appropriate biochemical stimuli.

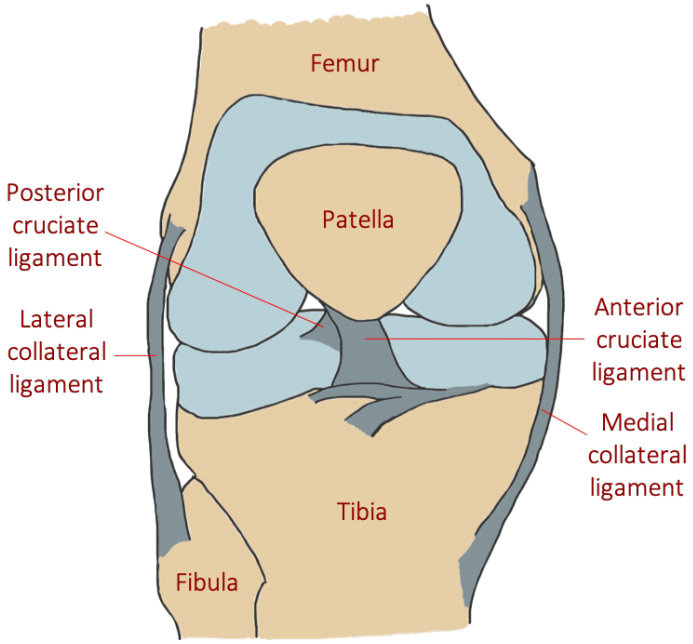

Figure 1.1: Knee joint anatomy depicting the four main ligaments present.

With regard to the biomaterial scaffold, electrospun fibers are widely utilized in the regeneration of fibrous tissues. Electrospun fibers mimic the structure of collagen fibrils found within the native extracellular matrix (ECM) of a variety of tissues (including ligament). However, electrospun fibers prepared from synthetic polymers are relatively inert, which can hinder the attachment, proliferation, and differentiation of cells into functional tissues. The presentation of bioactive cues (e.g., growth factors and adhesive proteins) to electrospun fibers better permits cell recognition of the fibers positively regulating required cell behavior [5, 6]. This, nevertheless, is only possible when bioactive agents are available in an active conformation and at an effective concentration. For instance, directly displaying agents on electrospun fibers or incorporating them with electrospinning polymer solutions often decreases their bioactivity due to enzymatic degradation or denaturation, respectively [7]. Another major concern of electrospun fibers is their

low porosity which makes cell infiltration through the scaffolds challenging. To address this, researchers have investigated diverse ways to increase pore sizes including the introduction of sacrificial fibers or porogens [8-10]. While these procedures increase porosity and cell infiltration, infiltration is rather slow and is at the expensive of the mechanical strength of fibers [11]. Instead, the addition of a space-filling hydrogel phase to electrospun fiber scaffolds may prevent fiber packing and improve cell infiltration [12].

1.2 Approach

Based on clinical evidence that graft integration within tibial and femoral bone tunnels is delayed in tendon-to-bone healing relative to bone-to-bone healing [13, 14], the focus of this project is to develop the bone region of an engineered ligament tissue, that could facilitate bony integration by permitting cell infiltration and stimulating new bone formation. Particularly, this work first examines a potential osteogenic fibrous scaffold. Next, methods to enhance the effectiveness of the added bioactive agents are studied through the utilization of a nanoparticle delivery system that can be combined with scaffolds. The clinical relevance of the fibrous scaffold is then expanded upon and further evaluated through the addition of a hydrogel component to the fibrous scaffolds to model fiber-hydrogel composites. While outside the scope of this work, it is anticipated that strategies developed through this work can then be applied to the fabrication of an entire ACL substitute.

1.3 Aim 1: Fabrication of Osteogenic Fibrous Meshes

One of the limitations associated with the use of electrospun scaffolds as biomaterials is the necessity to modify them with recognition sites for essential cell-scaffold interactions. Previous

studies have shown that functional materials with the capacity to regenerate bone can allow the healing of an engineered ACL substitute with native bone tunnels [13, 15]. To be functional, both the modification techniques as well as the material properties are important. The first aim involves the fabrication of growth factor immobilized electrospun fibrous scaffolds to induce osteoblastic differentiation. Specifically, bone morphogenic protein (BMP)-2 was immobilized to surfaces of electrospun fibers by adsorption and covalent conjugation. Concurrently, heparin was incorporated into polycaprolactone fibers to facilitate both BMP-2 adsorption and covalent conjugation mechanisms. Subsequently, the ability of the surfaces to support cell viability, proliferation, and osteoblastic differentiation were assessed using bone marrow derived mesenchymal stem cells (MSCs).

1.4 Aim 2: Delivery of Growth Factors with Nanoparticles

A major limitation of many growth factors is their short half-life *in vivo.* Nonetheless, competent strategies used to deliver growth factors can help enhance their clinical outcomes. The use of nanoparticles as delivery vehicles have demonstrated improved growth factor retention and higher biological efficiencies [16, 17]. In this aim, nanoparticle carriers were developed for the controlled delivery of growth factors to stimulate osteoblastic differentiation. Chitosan nanoparticles were fabricated through ionic gelation and characterized in terms of particle size and particle size distribution. The osteogenic growth factor BMP-2 was incorporated into nanoparticles by three approaches: 1) adsorbing growth factors on particle surfaces, 2) encapsulating them within the particles or 3) immobilizing them on particle surfaces. The incorporation efficiencies and subsequent release kinetic profiles of BMP-2 with the three approaches were examined. Finally,

the effects of nanoparticle carriers on cell viability and osteoblastic differentiation were determined.

1.5 Aim 3: Characterization of Fiber-Hydrogel Composites

Electrospun fibers that are densely packed can significantly hinder cell infiltration and subsequent tissue formation. To address this, various methods have been implemented to increase the porosities of fiber meshes as well as cell infiltration [11, 18]. Among those methods is the incorporation of a hydrogel phase with the fibers, which has the added benefits of facilitating three-dimensional cellularization. In this third aim, several approaches were taken to combine the fiber and hydrogel phases to form model fiber-hydrogel composites. *In vitro* composite models were fabricated, in which the fiber layer was either attached to a rigid support or elevated above the support. Collagen hydrogel and cells were added to the fibers in several different configurations, and the influence of configurations on cell viability, proliferation, and morphology were studied.

1.6 Dissertation Layout

The remainder of this dissertation consists of five more chapters. Chapter 2 provides background information on the medical problem and the history of treatments before focusing on the anatomical structure and function of the anterior cruciate ligament (ACL) as well as the tissue engineering triad. Chapter 3 addresses the modification of polycaprolactone fibrous meshes with heparin of different concentrations and bone morphogenic protein (BMP)-2 using different immobilization techniques. Chapter 4 discusses the development of BMP-2 nanoparticles through three incorporation approaches – adsorption, encapsulation, and conjugation – and the marked effects of those approaches on protein release and cell behavior. Chapter 5 focuses on the

fabrication of model fiber-hydrogel composites in both supported and elevated fiber configurations, and the evaluation of cell behavior in these composites. Chapter 6 summarizes the main findings of this work and proposes studies for the future continuation of these efforts.

Chapter 2: Background

2.1 Context of Medical Problem

Due to the high mechanical loading that an ACL is exposed to as well as the slow rate of healing, ACL tears are attributed to the accumulation of damage from repeated over-stretching. At the point of a full rupture, the proximal and distal stumps of the ACL are no longer in contact and therefore will not heal naturally; furthermore, surgical efforts to suture the stumps together have proven unsuccessful due to the limited vascularity and slow rate of healing of the ACL. Thus, the aim of ACL reconstructions is to bridge the gap while providing a foundation for cell migration and ligament regeneration. Generally, ligament or tendon tissues are used in reconstructions, and affixed to the tibia and femur by insertion into bone tunnels and anchoring with screws [19]. A result of affixing soft tendon or ligament tissue directly to bone is the creation of an interface – with mismatched mechanical properties – that is slow to integrate and is a major reason for graft failure [20].

2.2 Treatments

The function and structure of native ACL has long been studied. Its inability to heal itself necessitates surgical intervention in most torn ACL cases. One of the earliest is a 1895 effort to repair the injured ligament by suturing together the two ACL stumps with catgut ligatures [21]. Since then, various different materials have been used to suture the torn ends of the ACL, but the repaired injured ligament exhibited high rates of re-rupture as well as tissue morbidity due to the arthrotomy procedure (prior to the advancement of arthroscopic techniques in the 1990s) [21]. During the same time period, autologous tissue grafts (autografts) were utilized as ACL substitutes. Autografts involve using tissue from the patient, usually from the hamstring or patellar tendon, to

reconstruct the ACL. The concerns with autografts include donor site morbidity, pain and weakness in the harvest site, limited availability of donor tissue, and delayed return of the patient to normal activity [22]. Nevertheless, comparison studies have shown that introducing a graft to replace the injured ligament yields better outcomes than restoring it through suturing. This has led to abandonment of the latter [21, 23], making autografts the gold standard.

Starting in the 1970s, the development of non-degradable synthetic grafts was of keen interest due to their potentially unlimited supply, ease of surgery, and the elimination of donor site complications [22, 24, 25]. Based on encouraging initial results, carbon fiber-based devices such as Proplast, Polyflex and Intergraft ligaments were commercialized [24, 26]. However, complications including their early rupture and the accumulation of carbon deposits in the liver led to their abandonment. In the 1980s and early 1990s, alternative synthetic fibers, such as Gore-Tex and Dacron, were used in the Kennedy Ligament Augmentation Device (LAD) and the Leeds-Keio Artificial Ligament for ACL reconstruction [27]. Nonetheless, serious complications (including immunological responses, breakage, instability and osteoarthritis) led to their discontinuation as well [24].

In the 1980s, interest grew for the use of allogeneic tissue graft (allograft) for ACL reconstruction [23]. Allografts involve the use of patellar, hamstring, and Achilles tendons from human cadaveric sources. Although allografts eliminate donor site-related complications and are more readily available, they still have accompanying shortfalls, including the risks of disease transmission and immunological responses. Furthermore, the sterilization process can diminish their strength in comparison to native ACL. Nevertheless, by the late 1990s, the use of synthetic grafts was completely discontinued by orthopaedic surgeons, and ACL reconstructions were performed using either autografts or allografts (biological grafts) [21, 24].

Graft fixation to native bone tunnels and the graft-bone tunnel motion and healing are other crucial factors to graft selection and its initial tension that influence the success of ACL reconstruction [28-30]. Predominant clinical grafts do not exhibit suitable healing with native bone tunnels in contrast to the less commonly used, more invasive bone-patellar tendon-bone autografts [4, 31, 32]. This is particularly associated with the property mismatch between the soft ligament tissue and the hard bone tunnels. As a result, the insertion usually does not provide enough graft fixation strength and suffers from stress concentrations, making tissue integration difficult. Unfortunately, this adds to the previously mentioned issues.

To avoid ruptures, donor site morbidities, immunological responses and the absence of graft-bone healing associated with the use of these treatments (autografts, allografts, simple restorations and synthetics), better approaches are required to enhance the treatment of ACL injuries. To do so, a promising approach is tissue engineering. Based on the aforementioned limitations, a tissue engineered ACL must not only have the ability to regenerate the ligament of the intraarticular portion but also demonstrate osteointegration at both bone tunnel regions.

2.3 ACL Anatomical Structure and Function

The ACL, one of the four ligaments of the knee joint, is vital in stabilizing the knee joint, preventing the displacement of the tibia over the femur and resisting anterior tibial translation and rotational loads [33-35]. The ACL consists of two functional bundles, the anteromedial and the posterolateral bundle. Its average length, width and breadth are 32 mm, 8 mm, and 10 mm, respectively [36, 37] . The ACL has an ultimate tensile strength of 2000 N and a stiffness of 200 N/mm [22, 24, 38]. As depicted in Figure 2.1, the ACL can effortlessly stretch from a relaxed state (toe region) up to a certain extent (linear elastic region) and resists higher loads without further

stretching (start of yield region) while maintaining healthy relative bone motion. If the load, however, becomes too extreme for what the ACL can handle, the ligament tears (end of yield region). However, due to its poor vascularization, interarticular location and regular movements within the knee, the healing process (e.g., development of a fibrin-platelet clot, recruitment of tissue repair cells) is poor [21].

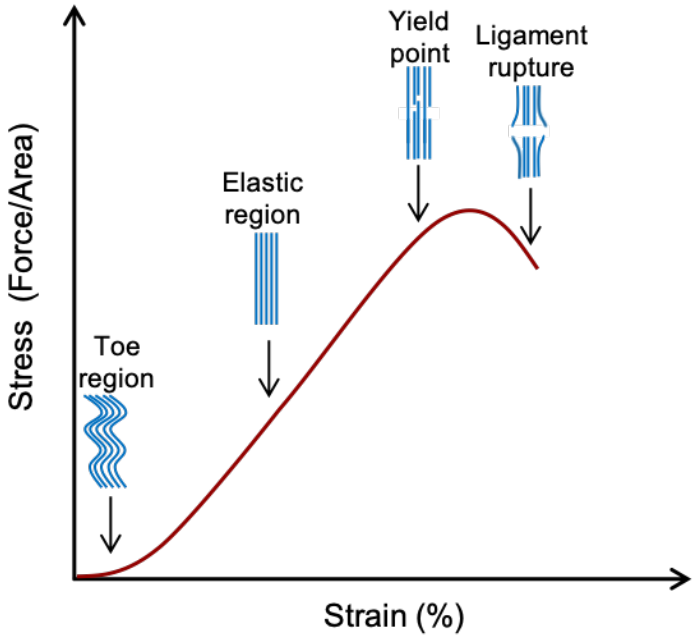

Figure 2.1: ACL structural behavior described by a load deformation curve.

Although the ACL is mainly a ligamentous tissue, histologically it is divided into three zones: the bony insertion ends, the bone-to-ligament interface, and the ligamentous zone. The orchestration between these distinct zones and their components allow the ACL to carry out its function. Each zone is compositionally and structurally systematized making the integration of soft and hard tissues possible and smooth [20, 39]. Although the ACL is considered avascular, a small amount of blood is delivered to the ligament region by the geniculate artery. The interface

and bony insertion sites are entirely avascular [38]. Different cell types occupy the different regions of ACL: osteoblasts in the bony insertion ends, fibrochondrocytes in the bone-to-ligament interface, and fibroblasts (the predominant ligament cell type) in the ligamentous zone (Figure 2.2). Below, each of these three regions is described in detail.

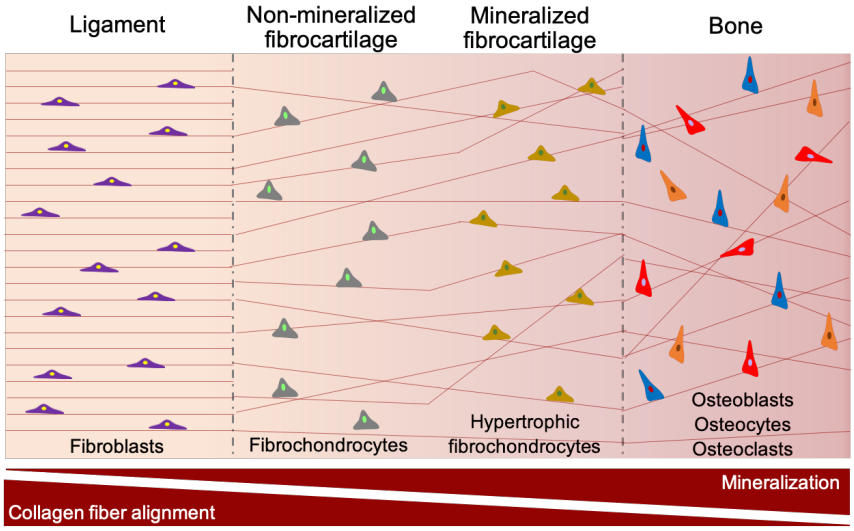

Figure 2.2: Schematic representation of ligamentous, bone-ligament interface and bony insertion zones depicting property transitions from soft tissue to hard tissue (adapted from [40, 41]).

2.3.1 Ligamentous Zone

The ligamentous zone is made of a highly organized and dense collagen matrix (70%) [42], some elastin (<5%), proteoglycans (1%) (such as decorin, hyaluronan, biglycan and lumican), fibroblast cells (20%), and water, all surrounded by synovial fluid [28, 36, 43-45]. The collagen matrix exists primarily in the form of fibers, accounts for 70-80% of ligament dry weight, and is comprised mainly of collagen types I (90%) and III (10%) [46]. These components join together in a highly organized hierarchical cord-like tissue with complex viscoelastic properties allowing it

to respond to stress in the manner shown in Figure 2.1. As illustrated in Figure 2.3, the smallest structural units of the ACL are aligned collagen fibrils (50-500 nm diameter) that are organized into fibers (10-50 μm diameter). Groups of fibers are then structured into primary (also known as sub-fasicles) and then secondary fiber bundles (known as fascicles) (50-500 μm) to form the entire ligament [36, 47].

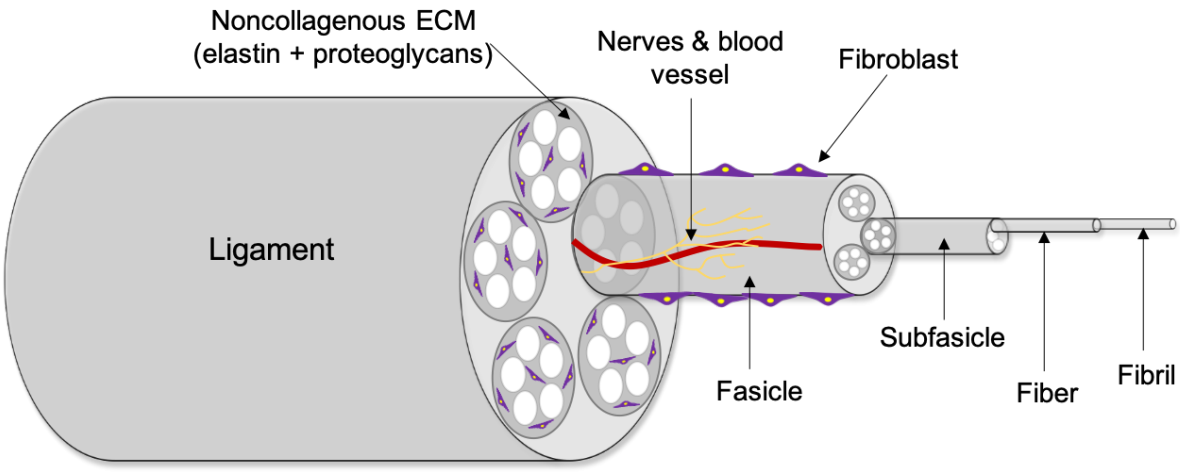

Figure 2.3: Hierarchical organization of collagen within ACL (adapted from [36, 48]).

2.3.2 Bone-Ligament Interface

The ligamentous zone of the ACL integrates to tibial and femoral bones through a bone-ligament interface, which helps facilitate load transfer as well as reduce stress concentrations that are naturally associated with soft to hard tissue attachment by gradually increasing in stiffness and acting as a shock absorber [3, 49]. This interface forms as cells present in this region are exposed to dynamic loads and compression to which they respond by creating a fibrocartilaginous matrix [50]. The bone-ligament interface is also known as the enthesis, is fibrocartilaginous in nature, and is further divided into a mineralized (or calcified) and an unmineralized (or noncalcified) zone

adjacent to the bone and ligament, respectively [29, 39]. Such subdividing within the interface is expected to be of functional significance as higher mineral content is linked to higher mechanical properties [29]. Although the mechanics of the enthesis are not well understood, its biological composition has been characterized. The enthesis is well-organized, rich in collagen, and poor in proteoglycans [39]. Yet in comparison with bone and ligament regions, the interface is low in collagen content [51]. The nonmineralized fibrocartilage section is comprised of collagen types I and II with fibrochondrocytes while the mineralized portion includes hypertrophic fibrochondrocytes within a collagen type X environment [29] (Figure 2.2).

2.3.3 Bony Insertion Ends

The bone-like regions present at the ends of the ACL connect to the tibia and femur. Macroscopically, long bones like the femur and tibia are made up of a less stiff, porous interconnected network at the inner surface known as trabecular or cancellous bone and a stiff, dense outer layer known as cortical or compact bone [52]. Compositionally, bone is comprised of 50-70% mineral, 20-40% organic matrix and 5-10% water [53]. The mineralized matrix is also referred to as the inorganic phase and is mostly composed of calcium hydroxyapatite, and some carbonate, magnesium, citrate, fluoride, chloride, sodium, potassium and strontium [44, 54]. The organic matrix, on the other hand, consists of type I collagen (88%), and non-collagenous proteins like osteocalcin, osteonectin, osteopontin and bone sialoprotein (10%) as well as lipids (2%) [54, 55]. As shown in Figure 2.2, cells embedded within the bone matrix are osteoblasts and osteocytes (bone forming and terminally differentiated bone cells, respectively), and osteoclasts (bone resorbing cells), all working together to remodel bone tissue [31]. The mineral and organic

components of bone contributes to its properties; the mineral phase provides bone stiffness in compression while the organic matrix offers bone toughness and strength in tension [56-58].

2.4 Tissue Engineering

Due to long-term instability concerns linked with current graft options, the development of tissue engineered devices as alternative approaches has received substantial attention to enhance ACL reconstruction. Tissue engineering is an interdisciplinary field that combines the application of engineering, biological and chemical principles with efforts to improve procedures for repairing damaged tissues and organs. Tissue engineered constructs, generally consisting of a biomaterial scaffold, cells, and/or pharmaceutical agents (Figure 2.4), are biocompatible, biofunctional, and do not elicit immunogenic responses. Essentially, tissue engineering strategies leverage a bioactive environment and deliver biologically relevant chemical and physical signals to stimulate tissue regeneration.

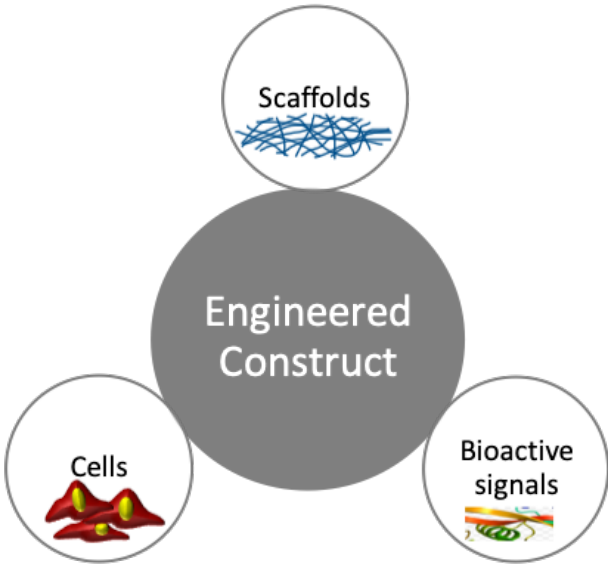

Figure 2.4: Traditional tissue engineering triad encompassing the scaffold materials, biologically active signals and cell supply sources.

A branch of tissue engineering is interfacial tissue engineering. Interfacial tissue engineering focuses on regenerating the anatomic interface between different types of tissue by generating gradients distinct in mechanical, chemical and biological properties. As such, it can potentially solve issues associated with soft graft-bone integration in ACL reconstruction by building upon successful tissue engineering fundamentals. To recapitulate the complex anatomical organization of each region of the ACL (i.e., bone, ligament, bone-ligament interface), efforts in this field have focused on combing different cell types, bioactive agents and/or biological scaffolds for each region to produce a single stratified tissue engineered graft.

Tissue engineering of the ACL aims to design a scaffold that offers initial stability and strength to the knee by supporting its normal functioning while also allowing *in situ* cells to infiltrate, organize and finally remodel the ACL tissue at a rate that is comparable to the scaffold's degradation rate. This helps smoothly shift the load from the implanted scaffold to the newly formed ligament tissue. Developing an ideal tissue engineered ACL remains a challenge due to the tissue's complex structure and our limited understanding of ACL development *in vivo.* Key challenges include the construction of multi-phased scaffolds containing many distinct yet continuous gradients as well as the use of multiple cell types to achieve functional tissue structures. Nonetheless, the works of numerous researchers focusing on various aspects of ACL tissue engineering are encouraging, and demonstrate that with further work, an *in vivo* engineered ACL analogous to native ACL could be utilized in place of current problematic treatment options.

In the following subsections, options and strategies for biomaterial scaffolds, pharmaceutical agents, and cells are discussed.

2.4.1 Biomaterial Scaffolds

Scaffolds are the fundamental element in engineering living tissue and act as a temporary structural support providing appropriate physical environment to which cells can attach, proliferate and differentiate to subsequently regenerate extracellular matrix (ECM) and form tissue. Scaffolds can also incorporate bioactive agents to guide the morphogenesis of tissue [38]. The incorporation of these agents into biomaterials can be carried out through multiple approaches including the direct adsorption or covalent immobilization of the agents onto scaffolds, or through utilizing biocompatible particles in the form of scaffolds for agent delivery to the implantation site [59-62]. The methods chosen to encompass bioactive signals to the scaffolds play a significant role in its biological activity, especially since sustained release profiles and suitable kinetics of signals are essential for tissue regeneration.

To serve as a suitable scaffold, the properties of a scaffold must mimic those of native ECM by possessing vital properties that foster cell-scaffold and cell-ECM interactions [63]. Scaffold biocompatibility, defined by its non-toxicity and non-immunogenicity upon implantation in patients, and biodegradability are among the most important properties. Other scaffold properties include its mechanical function and its architecture. Scaffolds must also match up with cell line requirements in their physical, mechanical, chemical and biomimetic capabilities to aid cell adhesion, growth and differentiation [64]. Furthermore, scaffolds must be porous enough to allow cell migration and nutrient transport [65]. Particular biochemical cues of the scaffold that influence cell behavior include its surface chemistry while physical cues include scaffold stiffness, fibrous structure and hydrophilicity [66, 67]. Thus, the selection of the scaffold material, its production technology, and the optimum balance of its characteristics are important choices for the advancement of tissue engineering scaffolds.

The following sections will focus on four subtopics of biomaterial scaffolds. The first section will examine the use of different materials and their application in ligament tissue engineering. The second section will discuss fibrous scaffolds and the ways their makeup affects cell response. The different techniques used to produce them will also be discussed in this section with an emphasis on electrospinning technique. The third section will focus on different hydrogel scaffolds and their utilization in regenerating ligament tissue. The last section will discuss the fabrication of composite materials with enhanced desirable properties by combining both a fibrous phase and a hydrogel component.

2.4.1.1 Material Choice

In fabricating scaffolds for ligament tissue engineering, there are several options within each of the natural and synthetic classes of materials that can be chosen to meet scaffold requirements. Contrary to short-term synthetic grafts of the 1970s and 1980s, tissue engineered synthetic materials focus on polymers that are both biocompatible and biodegradable. Poly-L-lactic acid (PLLA), polyglycolic acid (PGA), and poly-lactic-co-glycolic-acid (PLGA) copolymers are among the numerous synthetic biodegradable polymers for ligament tissue engineering. Polycaprolactone (PCL), a Food and Drug Administration (FDA) approved for multiple medical applications, is another synthetic polymer used in ligament tissue engineering [47, 68-74]. The advantages of synthetic polymers for ligament regeneration include the ease with which they can be melt- or solvent-processed, the ability to tailor their properties, such as tensile modulus and degradation rate, and their capacity to readily form into high mechanical strength scaffolds. This is important as scaffolds should maintain their mechanical properties until they are replaced by native tissue. Nonetheless, their lack of biological activity could affect their intended

function. Specifically, synthetic fiber polymers carry attractive mechanical and physiochemical properties yet their outer surface, unnatural composition as well as their lack of cell recognition can impede cell attachment and growth [75]. Synthetic polymers tend to degrade by simple hydrolysis whereas natural ones are susceptible to both hydrolytic or enzymatic degradation [76]. PLLA, PGA and PLGA produce hydrolytic degradation products that are ordinarily existent in the metabolic pathways of the body except when in their bulk degradation. Bulk degradation can result in the accumulation of acidic degradation products that lower both cell adhesion and angiogenesis and can be difficult to eliminate [77, 78]. PCL degrades at a much slower rate than PLLA, PGA and PLGA making it more appealing for longer term scaffolds like ligament scaffolds [79]. Its hydrophobicity, on the other hand, results in poor cell attachment. It is thus combined with other polymers when intended for ligament regeneration.

Natural materials have successfully been utilized in tissue engineering studies due to their biocompatible and biodegradable nature when incorporated in physiological environments. Collagen, silk and chitosan are among the natural materials that have been commonly used to produce scaffolds for ligament tissue engineering. Collagen is a polymer that has been extensively investigated for decades in clinical applications [80, 81]. It is the most common protein in our bodies and is particularly abundant in ACLs. As any other scaffolding material, cell behavior is determined by the micro features (such as diameter and porosity) of the collagen scaffold [80]. In addition, collagens contain binding sites for integrin-mediated cell adhesion and cell spreading. Collagen, nonetheless, degrades quickly *in vivo* and has low mechanical properties [82]. It is thus typically used to form hydrogels for soft tissue regeneration [83]. Silk, which has been utilized as a suture material for many years, is another biomaterial that has been investigated. Fabricated silk scaffolds have demonstrated cell guidance towards ligament lineages as a result of their

biocompatibility, suitable biodegradability and tensile strength that is similar to native ACL [22, 84-86], in contrast to most natural polymers which are incapable of withstanding heavy mechanical loads. However, silk scaffolds often limit cell adhesion and proliferation [22, 87]. Chitosan, the deacetylated form of chitin in marine crustaceans, is another natural polysaccharide that has been shown to have properties of biological activity, degradability and compatibility as well as excellent film properties. However, chitosan, like collagen, is inherently weak and difficult to form into scaffold constructs suitable for ligament regeneration. Hence, their modification or combination with other materials is necessary. Other natural materials that have been examined include hyaluronic acid and fibrin [63, 88].

The lack of cell recognition associated with synthetic materials can be avoided with the use of natural ones. Natural materials such as collagen and gelatin that exist as native proteins can additionally provide chemical cues [66]. This is due to the similar compositions of macromolecules such as proteins that are present in the ECM bearing domains to which cellular membrane integrins can attach to [75]. Additionally, natural polymers encompass functional groups to which other molecules like growth factors can be covalently conjugated; a property that is valuable for their application in tissue regeneration. Nonetheless, the poor mechanical properties and lower processing ability of natural polymers in comparison to synthetic ones can limit their application. A recognized tissue engineering approach to overcome this is the production of scaffolds that combine both natural and synthetic ingredients. This allows benefiting from the mechanical properties of synthetic materials while simultaneously allowing natural materials to stimulate cellular adhesion [75].

As in ligament tissue engineering, the use of both natural and synthetic materials has been explored in bone tissue engineering. Since bone is stiffer in comparison to ligament, similar

materials such as synthetic PCL, poly(ethylene glycol) (PEG), PLGA and natural collagen, gelatin, chitosan, silk fibroin, and hyaluronan, are used but combined with other materials or prepared using techniques that yield higher mechanical properties [10, 20, 59, 89, 90]. Additionally, some inorganic osteogenic ingredients specific to bone tissue engineering that continue to be employed are magnesium, calcium phosphates (mainly β-tricalcium phosphate and hydroxyapatite, as well as biphasic calcium phosphate) and glass ceramics which are used to favor the migration, proliferation and differentiation of bone cells [16, 59, 91, 92]. Overall, each class of materials has its advantages and disadvantages, and no explicit material is universally accepted for ligament tissue engineering. For specific applications, however, some materials have been demonstrated to be more fitting.

2.4.1.2 Fibrous Scaffolds

Processing techniques have allowed the fabrication of scaffolds with properties similar to those of native ECM. Specifically, fibrous scaffolds can recapitulate the fibrous structure of ligament ECM as it is its simplest anisotropic structure. Further, collagen fibers are generally the main component of the ECM of many tissues. Accordingly, fibrous scaffolds have been used numerously in both ligament and bone tissue engineering. Fibers have been organized in multiple ways including simple parallel alignment, twisted, braided, woven, crosslinked and knitted structures to form scaffolds [82]. The way fibers are organized determines scaffold mechanical properties and porosity. Fibrous scaffolds have the advantages of a large surface area to volume ratio and a porous structure which provides stronger cues by better mimicking ECM fibers and increasing cell to cell contact, respectively [93]. This in turn enhances mechanical properties and

supports cell growth within scaffolds. In a similar manner, larger surface areas increase cell attachment and smaller fiber diameters increase scaffold biocompatibility [65].

Many techniques have been developed for the fabrication of fibers from various ranges of materials including natural and synthetic polymers, ceramics and metals for bioengineering, drug delivery and predominantly tissue engineering applications. These techniques include melt blowing, self-assembly, phase separation and electrospinning [66]. Among these techniques, electrospinning is an inexpensive, consistent and simple method that produces fibers with nanometer to micrometer range diameters [93, 94]. It is the most popular method and many studies show that electrospun fibers foster cell attachment, growth and proliferation [94] due to their similar dimensions to natural ECM fibrils. Electrospinning forms nanofibers based on the uniaxial stretching of a viscoelastic polymer solution. This occurs by creating an electric field between a charged polymer solution and an oppositely charged or a grounded collector through applying a voltage [95]. As a result, molecules of the charged solution start repelling each other and are attracted to the collector. At the end of the capillary tube (the needle from which they leave the syringe), the polymer solution is held in a Taylor cone shape by its surface tension. Once the surface tension is overcome by electrostatic repulsive forces, the charged polymer leaves the tip of the Taylor cone in a rapidly whipping jet evaporating the solvent and forming a mechanically robust fibrous mesh on the oppositely charged or grounded collector. If the polymer solution is too dilute, repulsive forces would instead drive the whipping stream to break up into droplets (i.e., electrospraying). The collector can be in the form of a rotating mandrel, a flat plate, or two parallel plates [96-98]. As an example, Figure 2.5 illustrates an electrospinning setup with a slowly rotating cylindrical collector. The type of collector directly impacts the alignment of the depositing fibers. The whipping jet generally induces alignment of the polymer chains which results in fibers of high

tensile properties and cause “strain-induced crystallization.” This particularly applies with the use of rotating rather than stationary collectors which can further exert pulling forces on deposited fibers as they rotate. Furthermore, modifying electrospinning setup, processing parameters, and solution properties allow for porosity tuning and the ability to alter the fiber compositions to match specific sizes and anisotropy. For instance, polymer solution concentration, applied voltage, flow rate, and throw distance can be altered based on desired tissue applications. Additionally, the type of collector and the speed of a rotating one can be used to control fiber alignment.

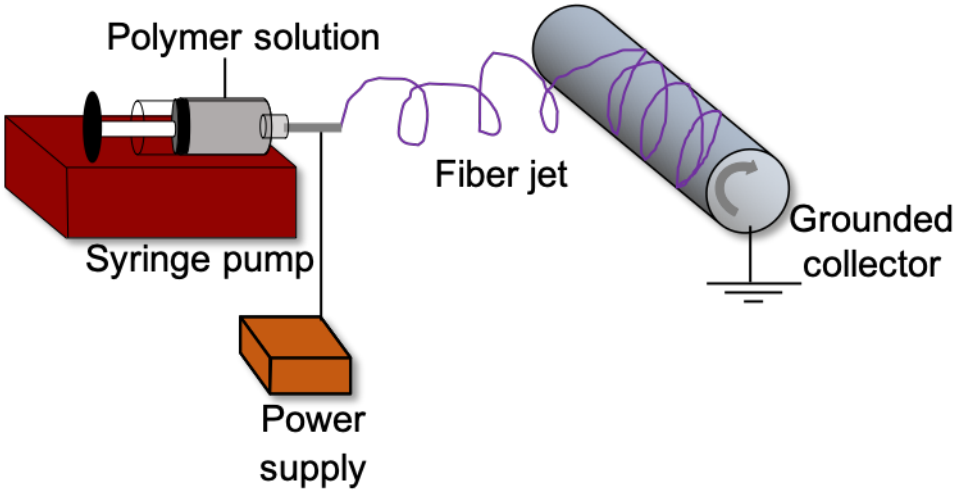

Figure 2.5: Illustration of an electrospinning setup, consisting of: power supply, syringe pump and a grounded rotating cylindrical collector.

Wide ranges of both natural and synthetic polymers have been used in electrospinning for several applications including the tissue engineering of ligaments, wound repairs, drug delivery and biosensor membranes [94, 99]. To enhance scaffolds to suit cell environments and improve cell recognition of scaffold surfaces, other materials such as biological molecules, particles and

minerals can be blended into polymer solutions prior to electrospinning [64, 78]. Additionally, electrospun meshes can be improved by modifying their surfaces [100, 101]. Although electrospun fibers are highly porous, the size of pores is likely on the order of fiber diameter (~ 1 μm) which is often smaller than the size of mammalian cells. This can interfere with cell infiltration which is essential for scaffold remodeling into functional tissue [10, 102]. To combat this, the formation of larger pores has been carried out by modifying the electrospinning process or using other fiber producing techniques. These include the introduction of sacrificial fibers and/or porogens like salt crystals [10, 47] that can then be leached out to increase porosity and pore size. Similarly, gas foaming has been widely used to increase the porosity of electrospun fibers by introducing a gas into the polymer solution [11, 103, 104]. The subsequent rapid release of the gas creates bubbles in the solution allowing the formation of larger pores within electrospun meshes [11]. Although these procedures aid cell infiltration, the rates of infiltration remain slow and these strategies significantly reduce the mechanical properties of the electrospun scaffolds. Additionally, larger pores are associated with a decrease in surface area and reduced cell adhesion [105].

2.4.1.3 Hydrogels

Hydrogel networks are another class of biomaterials. Hydrogels consist of three-dimensional hydrophilic polymer networks that are synthetically or naturally derived and are formed through either chemical or physical crosslinks. Typically, chemically crosslinked hydrogels have higher mechanical properties than physically crosslinked ones [106]. Hydrogels have the ability to absorb large amounts of water through swelling and are of a well-interconnected porous structure (> 90%) in comparison to bulk polymers. This highly hydrated porous structure can be designed to promote the migration and consequent proliferation of cells [65, 107, 108] as

well as the diffusion of oxygen and nutrients [109]. Furthermore, hydrogels are viscoelastic in nature and have the ability to release their absorbed water under the application of forces [43]. Thus, cells are provided with environments that mimic their native ECM both compositionally and structurally. As such, hydrogels are a huge class of materials potentially suitable for tissue engineering different tissues including ligament.

Naturally derived hydrogels include collagen, chitosan, alginate and elastin [89, 110, 111]. The presence of amino, amide, carboxyl, and hydroxyl moieties along the backbone chains contribute to the hydrophilicity of such hydrogels [112, 113]. Since they originate from living organisms and can be prepared from ECM proteins and polysaccharides, natural hydrogels are highly compatible and usually possess domains to which surface integrins of cells can attach to and promote proliferation. Among natural hydrogels, collagen is an especially appealing protein due to its abundance in ECM as well as its high cell binding sites content [110]. Another material is hyaluronic acid which is a natural polysaccharide present in human tissue. It can be designed to produce gels of varying mechanical strength while retaining its biochemical signaling abilities [114]. Natural hydrogels, on the other hand, are easily degraded and can be of low mechanical strength [111, 115].

Synthetic hydrogels that have been explored for tissue engineering applications include PEG [116], poly(vinyl alcohol) (PVA) [117], and poly(2-hydroxylethyl methacrylate) (PHEMA) [89]. In comparison to fibrous scaffolds, particular microarchitectures such as high alignment can be hard to recapitulate in hydrogels [118]. Moreover, paralleled to natural hydrogels, synthetic hydrogels can be highly customized as mechanical and chemical characteristics can be controlled through the formation of polymer blends and copolymers [89]. On the other hand, natural hydrogels are of higher bioactivity and can be more supportive of cell adhesion. Although

hydrogels are mechanically weak and seem to be inappropriate, particularly for harder tissue like bone, the presence of a hydrogel phase can actually enhance viscoelastic properties of scaffolds and provide a suitable matrix for cell maturation [43, 119]. In turn, this allows speeded tissue formation which provides the required mechanical support.

2.4.1.4 Fiber-Hydrogel Hybrids

While electrospun fiber meshes and hydrogels are commonly utilized in biomedical and biological studies, a small number of studies have involved fiber-hydrogel composites to overcome previously mentioned individual shortcomings. Combining fibers and hydrogel can yield benefit from a) the mechanical stability and the ECM mimicking architecture of the fibrous constituent as well as b) the similar three-dimensional ECM-like microenvironment, biocompatibility and functionality of the hydrogels [43, 118, 120-122]. For instance, Deepethi *et al.* fabricated PCL fiber meshes combined with chitosan-hyaluronic acid hydrogels and layered them for the regeneration of ligament tissue [123]. It was found that the presence of hyaluronic acid hydrogel on the fibers did not alter the tensile strength of the fibers yet allowed more cell attachment and infiltration. Additionally, Freeman *et al.* developed a fiber-hydrogel composite composed of PLLA fibers and a polyethylene glycol diacrylate (PEGDA) hydrogel in a braid-twist structure [43]. The incorporation of the hydrogel was found to improve composite viscoelasticity and to allow it to behave similar to natural ligaments in tension. In a similar manner but for bone regeneration, Kolambkar *et al.* produced a hybrid nanofiber mesh tube filled with a growth factor-modified alginate hydrogel phase tested *in vivo* [124]. Here, the delivery of growth factors as part of a fiber-hydrogel composite was found to restore bone defects. The designs of these three mentioned studies integrate fibers and hydrogels differently.

Commonly, fiber and hydrogel phases are assembled in a manner where the hydrogel supports the adhesion of electrospun meshes through the rolling and/or stacking of meshes, or through the incorporation of fibers within the hydrogel phase [118, 120, 125]. This is potentially due to physical combination of the two phases being the simplest approach [120]. Nonetheless, composites with homogenous properties can be difficult to achieve due to precise fabrication methods. Hence, in producing composites, it is essential to develop an approach that not only combines the individual advantages of the constituents creating a scaffold with novel characteristics, but one that also retains the fundamental properties required of a scaffold based on the targeted tissue.

2.4.2 Bioactive Agents

Tissue engineering research requires more than an inert template for cell attachment and is thus combined with biological cues and tissue cells. The presence of a cue, in the form of adhesion molecules and/or growth factors can guide and mediate the formation of tissue by mimicking the ECM's supply of bioactive signals which regulate cell behavior [126]. Furthermore, biological signals influence cell proliferation, differentiation and migration [22]. Therefore, the introduction of different signaling molecules including different cytokines, growth factors, and morphogens to the cell environment to direct the formation of target phenotypes is an important aspect of tissue engineering. In ACL tissue engineering, the use of signaling molecules and an understanding of their exact cell guiding schemes has become of deep interest and continues to be explored.

Growth factors are among the signaling molecules that can govern cell behavior, and several growth factors (such as fibroblast growth factor (FGF), transforming growth factor (TGF)-β and platelet-derived growth factor (PDGF)) have been demonstrated to increase fibroblastic

differentiation and to produce ECM to help in ligament healing [80]. Furthermore, the incorporation of growth factors into acellular scaffolds encourages *in situ* cells surrounding host tissue to migrate and grow into the scaffold [127]. Often, groups of growth factors that belong to proteins and are known to improve the deposition of ECM products are employed [1]. Such growth factors include bone morphogenic proteins (BMPs) which belong to the transforming growth factor (TGF)-β superfamily and were a major breakthrough in 1965 [128, 129]. BMPs are further known to have an inductive ability on their own [127].

Prominently, BMPs simulate chondrogenic and osteogenic differentiation of MSCs [1, 130] with BMP-2 being the most representative and osteoinductive member of the family. BMP-2 formulated in an absorbable collagen sponge carrier is FDA approved for use in spinal fusion applications [127]. As a result of its well-known critical role in bone formation, BMP-2 has been incorporated into biomaterial scaffolds in a number of different ways to stimulate osteoblastic differentiation *in vitro,* and bone healing in both animal studies and clinical procedures. Zhao *et al.* investigated the role of BMP-2 immobilized poly(lactide-*co*-glycolide)/hydroxyapatite (PLGA/HA) fibrous scaffolds produced by melt-spinning on MC3T3-E1 cells to promote the regeneration of bone tissue [131]. Here, the authors reported increased alkaline phosphatase activity, higher expression of osteogenesis related genes, and higher mineral deposition in cells with BMP-2 immobilized scaffolds in comparison to those in the absence of BMP-2. Andrews *et al.* reported a similar observation in the presence of BMP-2 when loading the protein in a chondroitin sulfate glycosaminoglycan (CS-GAG) scaffold or inserting its gene into mesenchymal stem cells (BMP-2 MSC) and studying it *in vivo* in a rat femoral defect model [132]. The presence of BMP-2 maintained a significant increase in bone volume, strength and stiffness illustrating its potential use for bone repair.

Similar to the importance of BMP-2 in the stimulation of an osteogenic pathway, the induction to tendinous and ligamentous pathways of MSCs are possible with growth and differentiation factors (GDFs), another distinct class belonging to BMPs [1]. Specifically, GDF-5, -6, and -7 are of significance in the development of tendon and ligament tissue and their repair process [133]. Farng *et al.* studied the effects of mechanical stimulation (with cyclic strain) and biochemical stimulation (with GDF-5) on the proliferation and differentiation of cells seeded on a highly porous, three-dimensional polycaprolactone (PCL) polymer scaffold [134]. Although the combination of both stimuli increased cellular proliferation, each stimulus on its own did not. GDF-5, nonetheless, increased the expression of ligament fibroblast markers: collagen I, collagen II and scleraxis. In a different study, Rickert *et al.* examined the influence of GDF-5 on rat Achilles tendon healing [135]. The sutures were either treated with a GDF-5 coat or left uncoated. At the end of 4 weeks, tendons were stiffer and the expression of collagen II in repair sites was upregulated in the GDF-5 coated group in comparison to the control. Again, this signifies the potential ability of GDF-5 to help accelerate soft tissue repair.

2.4.3 Cells

The third fundamental component for the success of a tissue engineering approach to ACL replacement is the choice of cell line to be incorporated onto/within scaffolds. Although cells can either be implanted with the scaffold (cellularized scaffolds) or be recruited to the scaffold *in situ* (acellular scaffolds) [136], cellularized scaffolds have shown to better enhance ACL healing since seeded cells can partake in its healing early on [80, 137]. This is possibly due to ACL's poor ability to heal and its unique mechanics. Yet the exact mechanism in which this occurs remains largely unidentified. In *in vitro* and *in vivo* investigations of tissue engineering, the selection of cell type

for the formation of cellular scaffolds or a model to *in situ* cells is key. Cell choice is generally based on the tissue of interest as well as the cell type availability, its capacity to proliferate, its potential to generate an ECM similar to that of native tissue, and to secrete trophic factors to recruit host cells to implantation sites assisting in the regenerative process. Specifically, cells incorporated for ligament regeneration must have the ability to remodel their generated ECM into collagen fibers of high tensile strength. Furthermore, the cells must stimulate integration of the scaffolds with tibial and femoral bone tunnels for complete healing.

In ligament tissue engineering, fully differentiated fibroblasts have been used as the cell source since ACL primarily consists of fibroblasts [138-140]. Typically, cells are seeded on scaffolds but sometimes other procedures are used to incorporate them to make up for certain cell-scaffold interaction limitations. The seeding of ligament-targeting scaffolds with fibroblasts *in vivo* has shown to allow higher cell ECM protein secretion in comparison to scaffolds implanted in the absence of fibroblasts [137]. Although their presence in ACL and their formation of an ECM make fibroblasts the logical cell choice, their limited quantity as well as the risk for local infection during harvesting restricts their use [1]. With the advancement in stem cell technology, nonetheless, many works support the use of mesenchymal stem cells (MSCs) over fibroblasts due to their higher and more robust proliferative potential and their capacity to produce more collagen [22, 141]. These findings were obtained when comparing MSC seeded scaffolds to fibroblast seeded scaffolds [141].

MSCs can be extracted from different body tissue such as the periosteum, dental pulp, hair follicle, fat, tonsil and skeletal muscle [22]. The most studied adult MSCs for skeletal tissue regeneration are those derived from bone marrow (BMSCs). With no significant surgeries, adult BMSCs can be harvested by suctioning bone marrow and expanding it rapidly *in vitro* [22].

BMSCs can self-renew and upon the introduction of signals, BMSCs can, among other pathways, differentiate into fibroblasts, osteoblasts and chrondocyte-like phenotypes. Undifferentiated MSCs are relatively more abundant than fibroblasts as they can be obtained from several different tissue sources and in a much easier manner than tendon or ligament fibroblasts [81, 142]. In bone tissue engineering, similarly, mesenchymal stem cells (MSCs) are the most commonly used cell line and are well known for their criticality in the bone healing process [64]. When stimulated correctly, MSCs have the ability to differentiate down well-defined pathways for the regeneration of different tissues, including bone, ligament, tendon and adipose.

2.5 Summary

This chapter discusses the distinctive characteristics associated with ACL injuries, the past and current treatments, as well as the various aspects related to the development of tissue engineering as an alternative approach to current treatments. The appropriate provision of stimuli, through the presence of bioactive agents and specific scaffolding properties, is necessary to guide tissue regeneration. The next three chapters will focus on the efforts embarked to develop scaffold materials and delivery systems to provide such stimuli to cells.

Chapter 3: Improving the Osteogenicity of PCL Fiber Substrates by Surface-Immobilization of Bone Morphogenic Protein-2

Dina Gadalla[1], Aaron S. Goldstein[1,2]

[1]Department of Chemical Engineering,
[2]School of Biomedical Engineering and Sciences
Virginia Tech, Blacksburg, VA 24061, USA

Accepted into *Annals of Biomedical Engineering*

Permission granted for reprinting from publisher

3.1 Abstract

Polycaprolactone (PCL) fiber scaffolds are attractive, albeit inert, substrates for ligament regeneration, that may be improved by incorporating trophic factors to guide tissue remodeling *in vivo*. In particular, immobilization of bone morphogenic protein (BMP)-2 to the scaffold surface may facilitate rapid and robust integration of the scaffold with adjacent bone tissues. As a first step toward testing this, model PCL surfaces were modified by the addition of heparin and BMP-2 to facilitate osteoblastic differentiation. Specifically, heparin was combined with PCL at 0, 0.5, and 1 wt% (denoted as PCL, PCL-0.5Hep, and PCL-1Hep), cast into films, and then BMP-2 was immobilized to surfaces by either adsorption and covalent conjugation. Here, BMP-2 concentration increased systematically with incorporation of heparin, and higher concentrations were achieved by covalent conjugation. Next, blends were electrospun to form thin meshes with fiber diameters of 0.54, 0.62, and 0.92 μm for PCL-1Hep, PCL-0.5Hep, and PCL, respectively. Mesenchymal stem cells (MSCs) had no difficulty attaching to and proliferating on all meshes.

Lastly, PCL-1Hep meshes were prepared with adsorbed or covalently conjugated BMP-2 and cultured with MSCs in the absence of osteogenic factors. Under these conditions, alkaline phosphatase activity and deposition of bone sialoprotein, osteopontin, and calcium minerals – markers of osteoblastic differentiation – were significantly higher on surfaces with immobilized BMP-2. Together, these data indicate that covalent immobilization of trophic factors confers bioactivity to scaffolds, which may be applied in a spatially controlled manner for ligament regeneration and bone integration.

3.2 Introduction

Anterior cruciate ligament (ACL) injuries are common, and incidents leading to such injuries continue to rise [143]. Indeed, the incidence of ACL reconstructions in the US was estimated to have risen from 87,000 in 1994 to 130,000 in 2005 [144]. In case of ACL replacement surgery, the graft must strongly integrate with the tibia and femur. However, reconstruction practices that involve directly affixing soft tissue to bone (e.g., quadriceps tendon, hamstring tendon graft) exhibit slower integration than bone-to-bone grafts (e.g., bone-patellar tendon-bone graft), and risk both mechanical instability and early pull out of the graft [15]. In ligament tissue engineering research, efforts have been made to overcome these limitations by constructing scaffolds with transition zones and hard regions to enhance integration with host bone [145].

To accelerate ligament regeneration and bony integration to bone, reconstruction strategies have involved the local delivery of osteogenic materials such as hydroxyapatite, magnesium, calcium carbonate, fibroblast growth factors (FGFs) and bone morphogenic proteins (BMPs) [146, 147]. BMP-2 in particular is a member of the transforming growth factor (TGF)-β superfamily and is involved in the osteogenic differentiation of mesenchymal stem cells (MSCs) and bone

formation both *in vitro* and *in vivo* [148, 149]. FDA-approved for lumbar fusion in 2002, BMP-2 recruits bone marrow and circulatory cells to areas of bone repair [150] and induces their osteoblastic differentiation and mineral deposition [151]. Nonetheless, BMP-2 has a short half-life *in vivo* and may lose biological activity shortly after release from its delivery vehicle, necessitating the use of superphysiologic concentrations. However, immobilization of BMP-2 on the delivery vehicle surface may extend its bioavailability and reduce the concentrations required for bone formation.

Polycaprolactone (PCL) is an attractive biomaterial for bone and ligament tissue engineering, and has been used to deliver BMP-2 [152] and other trophic factors. Although PCL is nontoxic, has a Young's modulus of ~400 MPa, and hydrolyzes in 6 months to 2 years, it is hydrophobic and lacks recognition sites for cell-scaffold interactions. Therefore, its modification with proteins, peptides, or polysaccharides – to increase biological compatibility – has been of great interest [153]. Heparin is a linear sulfated glycosaminoglycan (GAG) that has been shown to confer anti-inflammatory and blood compatibility properties to synthetic biomaterial surfaces [154]. In addition, it binds various trophic factors (e.g., BMPs, FGFs, VEGF, PDGFs) decreasing their diffusion rate and modulating their bioactivity [155-157].

With the ultimate goal of fabricating a contiguous 3D ligament scaffold with bony insertion regions, this work focuses on the fabrication of electrospun fibrous scaffolds capable of inducing osteogenic differentiation. To this end, PCL was mixed with heparin and electrospun to form PCL-heparin (PCL-Hep) films and fiber meshes to which BMP-2 was immobilized through adsorption and covalent conjugation. MSC responses – including cell viability, proliferation, alkaline phosphatase (ALP) activity, deposition of bone sialoprotein (BSP) and osteopontin (OPN), and mineralization – to the different bioactive fiber meshes were studied.

3.3 Materials and Methods

3.3.1 Materials

Polycaprolactone (PCL, Mn 80 kDa), heparin (sodium salt from porcine intestinal mucosa Grade I-A, average MW of 18 kDa), toluidine blue, Tween-20, Triton-X100, Alizarin red, neutral buffered formalin (NBF) and cetylpyridinium chloride were obtained from Sigma Aldrich (Saint Louis, MO). Extra pure 2,2,2-trifluoroethanol (TFE), 2-morpholinoethane sulfonic acid buffer (MES), bovine serum albumin (BSA) and sodium phosphate were obtained from Fisher Scientific (Suwanee, GA). N-hydroxysuccinimide (NHS), 1-ethyl-3-(3-dimethylaminopropyl) carbodiimide (EDC) and ABTS (2,2'-Azinobis [3-ethylbenzothiazoline-6-sulfonic acid]-diammonium salt) were obtained from Thermo Scientific (Grand Island, NY). Recombinant human bone morphogenic protein (BMP)-2 and phosphate buffered saline (PBS) were obtained from Invitrogen (Carlsbad, CA) and Corning cellgro (Manassas, VA), respectively. Primary antibodies against BSP (ab52128) and OPN (ab8448) as well as fluorescein thioisocyanate (FITC)-conjugated secondary antibody (ab6717) were obtained from Abcam Inc. (Cambridge, MA).

3.3.2 Electrospinning of Fiber Meshes

PCL and PCL/heparin blends (99.5/0.5 and 99/1 w/w%) were prepared at 9 wt% in TFE. To incorporate heparin into PCL, appropriate amounts of heparin were first dissolved in 100 μL of water and then mixed with 5 mL of TFE prior to the addition of PCL. The 99.5/0.5 and 99/1 w/w% blends are denoted as PCL-0.5Hep and PCL-1Hep. Fibers were electrospun from solutions in 10 mL plastic syringes equipped with 22-gauge stainless steel needles, using a flow rate of 3.0 mL/h, a throw distance of 11 cm, and a potential of 15 kV. Fibers were collected on an aluminum foil covered 7.5 cm diameter cylindrical mandrel rotating at 1600 rpm. Fibers collected on the foil

for 30 min were used for characterization of fiber properties and mechanical testing. Fibers for cell culture studies were electrospun for 5 min and collected onto 15 mm diameter coverslips attached to the rotating mandrel.

3.3.3 Fiber Characterization

The incorporation of heparin into PCL-0.5Hep and PCL-1Hep fiber meshes was visualized using toluidine blue. Electrospun meshes were incubated in a solution of 50 μg/mL toluidine blue in 0.01 M HCl and 0.2% NaCl under gentle shaking for 2 h at room temperature. Subsequently, color images of the stained meshes were collected as well as absorbance measurements of the resultant dye solution at 631 nm (using a SpectraMax M2 plate reader, Molecular devices, Sunnyvale, CA). In addition, the morphology of the electrospun fibers was examined by scanning electron microscopy (SEM). After sputter coating the fibers with a 5 nm conductive palladium layer (Model 208 HR, Cressington Scientific Instruments, Cranberry, PA), fibers were visualized with a LEO1550 field emission SEM (Oxford Instruments, Oxfordshire, UK) at an accelerating voltage of 5 kV. Average fiber diameters for the different meshes were determined by analyzing at least 100 fiber segments over 4 image fields using ImageJ (National Institutes of Health). To characterize the hydrophilicity of fiber meshes, water contact angles on electrospun fiber surfaces were measured with a FTA125 contact angle goniometer (First Ten angstroms, Portsmouth, VA).

3.3.4 Mechanical Testing

Mechanical testing was carried out on 5 cm × 2.5 cm meshes (with the longer dimension corresponding to the theta direction of the rotating mandrel) that had been incubated overnight in PBS at room temperature. Widths and lengths were measured with a precision caliper and the

thicknesses were measured using a laser displacement sensor (Keyence model LK-G82, Itasca, IL). Widths and thicknesses were averaged along the length of the meshes. Samples were mounted into the clamps of a material testing system (MTS Insight, Eden Prairie, MN) giving a mesh gauge length of approximately 3 cm. Tensile testing was conducted to failure at a strain rate of 0.3 mm/s at room temperature with a 50 N load cell. Young's Modulus and strain at peak, among other outputs, were automatically calculated by the MTS Test Works 4 software from generated load vs extension curves.

3.3.5 BMP-2 Immobilization and Quantification on Thin Films

BMP-2 was either adsorbed or covalently attached to the fibers. To quantify the concentration of BMP-2, polymer films were on 15 mm glass coverslips by spin coating. To adsorb BMP-2, coverslips were immersed in 0.5 mL of 250 ng/mL BMP-2 solution in PBS for 2.5 h at room temperature. For covalent attachment, coverslips were incubated in 25 mM EDC and 10 mM NHS dissolved in MES buffer (0.05 M MES in water, pH 6) for 30 min followed by immersion in 250 ng/mL BMP-2 solution in MES buffer for 2.5 h at room temperature.

The amount of BMP-2 adsorbed or covalently immobilized was quantified with a Quantikine Enzyme-Linked Immmunosorbent Assay (ELISA) (PeproTech) immediately following adsorption/conjugation and after 7 days of incubation in PBS (pH 7.4) at 37 °C. Samples on glass coverslips were rinsed twice with PBS, blocked for 1 h with 1% BSA in PBS, and washed thrice with 0.05% Tween-20. Samples were then incubated in 250 ng/mL biotinylated rabbit anti-human BMP-2 antibody (PeproTech, catalog #500-P195BT) for 2 h, washed thrice in Tween-20, and incubated in 550 ng/mL streptavidin-conjugated horseradish peroxidase (PeproTech) for 30 min. Coverslips were washed in Tween-20, transferred to new wells, and incubated for 5 min in

ABTS development solution under gentle agitation. Samples of development solutions were then transferred to a 96 well plate and the absorbances measured at 405 nm with wavelength correction set at 650 nm using a SpectraMax M2 plate reader. Absorbances were converted to nanograms of BMP-2 per volume of solution using a series of BMP-2 standards.

3.3.6 Mesenchymal Stem Cell (MSC) Culture

MSCs were derived from bone marrow explants from the femurs and tibias of juvenile male Sprague-Dawley rats weighing 125-150 g (Harlan, Dublin, VA) in accordance with the Institutional Animal Care and Use Committee at Virginia Tech as described previously [158]. Cells were cultured in growth medium consisting of alpha-modified Eagle medium (α-MEM, Invitrogen, Carlsbad, CA) supplemented with 10% fetal bovine serum (Gemini Biosciences, West Sacramento, CA) and 1% penicillin/streptomycin (Invitrogen), and used between passages 3 and 5.

Fibers on coverslips were sterilized by soaking in 70% ethanol for 30 min, exposing to UV light for 30 min, and washing twice with sterile PBS. Next, BMP-2 was deposited onto fibers by adsorption or conjugation under sterile conditions (as described previously). Coverslips were then transferred into 24 well plates and each incubated with 1 mL of growth medium for 30 min before seeding with 4×10^4 cells per fiber mesh. Cells were cultured in growth media, and the media was changed twice weekly.

3.3.7 Cell Viability Analysis

The viability of cells on the different fiber meshes were evaluated with a live/dead viability cytotoxicity kit (Biotium, Hayward, CA) at 1, 7 and 14 days after seeding cells. Briefly, fiber

meshes were incubated for 30 min at 37 °C in 2 μM calcein-AM and 4 μM ethidium homodimer I in PBS. Meshes were then rinsed with PBS and observed with an inverted Leica DM IL microscope (Leica Microsystems, Buffalo Grove, IL) with a blue band-pass filter to identify live cells and a green band-pass filter to indicate dead cells.

3.3.8 MSC Number

Quanti-iT PicoGreen kit (Invitrogen, Grand Island, NY) was used to quantify the DNA content of the PCL, PCL-0.5 heparin and PCL-1 heparin fiber meshes at 3, 7 and 14 days post seeding. After two PBS washes, the cells were lysed with 0.2% Triton-X100 followed by three freeze-thaw cycles, and thorough mixing. Equal volumes of sample and Quanti-iT PicoGreen dsDNA reagent were combined and incubated for 5 min following manufacturer's instructions. Fluorescence was then measured at excitation 480 nm and emission 520 nm with a SpectraMax M2 plate reader. Fluorescence data were converted to DNA mass using a prepared standards series. The number of cells was calculated from DNA content using the predetermined conversion factor of 8 pg DNA per cell and reported as relative to day 3 cell numbers within each group.

3.3.9 ALP Activity

Intracellular ALP activity was determined at 7 and 14 days of culture in growth medium. At each time point, fiber meshes were washed with PBS and the cells lysed for 1 h in 0.2% Triton-X100 and 5 mM $MgCl_2$ in deionized (DI) water. Activity was assayed according to manufacturer's protocol with a QuantiChrom ALP assay kit (BioAssay Systems) using *p*-nitrophenyl phosphate. Cell number for each sample was then determined by PicoGreen (as described previously), and the values were used to normalize ALP activity.

3.3.10 Alizarin Red Staining and Quantitative Analysis

Alizarin red staining was carried out at day 28. Cells were washed with PBS and fixed in 10% neutral buffered formalin for 30 min. After washing with DI water, samples were stained with 2% Alizarin red in DI water for 45 min in the dark at room temperature. Following that, samples were washed with DI water to remove unbound stain and the cells analyzed with a microscope. Quantitative analysis was carried out by dissolving the bound stain with 10% cetylpyridinium chloride in 10 mM sodium phosphate under shaking for 30 min. The solution was then centrifuged and the absorbance of the supernatant measured at a 570 nm wavelength with a SpectraMax M2 plate reader.

3.3.11 Immunofluorescent Staining

Immunofluorescent staining was carried out after 28 days of culture to detect OPN and BSP proteins. Cells were washed twice with PBS and fixed for 30 min with 10% NBF. After three PBS washes, cells were lysed for 15 min with 0.5% Triton-X100 in PBS. Samples were then rinsed thrice with PBS and blocked for 1 h with 1% BSA in PBS and then incubated with either rabbit polyclonal anti-BSP or anti-OPN primary antibody (both at 1:100 dilution) in PBS for 16 h at 4 ^{0}C. Following three PBS washes, samples were incubated in 1:1000 diluted FITC-conjugated goat polyclonal secondary antibody to rabbit immunoglobin G (IgG) in PBS for 1 h at room temperature. Samples were then rinsed twice with PBS and observed using an inverted Leica DM IL microscope with a blue band-pass filter to indicate the presence of BSP and OPN proteins.

3.3.12 Statistical Analysis

Data values are represented as mean ± standard error of the mean (SEM). *p* values were

determined by one-way analysis of variance (ANOVA) using StatPlus 2016 statistics package (AnalystSoft, Walnut, CA) and values $p \leq 0.05$ were considered statistically significant.

3.4 Results

3.4.1 Fiber Characterization and Mechanical Testing

The morphologies of the PCL, PCL-0.5Hep and PCL-1Hep fibers were visualized by SEM. Overall, the surfaces appear similar, with regular fibers and the absence of beads or broken fibers for all compositions (Figure 3.1). Some evidence of splaying (e.g., a mixture of thin and thick fibers, fibers branching, fibers twisted around one another) was noted. Quantitative analysis indicated a systematic decrease in fiber diameter with addition of heparin, with diameters of 916 ± 320 nm for PCL, 623 ± 307 nm for PCL-0.5Hep, and 537 ± 225 nm for PCL-1Hep. The presence of heparin was confirmed by toluidine blue assay, which revealed more purple-colored heparin-toluidine blue dye on the PCL-0.5Hep and PCL-1Hep fibers than on PCL fibers (Figure 3.2a-c). In addition, absorbances for the toluidine blue soaking solutions (following incubation with the meshes) decreased with increasing heparin content with values of 2.20 for PCL, 2.18 for PCL-0.5Hep and 2.15 for PCL-1Hep fiber substrates at 631 nm wavelength (Figure 3.2d). Similarly, surface contact angles decreased with increasing heparin content, with values of 98.5° ± 8.8°, 73.0° ± 0.5° and 64.0° ± 1.0° for PCL, PCL-0.5Hep and PCL-1Hep surfaces, respectively. Mechanical testing, demonstrated similar tensile properties of the different meshes, with Young's moduli of 28.3 ± 3.6 MPa, 28.0 ± 3.9 MPa and 30.7 ± 8.1 MPa for PCL, PCL-0.5Hep and PCL-1Hep surfaces, respectively.

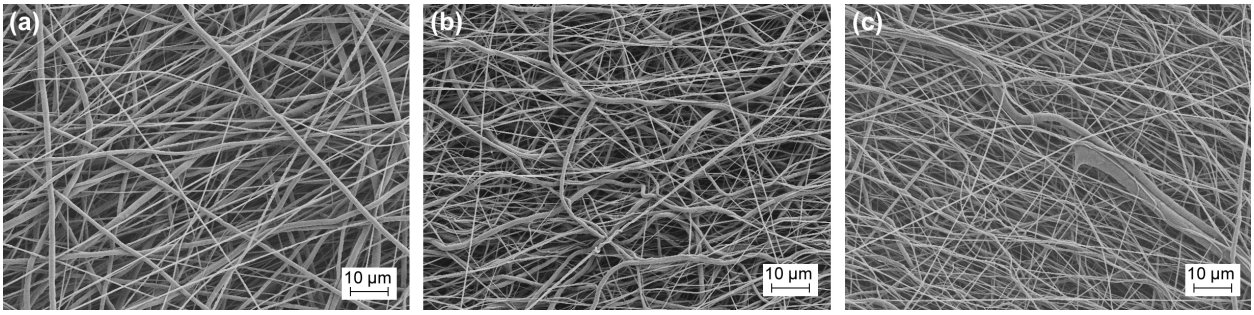

Figure 3.1: SEM images of (a) PCL, (b) PCL-0.5Hep and (c) PCL-1Hep electrospun fibers. Scale bars correspond to 10 µm.

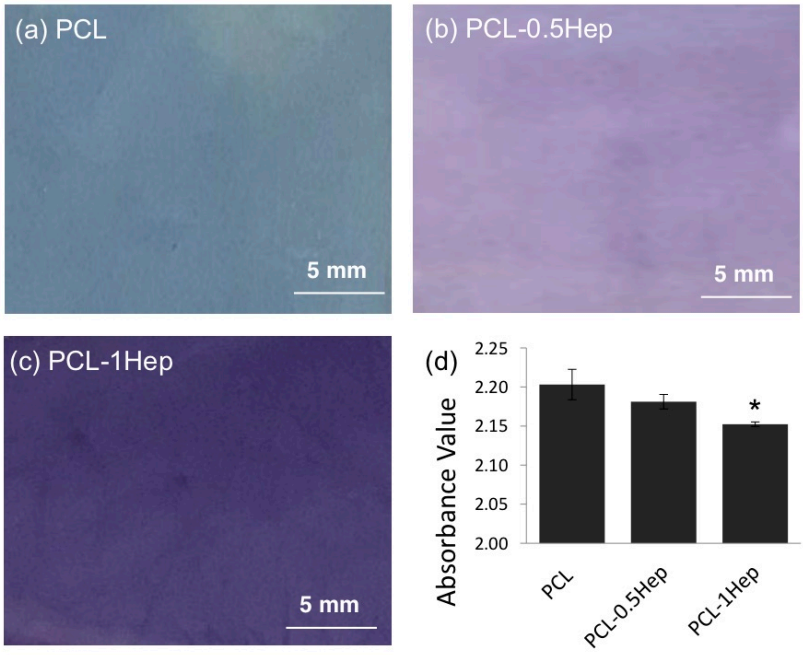

Figure 3.2: Observed toluidine blue staining on (a) PCL, (b) PCL-0.5Hep and (c) PCL-1Hep electrospun fibers. Scale bars correspond to 5 mm. (d) Absorbance values of toluidine blue solutions post-staining. *Indicates statistical significance ($p < 0.05$) relative to other groups.

3.4.2 BMP-2 Immobilization

BMP-2 was immobilized to spin-coated films of the three different materials by adsorption of 250 ng/mL BMP-2 or by activation of the surface with EDC and NHS followed by incubation with 250 ng/mL BMP-2. The surface concentration varied with both conjugation technique and substrate composition (Figure 3.3a). In particular, the concentration increased systematically with heparin content for both conjugation techniques but covalent conjugation achieved higher BMP-2 binding for all three substrates. Thus, PCL-1Hep surfaces with covalently conjugated protein had the highest BMP-2 surface concentration (5.1 ± 1.6 ng/cm^2), which was significantly different from the other groups ($p < 0.05$). In a separate study surfaces were incubated in PBS for 7 days prior to determination of BMP-2 concentration (Figure 3.3b), and qualitatively similar concentrations of BMP-2 were observed. That is, a significant decrease in protein – that could be associated with BMP-2 desorption or PCL degradation – was not observed. However, at the same time, the concentration of BMP-2 covalently conjugated to the substrates appeared to increase by roughly a factor of two relative to day 0. This could be a consequence of rearrangement of the proteins on the surfaces (e.g., denaturation) to expose more epitopes for antibody binding. Nevertheless, the data conservatively indicates that BMP-2 is not lost from any of the surfaces over 7 days of incubation and that covalent conjugation may achieve three to four times as much BMP-2 immobilization as adsorption.

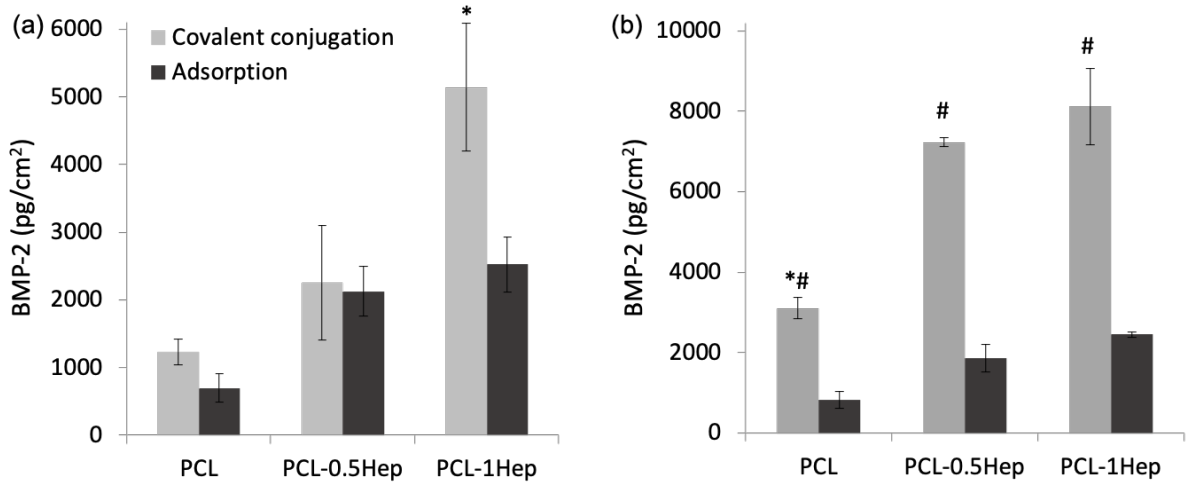

Figure 3.3: (a) Adsorbed and conjugated BMP-2 surface concentrations on PCL, PCL-0.5Hep and PCL-1Hep surfaces as measured by ELISA. (b) Adsorbed and conjugated BMP-2 surface concentrations on PCL, PCL-0.5Hep and PCL-1Hep surfaces at day 7 as measured by ELISA. Bars correspond to mean ± SEM ($n = 3$). *Denotes statistical significance ($p < 0.05$) relative to other groups. #Indicates statistical significance ($p < 0.05$) relative to same group for different immobilization chemistry.

3.4.3 Live/Dead Staining and Cell Proliferation

Live/dead staining showed that MSCs attached to the three different fiber meshes (absent BMP-2 conjugation) and exhibited high viability over 14 days of culture (Figure 3.4). In addition, cell numbers increased over 14 days on all surfaces (Figure 3.5), and were comparable to cells on tissue culture polystyrene (TCPS). Quantitative analysis indicated that all fiber meshes supported significant increases in cell number between day 7 and day 14. In addition, at day 7, cell numbers on PCL-1Hep fiber meshes were significantly higher than on the other surfaces.

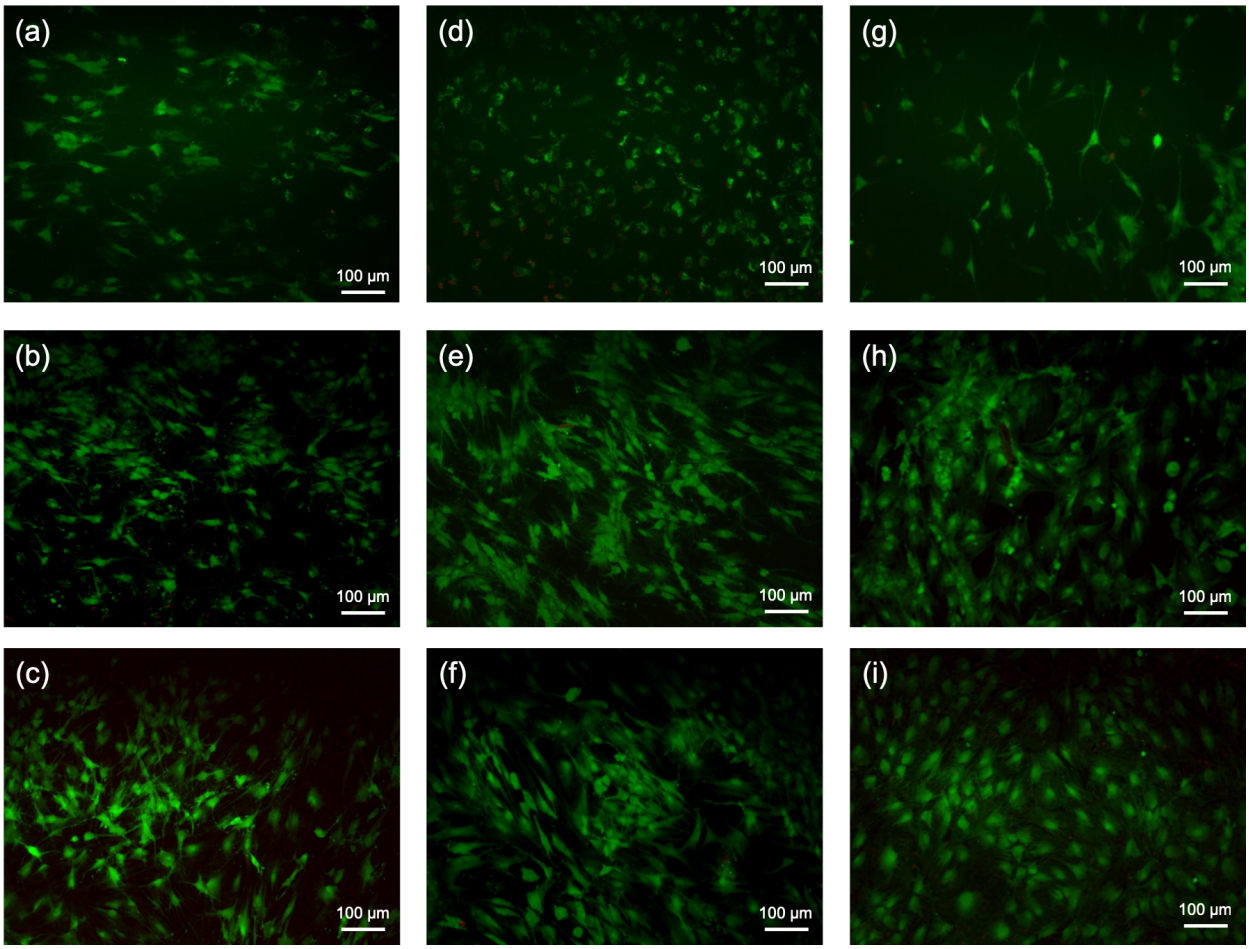

Figure 3.4: Live dead staining of MSCs seeded on PCL, PCL-0.5Hep and PCL-1Hep electrospun fibers at days 1, 7 and 14. Scale bars correspond to 100 µm.

3.4.4 MSCs Osteogenic Differentiation

Because spin-coated PCL-1Hep surfaces achieved the highest BMP-2 surface concentration (Figure 3.3), osteoblastic differentiation studies were performed on electrospun PCL-1Hep fiber meshes. Experimental groups were meshes with adsorbed and covalently conjugated BMP-2 and negative controls were meshes without BMP-2. For these studies, cells were maintained in growth medium (without osteogenic supplements such as dexamethasone, β-glycerophosphate and ascorbic acid).

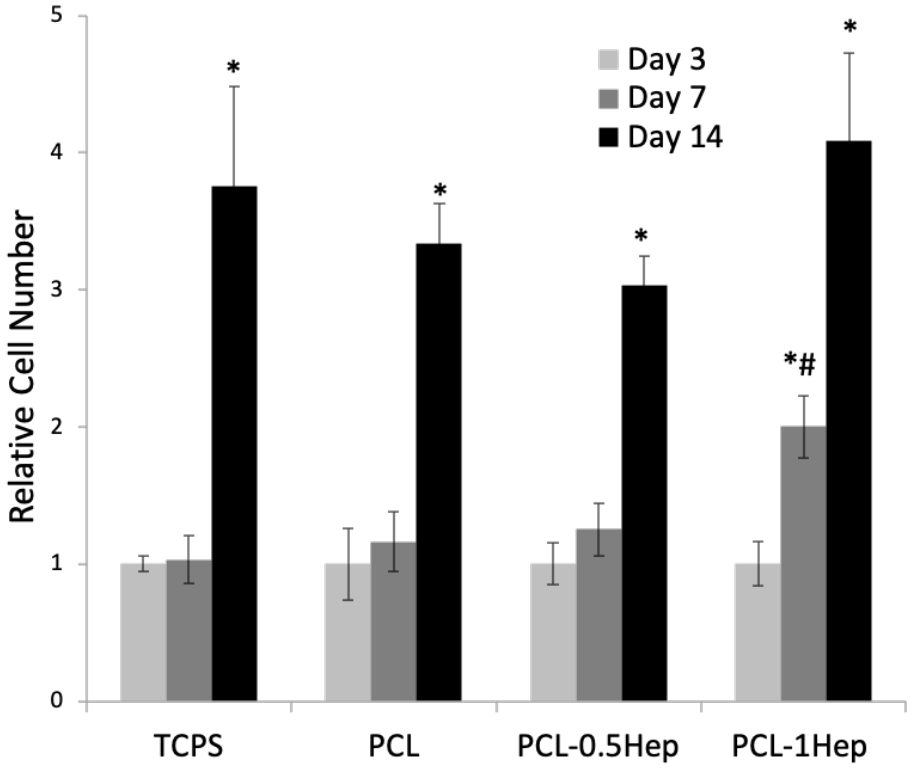

Figure 3.5: Relative cell number for MSCs seeded on PCL, PCL-0.5Hep and PCL-1Hep electrospun fibers at days 3, 7 and 14. Cell numbers on each surface were normalized by day 3 values. Cells on tissue culture polystyrene (TCPS) are included as a control group. Bars correspond to mean ± SEM for $n = 4$. #Indicates statistical significance ($p < 0.05$) relative to other groups at the same time point. *Denotes statistical significance ($p < 0.05$) relative to same group at previous time point.

Alkaline phosphatase activity, a marker of osteogenic potential of MSCs, was measured at days 7 and 14. As shown in Figure 3.6, ALP activity at day 7 was significantly higher with covalently conjugated BMP-2 than without BMP-2 or with adsorbed BMP-2. In addition, ALP activity increased from day 7 to 14 on fibers with covalently conjugated BMP-2, but remained similar at day 7 and 14 on fibers without BMP-2 or with adsorbed BMP-2.

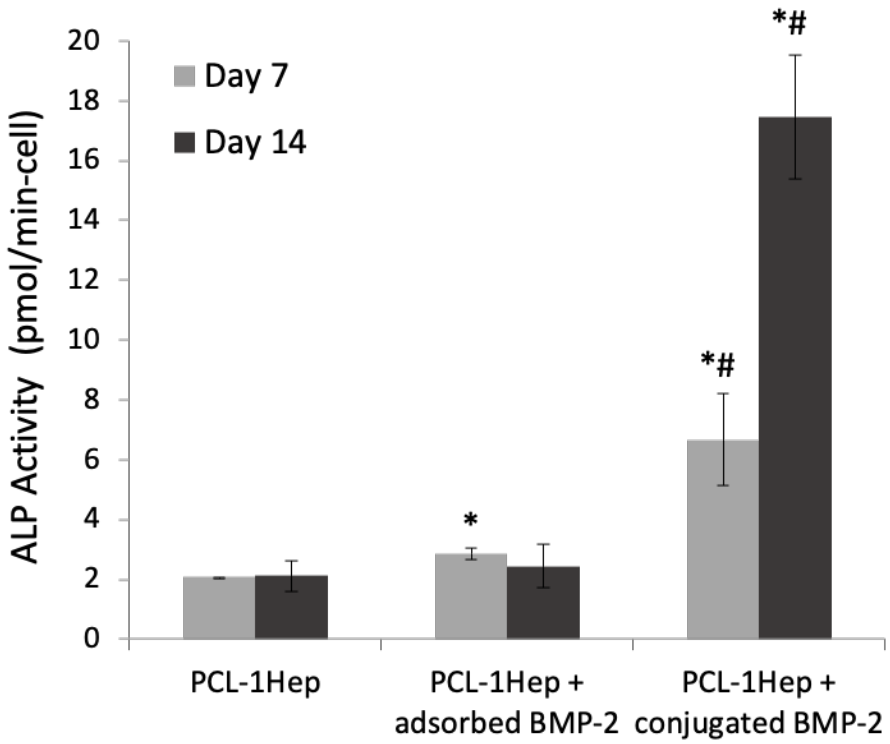

Figure 3.6: Alkaline phosphatase activity of MSCs on PCL-1Hep fibers and PCL-1Hep fibers with adsorbed and covalently conjugated BMP-2 at days 7 and 14. Bars correspond to mean ± SEM for $n = 3$. *Denotes statistical significance ($p < 0.05$) relative to PCL-1Hep. #Indicates statistical significance ($p < 0.05$) relative to other groups at the same time point.

To examine late osteogenic differentiation, the deposition of calcium minerals and BSP and OPN proteins by MSCs on PCL-1Hep fiber meshes was examined at day 28. As shown in Figures 3.7a-c, more calcium deposits are evident by Alizarin red staining on fibers covalently conjugated with BMP-2 than on fibers without BMP-2 or with adsorbed BMP-2. Furthermore, for covalently conjugated fibers, large mineral deposits that encompass cell colonies are evident (Figure 3.7c). Differences in Alizarin red staining between groups were verified by extraction of

the dye. Absorbances plotted relative to fiber surfaces without BMP-2 indicate 1.9 and 4.1 times higher mineralization deposition for fiber meshes with adsorbed BMP-2 and covalently conjugated BMP-2, respectively (Figure 3.7d). Immunofluorescent staining for BSP (Figure 3.8a-c) and OPN (Figure 3.8d-f) confirmed this trend with little staining in the absence of BMP-2, light staining for MSCs cultured on surfaces with adsorbed BMP-2, and more punctate staining for MSCs cultured on surfaces with covalently conjugated BMP-2.

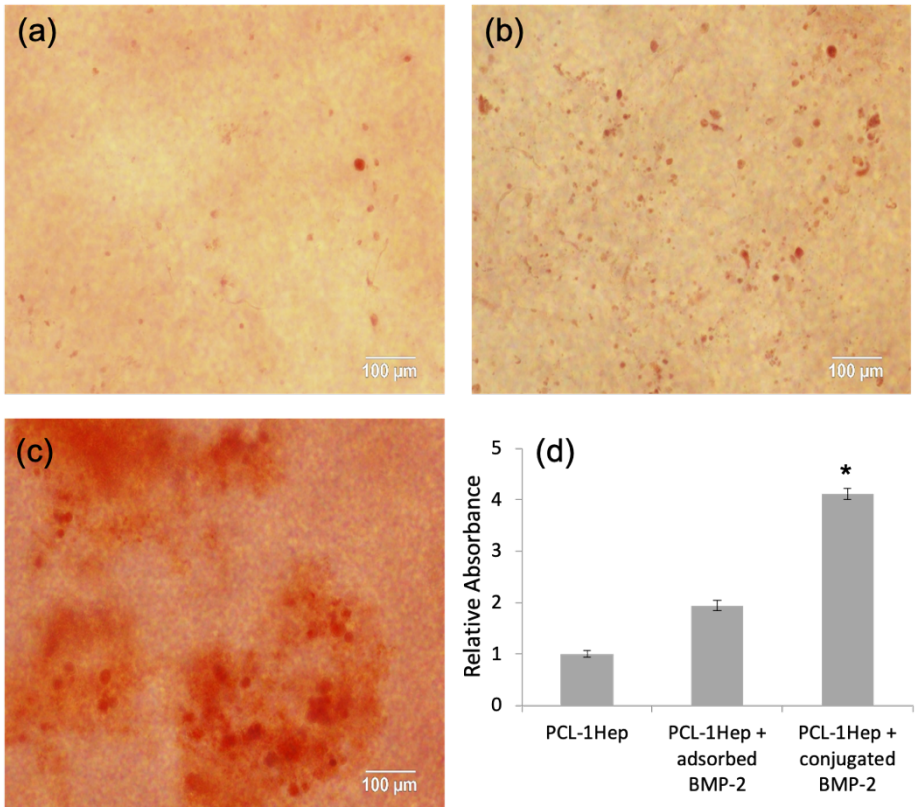

Figure 3.7: Alizarin red staining of MSCs mineral deposits on (a) PCL-1Hep fibers and PCL-1Hep fibers with (b) adsorbed and (c) covalently conjugated BMP-2 and (d) colorimetric quantification of mineralization, with absorbance values relative to PCL-1Hep, at day 28. Bars correspond to mean ± SEM for $n = 4$. *Denotes statistical significance ($p < 0.05$) relative to other groups.

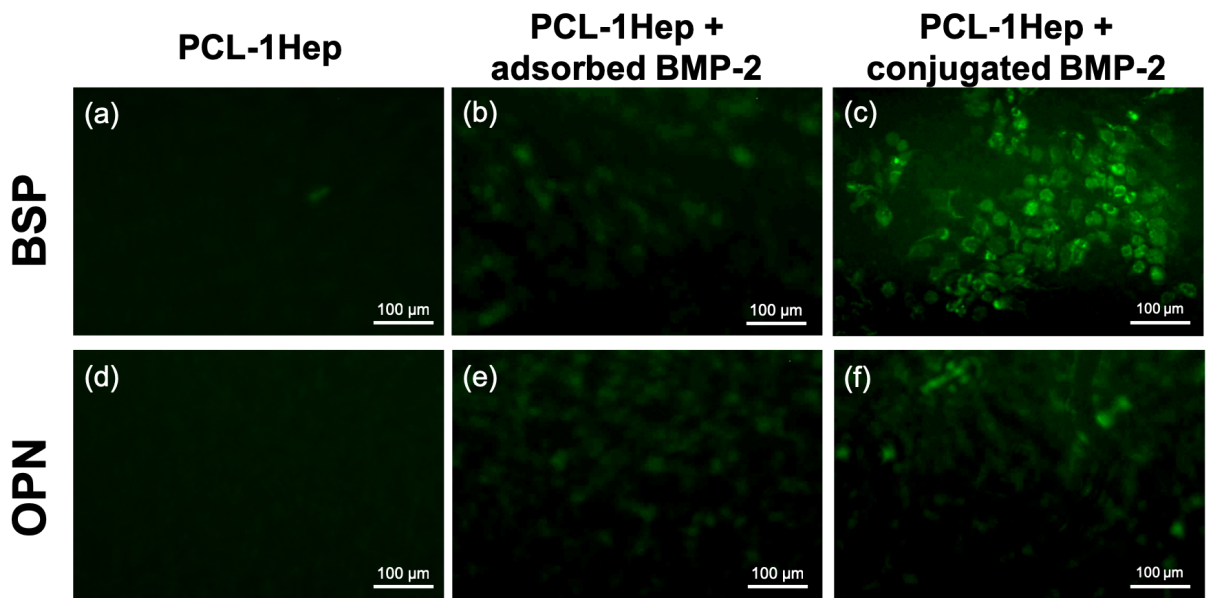

Figure 3.8: Immunofluorescence staining for (a-c) BSP on (a) PCL-1Hep fibers, PCL-1Hep fibers with (b) adsorbed and (c) covalently conjugated BMP-2, as well as for (d-f) OPN on (d) PCL-1Hep fibers, PCL-1Hep fibers with (e) adsorbed and (f) covalently conjugated BMP-2, at day 28. Scale bars correspond to 100 µm.

3.5 Discussion

Successful ACL reconstruction and regeneration requires robust integration of the graft with proximal and distal bones. In the context of synthetic grafts, this entails the modification of graft surfaces to facilitate host tissue infiltration and osteoblastic differentiation. To this end, BMP-2 was either adsorbed or covalently conjugated to electrospun meshes of PCL or PCL with 0.5 or 1 wt% heparin. Here, the addition of heparin was intended to increase surface hydrophilicity and BMP-2 binding. Overall, the goal was to determine if covalent conjugation produced fiber surfaces that were more osteogenic than surfaces produced by BMP-2 adsorption. The findings were that BMP-2 concentration increased with heparin content and that covalent conjugation yielded higher

surface concentrations than adsorption. Further, there was no apparent loss of BMP-2 from the surfaces over 7 days. Finally, MSCs were able to attach and proliferate on all electrospun fiber surfaces, but surfaces to which BMP-2 was covalently conjugated showed the highest levels of ALP activity, mineral deposition, and staining for BSP and OPN.

In this study, heparin was added to PCL scaffolds to increase their hydrophilicity and introduce sulfate and carboxylate groups to anchor BMP-2. Hydrophilic groups have been shown to improve fibronectin adsorption, cell adhesion, and osteoblastic differentiation on model synthetic substrates [159]. However, heparin was specifically incorporated into PCL surfaces to facilitate both adsorption and covalent conjugation of BMP-2. Like other members of the TGF-β superfamily, BMP-2 has a cationic heparin binding domain that interacts with the sulfate groups on heparin. Thus, the systematic increase in protein adsorption with heparin content observed in Figure 3.3a suggests heparin-mediated protein binding, consistent with the work of Cao *et al.* [160]. In addition, heparin contains carboxylic acid groups that can be activated with EDC, enabling a second mechanism for BMP-2 immobilization and explaining the higher BMP-2 concentrations achieved with covalent conjugation to PCL-0.5Hep and PCL-1Hep films. Interestingly, a higher BMP-2 concentration was also observed with covalent conjugation to PCL surfaces, suggesting that terminal carboxylic acid groups of PCL are also available for conjugation. Finally, it should be noted that the sulfate groups on heparin can also interact with heparin binding domains found within various growth factors found in serum (e.g., FGF-2, VEGF, PDGF), and that this adsorption of mitogenic serum proteins may explain the higher cell density observed at day 7 on the PCL-1Hep fibers (Figure 3.5).

SEM images confirmed that incorporation of heparin in the PCL polymer solution did not adversely affect electrospun fiber formation. Indeed, the primary observation was that

incorporation of heparin reduced the average fiber diameter. This can be attributed to the highly charged polysaccharide structure, which increases the conductivity of the polymer solution and causes a thinner fiber filament to leave the syringe needle tip during electrospinning. Indeed, this effect has been reported with the addition of proteins, salts and drugs into electrospinning polymer solutions [161-163]. Two consequences of smaller fiber diameters are more surface area per unit mass and a decrease in the mechanical properties of the fiber scaffold. While the former would enable higher quantities of BMP-2 to be immobilized to a three-dimensional scaffold, the latter might undermine osteoblastic differentiation, as differentiation has been shown to increase with substratum stiffness [164, 165]. However, mechanical testing indicated similar tensile properties for the three meshes. Further, fibers were intentionally deposited as thin layers on glass coverslips in this study so that adherent cells would perceive the mechanical properties of the underlying glass substrate and not behave in a manner sensitive to fiber stiffness.

Inclusion of osteogenic BMP-2-delivering materials have been shown to improve graft-to-bone integration in ACL reconstructions. Rodeo *et al*. reported that BMP-2 collagen I sponges direct tendon-to-bone healing and enhances new bone formation in the proximal tibia bone tunnels of adult mongrel dogs [151]. Similarly, Kawakami *et al*. reported that the incorporation of BMP-2 expressing ACL-derived stem cell sheets to ACL graft ends accelerated graft-bone integration in ACL reconstructions in rat [15]. *In vivo*, new bone formation has been attributed to the MSCs residing in the host that are recruited to bone tunnels to initiate tissue remodeling [166]. Therefore, in this study MSCs were employed to characterize the bone-forming potential of electrospun fibers displaying immobilized BMP-2. In this study, MSCs exhibited attachment, viability, and proliferation on all electrospun substrates. However, higher ALP activity at day 14 (Figure 3.6) and more extensive calcium deposits (Figure 3.7) and staining for BSP and OPN at day 28 (Figure

3.8) indicate that substrates covalently conjugated with BMP-2 are more osteogenic.

The different osteogenicities of PCL-1Hep fibers with adsorbed vs. covalently conjugated BMP-2 could result from different surface concentrations, different conformations of the immobilized protein, or even different rates of protein desorption or degradation. Examination of concentrations (Figure 3.3) indicated that the more osteogenic substrates had more immobilized BMP-2. Further, surface concentrations did not appear to decrease following 7 days of incubation in PBS. This differs from previous studies that have reported 20% and 84% losses of conjugated and adsorbed BMP-2, respectively, from chitosan over 3 weeks in PBS [167], and 16% and 70% losses of conjugated and adsorbed BMP-2, respectively, from silk fibroin over 1 week in cell culture [168]. (Interestingly, the more rapid loss in cell culture suggests that degradation and internalization mechanisms may also contribute to BMP-2 loss during cell culture.) Instead, in this study the concentrations of covalently conjugated BMP-2 appeared to increase over 7 days in PBS (Figure 3.3), and this may reflect changes in protein conformation to expose more epitopes for binding of the polyclonal antibody probe.

This study demonstrates that the incorporation of heparin into electrospun fibers improves BMP-2 surface conjugation and osteoblastic differentiation on model surfaces. The next step is to fabricate larger three-dimensional scaffolds suitable for ligament regeneration with macropores to permit cell infiltration. This will clearly introduce a number of challenges, including the integration of other scaffold fabrication techniques (e.g., foaming, three-dimension printing) to achieve macropores and suitable mechanical properties, and introduction of multiple trophic factors throughout the scaffold volume to stimulate host cell infiltration and tissue remodeling.

3.6 Conclusions

Electrospun PCL fibers were modified by the addition of heparin and by surface immobilization of BMP-2 (by adsorption and covalent conjugation) to improve osteogenicity. Heparin improved BMP-2 immobilization, higher BMP-2 concentrations were achieved by covalent conjugation than by adsorption, and desorption of BMP-2 from surfaces was not detected after 7 days in PBS. Cells attached and proliferated on all fiber meshes, but on those displaying covalently conjugated BMP-2 MSCs exhibited significantly more ALP activity, calcium (mineral) deposition, and production of osteoblast-specific ECM proteins.

Chapter 4: The Effect of Incorporation Strategy of BMP-2 with Chitosan Nanoparticles on Protein Release and Bioactivity

Dina Gadalla[1], Aaron S. Goldstein[1,2]

[1]Department of Chemical Engineering,
[2]School of Biomedical Engineering and Sciences
Virginia Tech, Blacksburg, VA 24061, USA

4.1 Abstract

The method used to incorporate signaling molecules into tissue engineered scaffolds plays a critical role in its biological activity. In particular, the use of nanoparticles to incorporate, present, and release bone morphogenetic protein (BMP)-2 may improve its biological efficacy in stimulating osteoblastic differentiation of stem cells *in vitro* and bone formation *in vivo*. Therefore, this study was designed to evaluate chitosan nanoparticles that incorporate BMP-2 through adsorption, encapsulation, or conjugation strategies. Chitosan nanoparticles were prepared by ionic gelation and characterized for particle size and BMP-2 incorporation efficiency for each incorporation approach. Further, BMP-2 release kinetics and bioactivity were evaluated. It was observed that the different incorporation approaches resulted in incorporation efficiencies ranging from 91.8% to 98.8%, and that mean particle sizes were 452 ± 2 nm, 620 ± 13 nm, and 4972 ± 2738 nm for adsorption, encapsulation, and conjugation, respectively. BMP-2 release from BMP-2 adsorption nanoparticles was sustained over a 28-day time period, while negligible release and a burst release followed by minimal release were observed for BMP-2 encapsulation and BMP-2 conjugation particles, respectively. Viability of mesenchymal stem cells (MSCs) was not adversely affected by the particles, but alkaline phosphatase activity (a marker of osteoblastic differentiation)

was highest for cells cultured with BMP-2 adsorption particles. These studies demonstrate that, although fabricated with similar ingredients, incorporation strategies can have a substantial effect on particle characteristics as well as subsequent cell response. BMP-2 adsorption nanoparticles developed in this work can be incorporated to the end regions of a biomaterial scaffold to facilitate graft integration with native bone tunnels.

4.2 Introduction

Anterior cruciate ligament (ACL) ruptures are widely known to be common knee injuries that particularly occur during high impact sports [169, 170]. Due to the poor healing capacity of native ACL, surgical reconstructions are essential and involve inserting a chosen substitute graft between the patient's tibia and femur by securing it to the bone tunnels. Frequently utilized grafts include widely accepted hamstring and quadriceps tendon autografts which are directly anchored to the bone [171-173]. In addition to the associated donor site morbidity issues that a patient goes through with such treatments, the property mismatch between the soft autograft tissue and the hard bone tissue results in early graft pullout [174, 175]. We postulate that engineered materials capable of inducing bone regeneration can be used to enhance integration of an implanted graft within the bone tunnels.

Bone morphogenetic protein (BMP)-2 is a member of the transforming growth factor (TGF)-β family and is well-known for its bone-inducing activity [176]. It is FDA-approved for spinal fusion procedures, and has shown promise in a variety orthopaedic applications including the integration of tendon and ligament grafts to bone [15, 177]. Nonetheless, BMP-2 has a short half-life *in vivo* and consequently must be administered at much higher dosages than physiological concentration (milligrams vs nanograms) to induce therapeutic effects [16, 147]. The use of such

high dosages results in complications such as ectopic bone formation and inflammation. Based on many previous studies [16, 122, 130, 178, 179], a low dose of BMP-2, particularly when locally retained and released sustainably, is enough to induce osteogenic differentiation both *in vitro* and *in vivo*. The strategy used to deliver BMP-2 is important and affects its clinical outcome [180]. For instance, the direct display of BMP-2 on scaffold surfaces may undermine its bioactivity by exposing it to degradative enzymes as well as denaturing agents [181]. As a result, the use of nanoparticles has attracted attention in the field of tissue engineering as a way to control protein release and improve its biological efficacy [182, 183].

The nature of the nanoparticle carrier is vital as the material properties can influence the formation of tissue. In this study, chitosan nanoparticles were chosen because they have many advantages including their simple synthesis methods, non-toxicity, and stability [184]. Chitosan is a cationic glycosaminoglycan derived from chitin through deacetylation and is sparingly soluble at neutral pH. Chitosan nanoparticles prepared by ionic gelation exhibit strong electrostatic interactions with polyanionic crosslinkers and avoid the negative side effects of residual solvents associated with oil-in-water emulsion techniques [185]. Among polyanions for ionic crosslinking of chitosan, tripolyphosphate (TPP) was chosen as it is non-toxic and can quickly gel chitosan. Chitosan particles crosslinked with TPP have been shown to be homogenous in size, and their sizes can be easily altered with diameters ranging from 200-2500 nm by changing process conditions [185, 186]. Chitosan nanoparticles also present functional amine groups for ionic interactions and permit bioconjugation of BMP-2. However, chitosan does not have any specific binding sites for BMP-2 and other proteins.

An ideal BMP-2 delivery system would be one that stores or presents BMP-2 in an active conformation as well as release it in a sustained and controllable manner [61, 187]. Hence, it is

vital to find an appropriate approach to incorporate BMP-2 on or within chitosan nanoparticles for the fabrication of a BMP-2 delivery system that can be combined with a macroscopic biomaterial scaffold to stimulate bone formation. We envision that such a combination of a BMP-2 delivery system and an appropriate biomaterial scaffold could be used to enhance ACL graft integration with bone.

The overall goal of this study was to fabricate 500-1000 nm chitosan nanoparticles to serve as delivery vehicles for BMP-2, and to evaluate three approaches to incorporate BMP-2: adsorption, encapsulation, and conjugation. BMP-2 encapsulation particles were prepared by combining BMP-2 and chitosan prior to ionic gelation, while BMP-2 adsorption particles were achieved by incubating nanoparticles with BMP-2. BMP-2 conjugation particles were achieved using the heterobifunctional crosslinker sulfo-SMCC. BMP-2 incorporation efficiency and its release rate from the different particles was measured. Finally, cell number and alkaline phosphatase (ALP) activity of bone marrow derived mesenchymal stem cells (MSCs) cultured in the presence of the nanoparticles was determined.

4.3 Materials and Methods

4.3.1 Materials

Chitosan of medium molecular weight (190-310 kDa) and 75-85% degree of deacetylation was obtained from Sigma-Aldrich (Saint Louis, MO). Sodium tripolyphosphate (TPP), sodium salt of ethylenediamine tetraacetic acid (EDTA), trypsin/EDTA, Triton-X100 and Tween-20 were also purchased from Sigma-Aldrich. Bovine serum albumin (BSA), Tris Base, magnesium chloride, sodium chloride (NaCl) and acetic acid were purchased from Fisher Scientific (Suwanee, GA). Phosphate buffered saline (PBS) was obtained from Corning cellgro (Manassas, VA), and

recombinant human bone morphogenic protein (BMP)-2 from Invitrogen (Carlsbad, CA). Sulfosuccinimidyl 4-(N-maleimidomethyl)cyclohexne-1-carboxylate heterobifunctional crosslinker (sulfo-SMCC) and ABTS (2,2'-Azinobis [3-ethylbenzothiazoline-6-sulfonic acid] - diammonium salt) were obtained from Thermo Scientific (Grand Island, NY).

4.3.2 Chitosan Particle Synthesis

Chitosan was dissolved in 1% acetic acid to make up a 1.5 mg/mL chitosan solution and left overnight under magnetic stirring to dissolve completely. TPP solutions of 1.25, 2.5, 5.0 and 10 mg/mL were prepared in deionized (DI) water. Chitosan and TPP solutions were sterilized by filtration through a 0.2 μm surfactant-free cellulose acetate syringe filter (Thermo Scientific). Chitosan-TPP nanoparticles were synthesized by ionic gelation of the cationic chitosan solution with the polyanionic TPP as adapted from Calvo *et al.* [188]. For each batch, 400 μL TPP was added dropwise with a syringe needle to a magnetically stirring 1 mL chitosan solution to produce a solution of 1.1 mg/mL chitosan and 0.36, 0.72, 1.4 or 2.8 mg/mL TPP. Magnetic stirring was continued for 10 min to permit particle formation. Subsequently, solutions were transferred to microcentrifuge tubes and centrifuged at 13,000 rpm for 5 min. The supernatant was then discarded and the particles dispersed in PBS by ultrasonicating for 10 min in a VWR Scientific Aquasonic (model 75T) bath sonicator.

4.3.3 BSA and BMP-2 Encapsulation Particles

Particles encapsulating BSA or BMP-2 were prepared by combining BSA or BSA/BMP-2 mixtures to the chitosan solution prior to the addition of TPP. BSA encapsulation particles were prepared by adding 0, 0.28, 2.8, 28, or 280 μg BSA to 1 mL of 1.5 mg/mL chitosan solutions.

Addition of 400 µL of 0.5 mg/mL TPP resulted in final BSA concentrations of 0, 0.2, 2, 20, or 200 µg/mL. BMP-2 encapsulation particles were prepared by the addition of 28 µg BSA and 280 ng BMP-2 to 1 mL of 1.5 mg/mL chitosan solutions followed by the dropwise addition of 400 µL of 5 mg/mL TPP to yield final BSA and BMP-2 concentrations of 20 µg/mL and 0.2 µg/mL, respectively. Following centrifugation, the supernatant was retained to evaluate BSA and BMP-2 encapsulation efficiency, and the particles resuspended in 1 mL PBS.

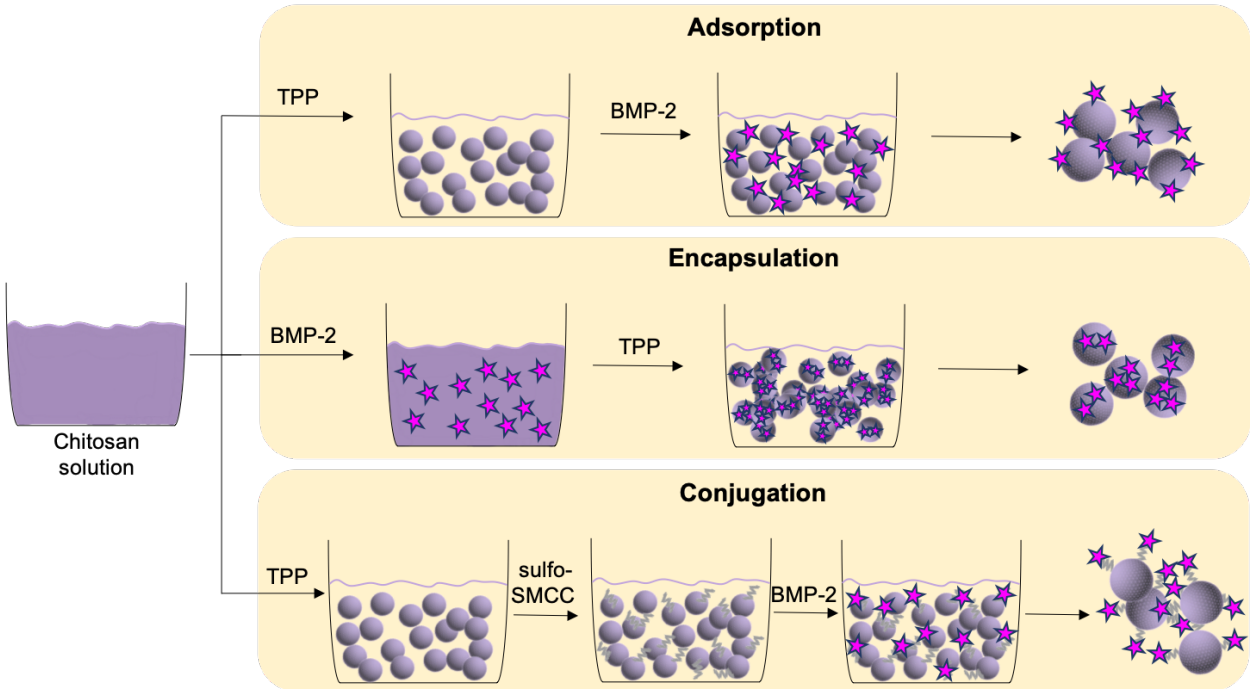

Figure 4.1: Schematic illustration of the fabrication of BMP-2 adsorption, BMP-2 encapsulation, and BMP-2 conjugation chitosan nanoparticles using TPP as the crosslinker.

4.3.4 BMP-2 Adsorption and BMP-2 Conjugation Particles

BMP-2 adsorbed particles were prepared from base particles (1 mL of 1.5 mg/mL chitosan with 0.4 mL of 5 mg/ml TPP as described above). After dispersion in PBS, base particles were incubated with 280 ng BMP-2 in PBS solution for 3 hours at room temperature. BMP-2 adsorption particles were then centrifuged, the supernatant retained for evaluation of BMP-2 incorporation efficiency, and the particles resuspended in 1 mL PBS.

BMP-2 conjugation particles were prepared from the same base particles, but following centrifugation, they were suspended in activation buffer (0.1 M PBS and 0.15 NaCl) by ultrasonication for 30 min. Particles were then centrifuged, resuspended in 4 mg/mL sulfo-SMCC in DI, incubated for 1 h at room temperature. Particles were then centrifuged, resuspended in conjugation buffer (activation buffer with 0.1 M EDTA to reduce disulfide formation), centrifuged again, and resuspended then incubated overnight at 4 °C with the protein mixture: 28 μg BSA and 280 ng BMP-2 in 1.4 mL conjugation buffer. Following incubation, particles were centrifuged and their supernatants were retained to evaluate BSA and BMP-2 encapsulation efficiency. Particles were then resuspended in 1 mL PBS.

4.3.5 BSA-FITC Particles

BSA-FITC particles were used as an alternative method for measuring protein incorporation efficiency and release rate. BSA-FITC particles were prepared in the same manner as BMP-2 encapsulation, BMP-2 adsorption, and BMP-2 conjugation particles except that BMP-2 was replaced with BSA-FITC. The mass of BSA in BSA-FITC was the same as that of BMP-2 (280 ng).

4.3.6 Control Particles

Control particles were prepared in the same ways as BMP-2 adsorption, BMP-2 encapsulation, and BMP-2 conjugation particles except that BMP-2 was omitted. These control particles were used to determine the effect of incorporation strategy on particle size, to determine background noise in measurements of BMP-2 incorporation efficiency and release, and as control groups in cell culture studies.

4.3.7 Particle Diameter Evaluation

Particle sizes and polydispersity index (PDI) of freshly prepared nanoparticles were measured using dynamic light scattering (DLS) technique with a Zetasizer Nano-ZS from Malvern instruments (Malvern Instruments, UK). Briefly, 1 mL suspended particles were transferred into plastic sizing cuvettes for measurement at room temperature. Data meeting DLS quality criteria was evaluated using Malvern Zetasizer software version 7.12. Results are reported as mean ± standard deviation.

4.3.8 BMP-2 Incorporation Efficiency

Following the encapsulation of BMP-2 into particles or adsorption/immobilization of BMP-2 to particle surfaces, particles were centrifuged and the BMP-2 concentration of the supernatant, C_{BMP2}, was measured with a Quantikine Enzyme-Linked Immmunosorbent Assay (ELISA) (PeproTech, Rocky Hill, NJ). Briefly, wells of a 96 well ELISA Nunc^{TM} MaxiSorp (Thermo Scientific) plate were incubated with 0.50 μg/mL of rabbit anti-human BMP-2 capture antibody (PeproTech) overnight at room temperature. Wells were then washed three times with 0.05% Tween-20 before blocking with 1% BSA in PBS for 1 h. Wells were again washed thrice

with Tween-20. One hundred μL of sample was then added to each well in duplicates for 2 h, washed thrice with Tween-20, followed by the addition of 1.0 μg/mL biotinylated rabbit anti-human BMP-2 detection antibody for 2 h. Wells were washed thrice with Tween-20, 550 ng/mL streptavidin horseradish peroxidase-conjugate (GE Healthcare, Little Chalfont, UK) was added for 30 min, washed thrice, and 100 μL of ABTS development solution was added to each well and incubated for 5 min. All incubations were carried out at room temperature. Absorbance values were measured with a SpectraMax M2 plate reader (Molecular Devices, Sunnyvale, CA) at 405 nm with wavelength correction at 650 nm and converted to BMP-2 concentration using a series of BMP-2 standards.

Using the measured BMP-2 concentrations, the volume of supernatant, V_{sup}, and the initial mass of BMP-2, m_{BMP2} (typically 280 ng), the percentage of BMP-2 incorporated was estimated by the following the equation:

$$\%BMP2_{incorporation} = \frac{m_{BMP2} - C_{BMP2}V_{sup}}{m_{BMP2}} \times 100\%$$

4.3.9 BSA-FITC Incorporation Efficiencies

Similar to BMP-2 incorporation efficiencies, BSA-FITC incorporation efficiencies were determined indirectly from the concentrations of supernatants of centrifuged BSA-FITC encapsulated, BSA-FITC adsorbed, and BSA-FITC conjugated particles. To determine BSA-FITC concentrations, fluorescence of supernatants were first measured with a SpectraMax M2 plate reader at 494 nm excitation and 520 nm emission. Using a series of prepared standards, fluorescence values were converted to BSA-FITC concentrations. Incorporated BSA-FITC was estimated by the same above equation after substituting the 'BMP-2' subscript with 'BSA-FITC'.

$$\%BSA - FITC_{incorporation} = \frac{m_{BSA-FITC} - C_{BSA-FITC}V_{sup}}{m_{BSA-FITC}} \times 100\%$$

4.3.10 BMP-2 Release

BMP-2 release from particles was determined by incubating ~ 3 mg of particles in 1 mL PBS at 37 °C. At days 1, 3, 7, 14, 21, and 28, a volume of 0.5 mL of solution was collected and replaced with 0.5 mL PBS. The concentrations of BMP-2 in samples were determined by ELISA as described above and the cumulative mass release and cumulative percent mass released were calculated. Particles prepared without BMP-2 were used as the negative control.

4.3.11 BSA-FITC Release

BSA-FITC release from particles was determined by incubating ~ 3 mg of particles in 0.5 mL PBS at 37 °C. At days 1, 3, 7, 17, 21, and 28, the entire supernatant was collected, replaced with PBS, and the concentrations of BSA-FITC determined by fluorescence as described above. The cumulative mass release and cumulative percent mass released were calculated. Particles prepared without BSA-FITC were used as the negative control.

4.3.12 Cell Studies

Mesenchymal stem cells (MSCs) were extracted from bone marrow explants from the femurs and tibias of juvenile male Sprague-Dawley rats weighing 125-150 g (Harlan, Dublin, VA) in accordance with the Institutional Animal Care and Use Committee at Virginia Tech. Extracts were thoroughly dispersed before plating on two 100 mm tissue culture polystyrene (TCPS) dishes per rat. Cells were cultured in growth medium consisting of alpha-modified Eagle medium (α-MEM, Invitrogen, Carlsbad, CA) supplemented with 10% fetal bovine serum (Gemini

Biosciences, West Sacramento, CA) and 1% penicillin/streptomycin (Invitrogen) for 10 days at 37 °C and 5% CO_2. Cells were re-plated at 10^5 cells/ 100 mm Petri dish after lifting every 4 days using trypsin/EDTA. Cells used in this study were at passage 5.

BMP-2 adsorption particles, BMP-2 encapsulation particles, BMP-2 conjugation particles and each of their control particles used for cell studies were prepared using filter-sterilized solutions. After nanoparticle preparation, each individual sample of particles (3 mg) was added in 200 μL growth media to one well of a 24 well plate for 30 min. Fifty thousand cells were then seeded on the particles in each well. Cells were cultured in 500 μL growth media and the media was replenished with an additional 250 μL every three days. Cells on TCPS and cells on TCPS with 80 ng BMP-2 added in media per well were included as control groups.

4.3.13 Cell Number

Cell numbers were determined 21 days after cell seeding using the Quanti-iT PicoGreen kit (Invitrogen, Grand Island, NY). Cells were washed twice with PBS and then lysed for 1 h in 400 μL 0.2% Triton-X100, 8 mM $MgCl_2$, 50 mM Tris Base and 150 mM NaCl in deionized (DI) water. Fifty μL samples of lysate were removed for alkaline phosphatase analysis. Three freeze-thaw cycles were carried out on remaining lysate and samples were thoroughly mixed. One hundred μL of lysate was then combined with 100 μL Quanti-iT PicoGreen dsDNA working reagent and the fluorescence of the mixture measured at 480 nm excitation and 520 nm emission with a SpectraMax M2 plate reader.

4.3.14 ALP Activity

ALP activity was measured at 21 days using a QuantiChrom ALP assay kit (BioAssay Systems) following the manufacturer's instructions. Briefly, lysed cells (prepared as described in the previous section) were assayed prior to undergoing the freeze-thaw cycles. One hundred and fifty μL *p*-nitrophenyl phosphate working solution was then mixed with 50 μL samples and the absorbance measured at a 405 nm with a SpectraMax M2 plate reader. Calculations provided with the kit were used to quantify ALP activity, which was then normalized by cell number (as determined by PicoGreen). Data is reported relative to ALP activity of cells cultured on TCPS without nanoparticles.

4.3.15 Statistical Analysis

Experimental values are presented as mean ± standard deviation or ± standard error of the mean (SEM), as indicated. Comparisons between the different groups were performed with one-way ANOVA using StatPlus (AnalystSoft, Walnut, CA) statistics package. $p \leq 0.05$ indicated statistical significance.

4.4 Results

4.4.1 Development and Characterization of Nanoparticles

Chitosan nanoparticles formed instantaneously upon the addition of anionic TPP to cationic chitosan. Resulting particle sizes made using 1.25, 2.5, 5.0 and 10 mg/mL TPP concentrations and a fixed 1.5 mg/mL chitosan concentration were characterized in terms of particle size and PDI using DLS (Figure 4.2). Particle size increased with increasing TPP concentration with the smallest and largest particle sizes at 117 ± 3 and 2978 ± 216 nm for TPP concentrations of 1.25 and 10

mg/mL, respectively. Although the dispersion of particles resulted in relatively clear solutions, particle solutions became turbid as TPP concentration was increased, indicating the formation of larger particles and the possible aggregation of particles. Overall, polydispersity indices did not follow a trend and were less than 0.5 at all TPP concentrations. Nanoparticles prepared with 5.0 mg/mL TPP were chosen for subsequent studies as will later be discussed.

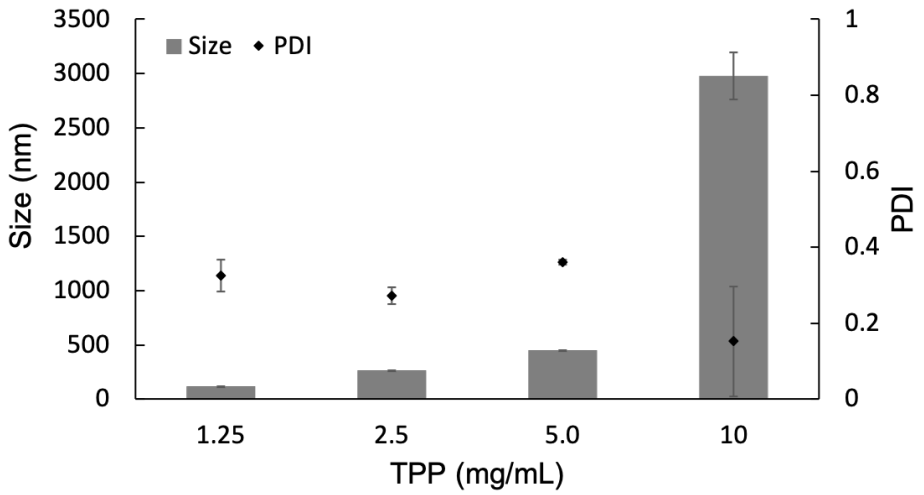

Figure 4.2: The effect of using 1.25, 2.5, 5.0 and 10 mg/mL TPP concentration on chitosan nanoparticles size (nm) and PDI as measured by DLS. Data is presented in mean ± standard deviation (n = 3).

In the next step, BSA was incorporated into nanoparticles through encapsulation. To this end, a range of BSA concentrations were combined with 1.5 mg/mL chitosan and then crosslinked by the addition of 5.0 mg/mL TPP. Figure 4.3 shows particle size and PDI as function of BSA concentration. Interestingly, particle sizes ranged from 390 nm to 620 nm and did not change significantly for BSA concentrations of 0-20 μg/mL, but exhibited a large increase with 200 μg/mL

BSA. The 20 μg/mL BSA concentration was chosen for subsequent BMP-2 incorporation for reasons later discussed.

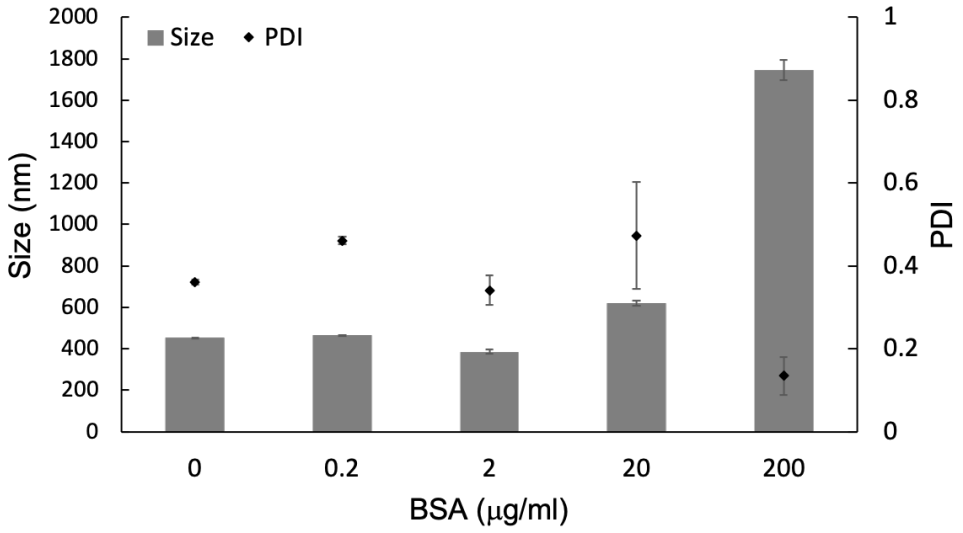

Figure 4.3: The effect of encapsulating 0, 0.2, 2, 20 and 200 μg/mL BSA on chitosan nanoparticles size (nm) and PDI as measured by DLS. Data is given in mean ± standard deviation (n = 3).

4.4.2 BMP-2 Incorporation Efficiency and Release Kinetics

Following particle characterizations, BMP-2 was incorporated with the particles using the same three approaches (Figure 4.1) to evaluate BMP-2 incorporation efficiencies and release rates. Percent of BMP-2 incorporated was determined using ELISA and BSA-FITC fluorescence methods. Indirect measurement of BMP-2 incorporation efficiencies (by assaying for unincorporated BMP-2 that remained in supernatant) indicated 96.9%, 98.8% and 91.8% incorporation by adsorption, encapsulation, and conjugation methods, respectively (Figure 4.4a). Separately, direct measurement of the incorporation of BSA-FITC into nanoparticles indicated

78.3%, 88.3% and 62.5% for adsorption, encapsulation, and conjugation methods, respectively (Figure 4.4b).

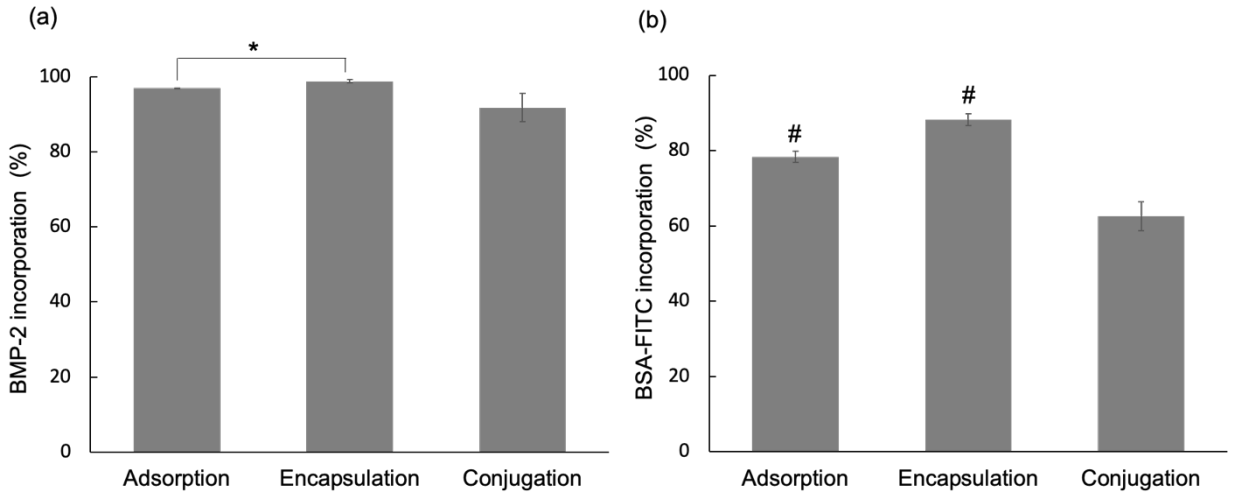

Figure 4.4: The influence of incorporation strategy on (a) BMP-2 incorporation efficiency as measured by ELISA and (b) BSA-FITC incorporation efficiency as measured with fluorescence. Data are given in mean ± SEM (n = 3). *Denotes statistical significance ($p < 0.05$) between groups. #Indicates statistical significance ($p < 0.05$) relative to other groups.

Next, the release of BMP-2 from nanoparticles into PBS was measured over a 28 day period. The concentrations of BMP-2 measured in the supernatants indicated a burst release of 28% of the protein during the first day from BMP-2 adsorption particles, followed by a more gradual and sustained release pattern over the remaining 27 days to a cumulative extent of 81% (Figure 4.5a). In contrast, BMP-2 conjugated particles exhibited a burst release of 15% of BMP-2 in the first day, followed by another 10% over the next two days, and a negligible release thereafter.

Finally, BMP-2 encapsulation particles exhibited negligible BMP-2 release with only an 8% cumulative release over 28 days.

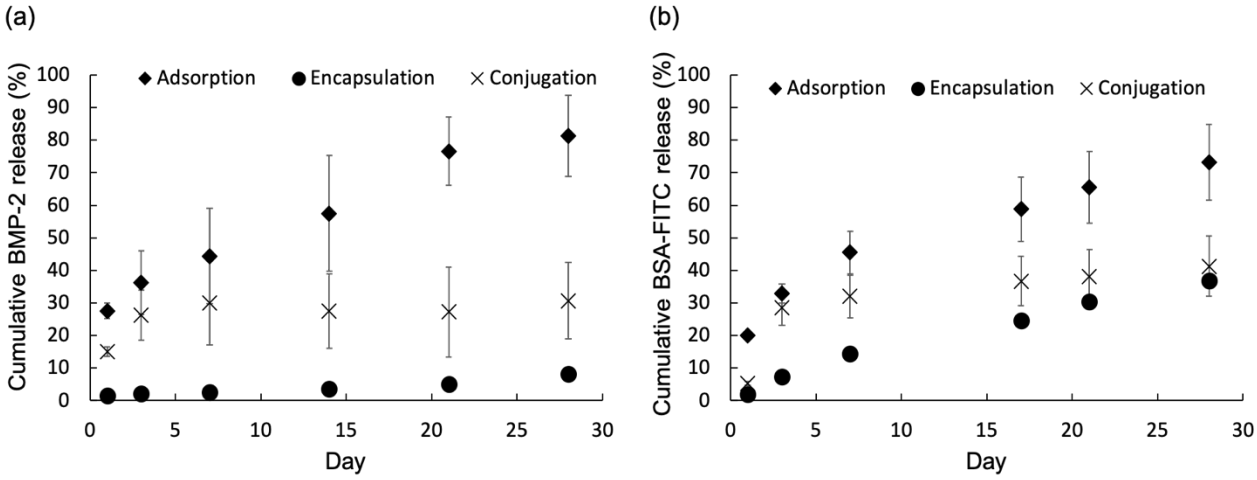

Figure 4.5: Cumulative release of (a) BMP-2 (measured by ELISA) and (b) BSA-FITC (measured by fluorescence) from particles prepared with adsorption, encapsulation and conjugation techniques over a 28-day time period. Data is given in mean ± SEM (n = 3).

Release profiles were determined using BSA-FITC fluorescence to further confirm the release trends associated with each incorporation strategy. BSA-FITC fluorescence showed very similar trends to those measured by ELISA (Figure 4.5). However, the release percentages were different for adsorption and encapsulation particles. The burst release for BSA-FITC adsorption particles was 20% (versus 28%) and the cumulative at day 28 was 73% (versus 81%). Although similar in release pattern, BSA-FITC encapsulation particles demonstrated a much higher release of 37% (versus 8%) over the entire 28 days time period. BSA-FITC conjugation particles showed similar percentages as those measured by ELISA at day 3 with cumulative release reaching 28.6% (versus 26.2%). However, the burst release measured using ELISA occurred partially at each of

days 1 and 3, while the total 29% BSA-FITC release mainly occurred at day 3 with only 5% of it occurring at day 1.

4.4.3 MSCs Cell Number and ALP Activity

To investigate the effects of BMP-2 incorporation with the different nanoparticles on MSCs response, cells were seeded over the different particles, cultured for 21 days, and then assayed for cell number and ALP activity. After 21 days, cell numbers in all groups were similar to those grown without nanoparticles suggesting that nanoparticles fabricated using adsorption, encapsulation and conjugation techniques did not significantly affect cell viability or proliferation (Figure 4.6).

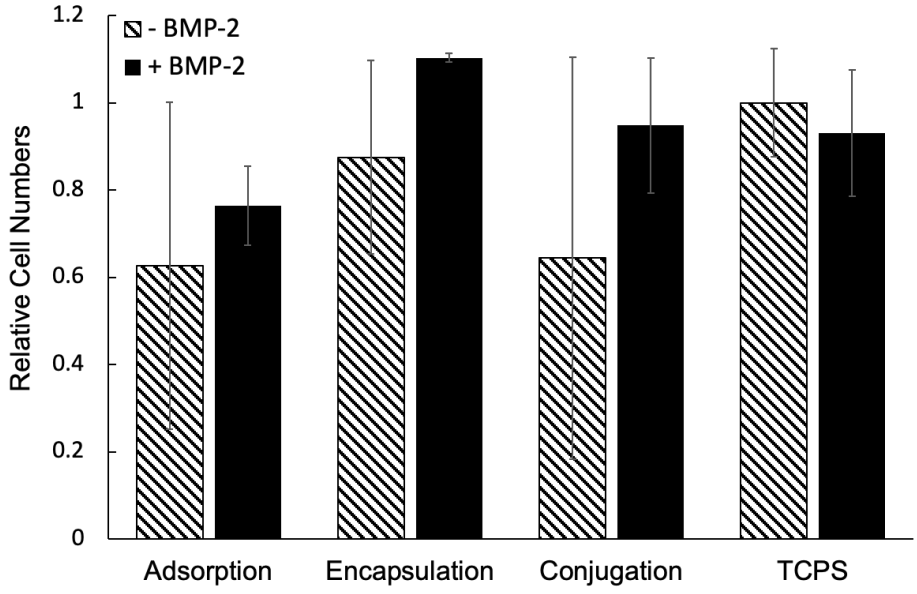

Figure 4.6: Cell numbers for MSCs seeded on both control (-BMP-2) and BMP-2 adsorption, BMP-2 encapsulation and BMP-2 conjugation particles at day 21 as measured by PicoGreen. Cell numbers are reported relative to the TCPS -BMP-2 control group. Bars correspond to mean ± SEM (n = 3).

To investigate the effects of the nanoparticles on osteoblastic differentiation of MSCs, an ALP assay was performed at day 21. Cells cultured with BMP-2 incorporated nanoparticles were compared to cells cultured with 80 ng/well BMP-2 (positive control) and cells cultured with BMP-2 free nanoparticles (negative controls). ALP activity was elevated for cells cultured with BMP-2 adsorption nanoparticles relative to the negative control (Figure 4.7). This was not the case with BMP-2 encapsulation and BMP-2 conjugation particles, however. These results suggest that BMP-2 adsorption particles had a stronger ability to induce ALP activity as compared to both BMP-2 encapsulation and BMP-2 conjugation particles.

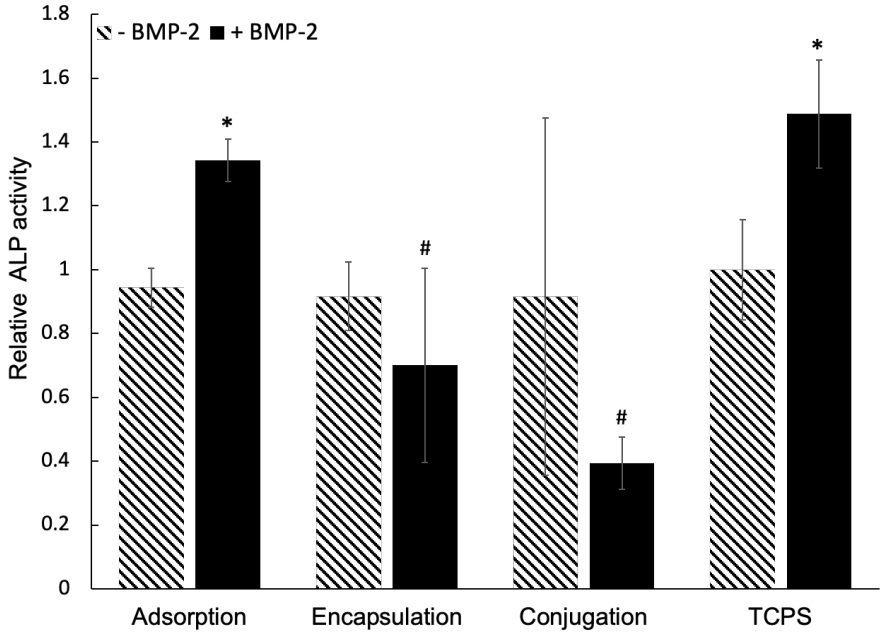

Figure 4.7: Alkaline phosphatase activity of MSCs on both control (-BMP-2) and BMP-2 adsorption, BMP-2 encapsulation and BMP-2 conjugation particles at day 21. ALP activities are reported relative to TCPS -BMP-2 control group. Bars correspond to mean ± SEM ($n = 3$). *Denotes statistical significance ($p < 0.05$) relative to the control (-BMP-2) of the same group. #Indicates statistical significance ($p < 0.05$) relative to +BMP-2 control.

4.4.4 Further Characterization of Nanoparticles

To assess the effect of BMP-2 incorporation steps of each of the three strategies on particle size and PDI, particle sizes and distributions of BMP-2 free control particles were examined. Table 4.1 shows the average particle size and degree of dispersion of control adsorption, encapsulation and conjugation nanoparticles. In particular, conjugation control particles (4972 ± 2738 nm) were much larger than adsorption and encapsulation control nanoparticles (452 ± 2 nm and 620 ± 13 nm, respectively). The larger standards of deviation for conjugation particles coincided with the multiple peaks observed in particle sizes measured by intensity in comparison to monomodal peaks observed in adsorption and encapsulation particles (Figure 4.8). Together, these data suggest that the process for preparing BMP-2 conjugation particles may lead to significant particle aggregation.

Table 4.1: The effect of preparation procedures of adsorption, encapsulation and conjugation techniques on chitosan control nanoparticle sizes (nm) and PDI as measured by DLS.

Incorporation method	Average diameters (nm)	PDI
Adsorption	452 ± 2	0.36
Encapsulation	620 ± 13	0.47
Conjugation	4972 ± 2738	-

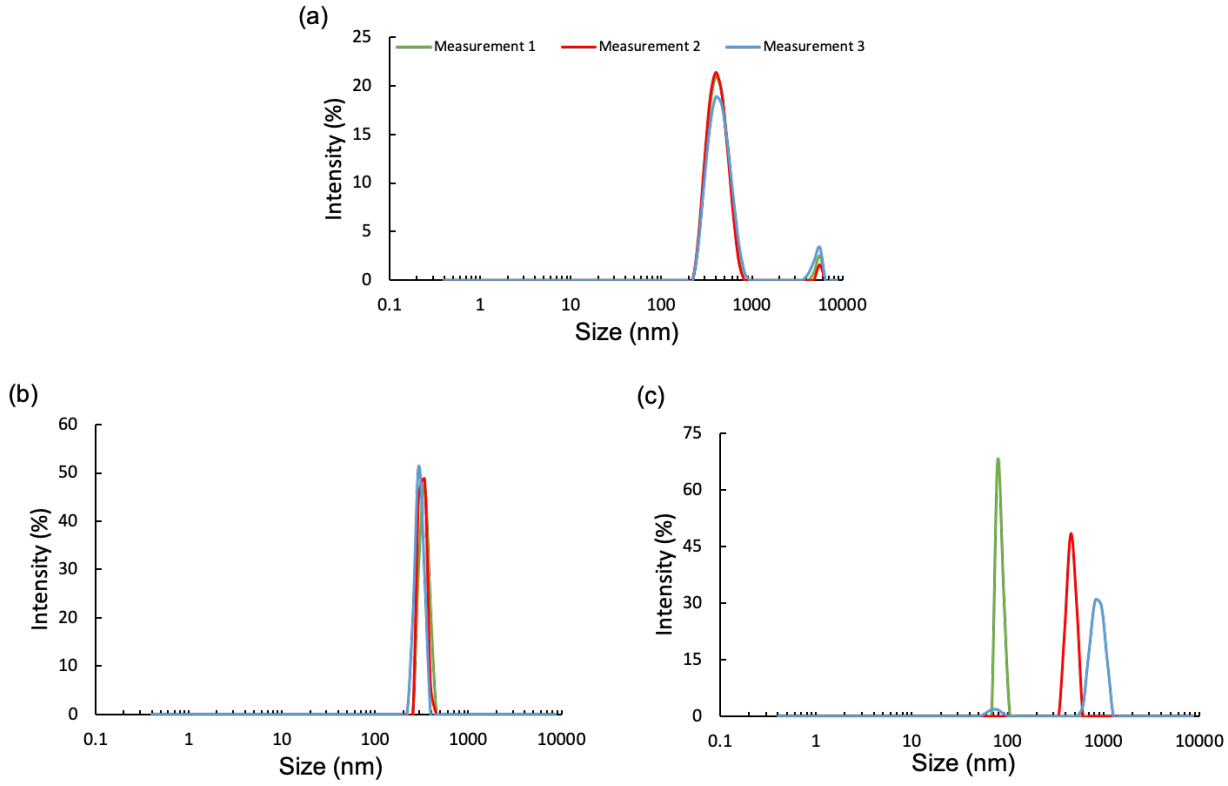

Figure 4.8: Corresponding nanoparticle size distribution by intensity for (a) adsorption, (b) encapsulation and (c) conjugation techniques.

4.5 Discussion

BMP-2 nanoparticles were fabricated as carriers to enhance the efficiency and delivery of loaded BMP-2. Adsorption, encapsulation and conjugation strategies were utilized to fabricate BMP-2 adsorption, BMP-2 encapsulation and BMP-2 conjugation chitosan nanoparticles, respectively. The different strategies, their ability to incorporate and release BMP-2, as well as how they affect the growth and osteogenecity of MSCs were analyzed. It was found that incorporation approach did not affect incorporation efficiency but did affect release kinetics. Concurrently, MSCs did not experience any adverse effects in the presence of the different

nanoparticles, yet the BMP-2 adsorption particles – which exhibited the highest extent of BMP-2 release – resulted in the highest ALP activity.

BMP-2 delivering nanoparticles have vast potential for facilitating bone regeneration, but we are particularly interested in their application in facilitating the anchoring of tendon and ligament grafts (e.g., ACL grafts) to bone. In ACL surgeries involving reconstruction with the hamstring or quadriceps tendon graft, the graft is secured within the bone tunnel with a screw, but typically takes at least three years for proper soft tissue graft healing with the host bone [189]. Consequently, pullout of an ACL graft remains a risk. To tackle this issue, we envision that BMP-2 delivering nanoparticles and an appropriate macroscopic delivery material could be employed in the region where the soft graft contacts the native bone. Hence, different BMP-2 delivering nanoparticles were developed and tested in this study. BMP-2 is a powerful inducer of osteogenesis. However, its short half-life has necessitated the use of superphysiological concentrations clinically. The use of nanoparticles as carriers can enhance the efficiency and delivery of loaded therapeutics and have proven to achieve a slower and more controlled BMP-2 release to the required site [17].

In this study, ionic gelation method was utilized to fabricate chitosan nanoparticles due to its simplicity and biocompatibility. Further, the use of more harsh techniques such as the exposure to organic solvents or high temperatures with the incorporation of biomolecules to carriers is known to result in a loss of molecule bioactivity [7]. Characterization studies show the feasibility of preparing the particles under different conditions. Encapsulated BMP-2 was first mixed with cationic chitosan solution which then formed particle complexes with the electrostatic interaction and binding with the negatively charged TPP. BMP-2 adsorption and conjugation, on the other hand, introduced the protein on the particle surfaces after the complexes were formed. Since the

ratio of chitosan to TPP is important in controlling particle size, the effect of TPP concentration on unloaded particle sizes was studied. The size of resultant nanoparticles fabricated with different TPP concentrations can be adjusted between 200 nm to 900 nm (Figure 4.2) and the observed trend of increasing particle sizes with TPP concentration has been previously reported [190-193]. The sudden onset of growing particles with more TPP (at 10 mg/mL) may be due to the presence of excess TPP [194] surrounding crosslinked cationic chitosan molecules such that TPP further links chitosan and brings different particles together. Particles fabricated with 5 mg/mL TPP were chosen for remaining studies as ~ 500 nm particles are not too small for endocytosis, not too big to still benefit from a high surface area to volume ratio for protein incorporation and release, and have the ability to uniformly be incorporated in scaffolds while maintaining their integrity and porosity [7]. To further improve the stability of BMP-2 chitosan nanoparticles (particularly with the relatively harsher encapsulation and conjugation techniques-as discussed later), BMP-2 was blended with BSA. BSA is often used as a protective agent and carrier for growth factors as well as a matrix in nanoparticles. Thus, adding it to nanoparticles can further help preserve BMP-2 biological activity [60, 61, 92, 122]. Although BSA encapsulation had no effect on particle size at low concentrations, the significantly larger size with 200 μg/mL concentration is due to the molecular weight and size of BSA molecules that take up more space within the particles. Twenty μg/mL was the chosen BSA concentration as it allowed particles to remain in the targeted particle size range (500-1000 nm) while benefiting from its properties.

A few studies have investigated the use of chitosan nanoparticles (both modified and unmodified with other materials) to incorporate BMP-2 [184, 195-197]. The focus of all those studies is the encapsulation of BMP-2 as a way to protect it and preserve its bioactivity. In this work, however, we evaluate three different approaches to understand how the method used to

integrate the protein with the particles affects its release, bioactivity as well as cell response. Among BMP-2 encapsulation particle studies, including this study, as well as postulated curves, the release patterns tend to differ [109, 198]. For instance, Bastami *et al.* found a continuous BMP-2 release that plateaued after 9 days with a 42% cumulative release [184]. Cao *et al*., on the other hand, determined a non-linear pseudo-second order pattern for their release [196]. Nonetheless, both of those studies reported significant release of BMP-2, which we did not observe with our BMP-2 encapsulation particles. In fact, release studies suggested that release was very minute over the entire 28-day time period with a very minor (~2%) BMP-2 release at day 1. Although in much higher amounts than 2%, this initial release trend is commonly observed for the release of drugs and proteins entrapped in particles with the initial release possibly due to the release of weakly adsorbed molecules on particle surfaces [199]. The way BMP-2 is released from encapsulation particles could be based on its diffusion, the degradation of carrier material, and the interactions of the protein with the carrier material. An understanding of the method through which BMP-2 is released remains incomplete. For example, although the work of Cao *et al.* indicates that BMP-2 release is a combination of both diffusion and degradation [196], Poth *et al.* claims that it is merely based on the degradation of particles [195]. Since the release of encapsulated BSA-FITC was significant compared to BMP-2, release does not seem to only be based on the degradation of our fabricated particles.

With an isoelectric point of 8.5 [200], BMP-2 is positively charged at a pH of 7.4 and is expected to repel the chitosan surface which is also positively charged [201], particularly in BMP-2 adsorption particles. Instead, the continuous release pattern exhibited by BMP-2 adsorption particles demonstrated otherwise. This can be attributed to the fact that the existing chitosan degree of deacetylation and pH experimental parameters significantly increase the interactions between

glutamic and aspartic acid residues of BMP-2 and the chitosan surfaces [202]. BMP-2 conjugation particles released around 28% of its incorporated BMP-2 in the first 3 days followed by no release thereafter. The observed initial release could be attributed to the relatively weaker adsorption binding between BMP-2 and chitosan particles. The following lack of release potentially illustrates that the remaining BMP-2 is immobilized on the particle surfaces. This could either be due to the strong covalent conjugation chemistry, the aggregation of particles preventing BMP-2 release, or a combination of the two. An initial burst release can help provide BMP-2 close to particle administration time yet an excess can result in side effects associated with site diffusion [203]. However, the burst release observed with BMP-2 adsorption and BMP-2 conjugation particles was no more than 30% (< 75 ng BMP-2). The high incorporation efficiencies measured by ELISA suggest that BMP-2 could almost be completely integrated with chitosan nanoparticles regardless of the incorporation technique. Although these efficiencies are determined indirectly from the amount of BMP-2 in supernatant, BSA-FITC particles also demonstrated high incorporation efficiencies, further supporting high incorporation percentages. The lower incorporation values of BSA-FITC could potentially be due to lower hydrogen bonding and hydrophobic attractions between BSA-FITC and chitosan in comparison to BMP-2 and chitosan. Similarly, the higher thiol content of BMP-2 compared to BSA-FITC can allow higher conjugation to particles.

PDI indicates the width of overall particle distribution assuming a single mean and ranges from 0 to 1. Commonly, a PDI value higher than 0.5 signifies the aggregation of particles and a value closer to zero indicates size homogeneity [61]. Although no specific PDI trends were observed in Figures 4.2 and 4.3, it is interesting that PDI values were significantly lower at the highest TPP and BSA concentrations. This is possibly due to the fact that larger particles could exhibit better uniformity due to the nature of their large sizes. PDI values were less than 0.5 (no

aggregation) and particle sizes measured by intensity expressed monomodal peaks for particle size characterization studies carried out on control adsorption and encapsulation particles. Control conjugation particles, on the other hand, had multiple peaks of particle sizes (and a PDI value of 0.979 which is not a useful measure due to the absence of monomodal intensity peaks (Figure 4.8)) as measured by intensity denoting possible particle aggregation. This aggregation which was not demonstrated with either adsorption or encapsulation particles is potentially due to the multiple centrifugations and resuspensions associated with covalent conjugation steps allowing strong hydrogen bonding between different molecules that lead to particle aggregation [7].

The recruitment of cells and subsequent osteoblastic differentiation play a vital role in bone regeneration. Cell number studies confirmed that cells were not adversely affected demonstrating the biocompatibility of the different particles. This was expected since chitosan is known to promote cell attachment and growth especially when combined with a safe non-toxic material, TPP. Further, the ability of the different particles to facilitate ALP activity of MSCs was studied and it was demonstrated that BMP-2 adsorption particles support osteogenic differentiation. Although BMP-2 encapsulation particles were expected to increase ALP activity in comparison with adsorption and covalent techniques due to the protection they provide, this was not the case. This can be attributed to the negligible BMP-2 release observed with these particles which are not valuable for osteogenic induction [184], as well as the possibility of protein deactivation associated with adding proteins during particle preparation (mixing with chitosan in acetic acid) versus after their preparation (as in adsorption and conjugation) [204]. Further, we hypothesized that BMP-2 conjugation particles will immobilize BMP-2 (as suggested by their release pattern) allowing continuous exposure and the interaction between proteins and cells. Nevertheless, results revealed that MSCs in the presence of these particles exhibited the lowest ALP activity. This could be due

to the aggregation of particles which would result in BMP-2 masking preventing its exposure to cells or the denaturation of BMP-2 associated with conjugation steps. The conjugation of BMP-2 using sulfo-SMCC chemistry is in itself not harsh and has been previously utilized without affecting BMP-2 bioactivity [205]. In addition to the presence of residual crosslinkers that may cause protein denaturation [206], yet and again, the multiple centrifugation and sonication steps involved in applying it to particle surfaces rather than flat surfaces could somehow alter the biological activity of BMP-2. Finally, the direct expose of BMP-2 by a passive approach in BMP-2 adsorption particles, on the other hand, allowed higher ALP activity. This is due to the mild processing conditions, the proper binding of the protein with particles (as previously discussed), as well as the sustained release of BMP-2 over a longer time period.

An ideal ACL grafts serves as both a mechanical structure (for physical characteristics) as well as a delivery system for various biomolecules. Particularly, this encompasses the inclusion of the delivery of osteogenic materials at the native bone tunnel site for proper graft-bone integration. This study demonstrates that delivering BMP-2 at low but efficient doses is possible with BMP-2 adsorption particles. The next step will be to integrate the particles into three-dimensional scaffolds and to test the scaffolds for their capacity to stimulate osteoblastic differentiation of MSC *in vitro* and bone formation *in vivo*.

4.6 Conclusions

Chitosan nanoparticles were prepared by ionic gelation to adsorb, encapsulate or conjugate BMP-2. High BMP-2 incorporation efficiencies were obtained with all particles yet different release patterns were observed. Lower quantities of BMP-2 release were associated with BMP-2 encapsulation and BMP-2 conjugation particles, while BMP-2 adsorption particles allowed higher

release over 28 days. Cells proliferated in the presence of the particles but exhibited higher ALP activity with BMP-2 adsorption particles. In contrast, BMP-2 conjugation particles exhibited lower ALP activity but appeared to form into aggregates during their preparation. These studies together illustrate the significance of BMP-2 integration approaches on the development of a suitable BMP-2 delivery system.

Chapter 5: Evaluating Cell Response in Fiber-Hydrogel Composite Models for Three-Dimensional Substitute Grafts

Dina Gadalla[1], Aaron S. Goldstein[1,2]

[1]Department of Chemical Engineering,
[2]School of Biomedical Engineering and Sciences
Virginia Tech, Blacksburg, VA 24061, USA

5.1 Abstract

Electrospun fibers have been widely considered ideal scaffolds for the regeneration of oriented tissues, including ligament tissue. However, the small fiber diameters (typically 0.2-5 μm) result in small pores that can often interfere with cell infiltration and subsequent formation of a functional three-dimensional tissue. In contrast, cells do not experience this limitation when cultured in three-dimensional hydrogels. Therefore, we postulate that a fiber-hydrogel composite could potentially permit cell infiltration and subsequent ECM formation. Hence, in this study, model fiber-hydrogel composites for a three-dimensional ligament regenerating composite were fabricated. Specifically, a 99/1 polycaprolactone (PCL)/heparin blend was electrospun on either cover slips or on elevated PDMS rings to produce supported and elevated thin fiber layers, respectively. Collagen was then added to the fibers as an adsorbed coating or as a hydrogel layer of different thicknesses, and mesenchymal stem cells (MSCs) were introduced by either directly seeding onto the surfaces or embedding within the collagen gel phase. Cells in or on composites were cultured for 7 days and then assayed for metabolic activity, viability, and cell number. Here, incorporating collagen as a coating or a thin gel layer were more supportive of cell metabolic

activity and allowed cells to sense the underlying substrates and align with the fibers. In contrast, the use of thicker collagen layers resulted in the rounding of cells and their decreased ability to sense underlying substrates. Together, these data indicate that minor changes in the structure of the fiber and hydrogel phases could significantly alter cell function in the formation of three-dimensional fiber-hydrogel composites for tissue regeneration.

5.2 Introduction

Anterior cruciate ligament (ACL) tears are widely common among athletes and result in around 350,000 ACL reconstruction surgeries annually in the United States [207]. Surgeries typically replace the torn ACL with an autogenic or allogenic tissue graft. Autologous tissue – transplanted from one part of the patient to another – results in additional pain and risks tissue morbidity at the donor site. Allogenic tissue – typically obtained from cadaver – circumvents donor-site morbidity and is widely available, yet can transmit disease and can take longer to incorporate with native tissue [208]. Additionally, the integration of both autografts and allografts with native bone tunnels is often slow impairing graft success by resulting in future re-injuries and knee osteoarthritis [207]. To overcome these drawbacks, ACL tissue engineering has become of interest and seeks to create graft substitutes that can stimulate host cell infiltration, proliferation, and differentiation into a functional ACL tissue.

Fibrous scaffolds are appealing for an engineered graft substitute due to their high surface area for cell attachment and their extracellular matrix (ECM) mimicking architecture [93]. Specifically, fibrous scaffolds produced by electrospinning have been shown to positively foster cell behavior and to produce nanofibrous ideal substrates for ligament tissue engineering [94, 209]. Additionally, they are widely used mainly due to the large similarity between electrospun fiber

properties and native fibers that make up ligament tissue [209]. Nonetheless, two-dimensional tightly packed fibers or thin layers of electrospun fibers in the absence of a chemical gradient and with only a superficial porous network make it difficult for cell infiltration and for the generation of tissues with thicknesses appropriate for clinical application [210, 211]. Three-dimensional scaffolds better mimic natural tissue architecture for cell growth in comparison to two-dimensional scaffolds [105, 112], yet braided or knitted electrospun fiber three-dimensional scaffolds are unable to recapitulate the native complex microenvironment which signals ligamentous differentiation [118]. This inability is again due to cell restrictions caused in the absence of chemical gradients on the fibers and their pore sizes being smaller than 10 μm, whilst mammalian cells are typically greater than 10 μm in size [86]. To address this, the formation of larger pores has been carried out by modifying the electrospinning process or using other fiber producing techniques. These include the introduction of sacrificial fibers or porogens like salt crystals [10, 47], as well as gas foaming [103, 104]. Although those procedures have been shown to help with cell infiltration, cell migration remains slow.

Hydrogels, on the other hand, provide a three-dimensional microenvironment that resembles the ECM of native tissues and their highly hydrated interconnected porous networks allow for the diffusion of nutrients to tissue repair sites [108, 123, 125]. Alternative to the use of only electrospun fibers, a space-filling hydrogel can be introduced to form fiber-hydrogel composites [212, 213]. The presence of the hydrogel can relax the structure of the fibers by reducing fiber bonding. In turn, this favors cell infiltration deep through and into the fiber scaffolds promoting three-dimensional cellularization and the formation of new ECM [11, 212]. Furthermore, the presence of a hydrogel phase can better regulate stem cell fate and tissue formation by improving cell morphogenesis, migration and cell to cell interactions [214, 215].

Synthetic hydrogels are inert and may compromise the functionality of scaffolds, resulting in unregulated cell behavior [210]. Natural hydrogels, on the other hand, originate from living organisms and are thus more familiar to cells. Collagen, a natural hydrogel, is substantially more bioactive than most polymers and is the most abundant ECM component in ligament tissue. Collagen is highly versatile and provides cell adhesive moieties [109, 112]. The combination of collagen with synthetic fibers potentially produces a scaffold that meets both the biomedical and mechanical property needs, with the fibers anticipated to provide mechanical strength and the collagen to permit better cell infiltration and proliferation [45, 82].

The objectives of this study were to construct model electrospun fiber-collagen hydrogel composites that could mimic the properties of large three-dimensional scaffolds for ligament regeneration, and determine how the structure of the scaffolds affects cell viability, proliferation, and morphology. To this end, a blend of polycaprolactone and heparin was electrospun to produce thin fiber mesh layers that were either supported or elevated. The introduction of collagen to fiber meshes as a top coat, as a top layer of different thicknesses or as an entire phase surrounding fibers was investigated. The effect of configuration on cellular behavior was examined through measurements of cell metabolic activity, viability, proliferation and orientation. Furthermore, the possibility of embedding cells in a collagen layer instead of direct surface seeding was evaluated in terms of cell viability and metabolic activity.

5.3 Materials and Methods

5.3.1 Materials

Polycaprolactone (PCL, Mn 80 kDa) and heparin (sodium salt from porcine intestinal mucosa Grade I-A, average MW of 18 kDa) were obtained from Sigma Aldrich (Saint Louis, MO).

Extra pure 2,2,2-trifluoroethanol (TFE) and 15 mm glass coverslips were obtained from Fisher Scientific (Suwanee, GA). Phosphate buffered saline (PBS) and silicon medical adhesive Type A were obtained from Corning cellgro (Manassas, VA) and Dow Corning (Midland, MI), respectively.

5.3.2 Fiber Layer Configurations

A 9 w/w% PCL solution in TFE was mixed with 50 mg/mL heparin in distilled water (DI) to give a 99:1 w/w% PCL-heparin (PCL-Hep) solution. PCL-Hep was electrospun for 5 min from a 22-gauge stainless steel needle with a 3 mL/h flowrate, 11 cm throw distance, and 15 kV potential, and the fibers were collected on a 7.5 cm diameter cylindrical mandrel rotating at 1600 rpm. Fiber layers approximately 300 μm thick were electrospun using two different approaches to give a supported and an elevated set up. The supported setup involved electrospinning onto 15 mm diameter glass coverslips that were secured to the rotating mandrel. The elevated setup involved depositing the fibers onto circular 15 mm diameter, 1 mm thick polydimethylsiloxane (PDMS) rings. Briefly, the collecting mandrel was covered with aluminum foil and PDMS rings were placed on the foil covered mandrel by securing the bottom edges using insulation tape. Right before electrospinning, the PDMS rings were lightly coated with silicon medical adhesive Type A to facilitate fiber adhesion. Fibers were allowed to dry overnight prior to being removed from the mandrel.

5.3.3 Collagen Hydrogels

Collagen harvested from rat tail tendons as described in [216] was used in preparing collagen hydrogels. Briefly, tendons were excised from rat tails and cleaned in 70% ethanol before

digesting for 48 h at 4 °C in a 0.1% acetic acid solution (100 mL acetic acid per gram of tendon). Soluble and insoluble components of the resulting suspension from digestion were then separated by centrifuging at 8800×g for 90 min at 4 °C with a Beckman Coulter Avanti TM J-25 Centrifuge (Beckman Coulter, Pasadena, CA). The clear supernatant containing the collagen was frozen overnight at -80 °C and stored at -20 °C. When ready for use, this dried collagen was prepared in a stock solution of 15 mg/mL by dissolving in 0.1% acetic acid for 3-4 days at 4 °C with the solution inverted 2-3 times a day to form a clear solution. Stock solutions were diluted to 5 mg/mL for the fabrication of collagen gels. Dilution was carried out using 1 N sodium hydroxide, 10× alpha-modified Eagle medium (α-MEM, Invitrogen, Carlsbad, CA), and 1× α-MEM in a 1:10:56 volumetric ratio.

5.3.4 MSC Culture

MSCs were harvested from the bone marrow of femurs and tibias of juvenile male Sprague-Dawley rats weighing 125-150 g (Harlan, Dublin, VA) in accordance with the Institutional Animal Care and Use Committee at Virginia Tech as previously described [158]. Growth medium consisting of α-MEM supplemented with 10% fetal bovine serum (Gemini Biosciences, West Sacramento, CA) and 1% penicillin/streptomycin (Invitrogen) was used in cell culture. Cells of passage 4 or 5 cells were used for these experiments.

Fibers on coverslips and PDMS rings were soaked in 70% ethanol for 5 min, exposed to UV light for 10 min and incubated in PBS for 20 min. Each coverslip or PDMS ring was then transferred to a well of a 24 well plate. For each sample, 5×10^4 cells were either seeded directly onto fiber meshes, seeded onto collagen coated fiber meshes or encapsulated within a collagen layer. Each sample was incubated in 1 mL of growth medium.

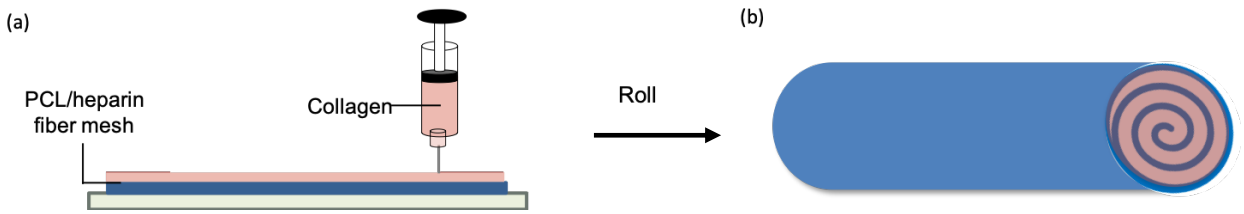

Figure 5.1: Illustrations of (a) collagen casted over a PCL-Hep fibrous mesh followed by rolling into a (b) three-dimensional fiber-hydrogel cylindrical composite.

5.3.5 Supported Fiber-Hydrogel Configurations

Composite materials to model the three-dimensional composite illustrated in Figure 5.1 were created in supported (Figure 5.2) and elevated (Figure 5.3) configurations. In the supported configuration, different collagen addition techniques were examined. The first, "collagen coat," involved incubating the fibers with 0.5 mL of collagen for 5 min (with gentle shaking) followed by aspiration of the excess collagen. Subsequently, the remaining collagen was gelled for 5 min at 37 °C. The second and third techniques, "collagen layer," involved seeding cells onto PCL-Hep fibers, allowing them to attach for 30 min, and then casting either a 500 μm or 1500 μm collagen layer on top of the seeded fibers. The collagen layers were allowed to gel for 5 min at 37 °C. The control groups were cells on PCL-Hep fibers in the absence of collagen and cells on tissue culture polystyrene (TCPS).

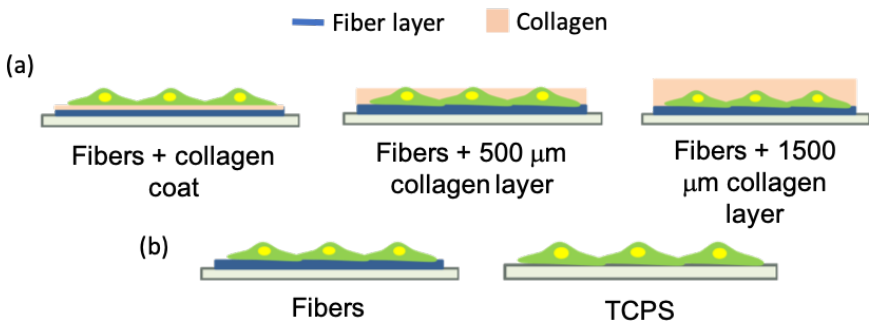

Figure 5.2: Illustrations of (a) the different approaches taken to assemble the fiber and hydrogel phases of supported fiber-hydrogel configurations and (b) their control groups in the absence of collagen.

The possibility of encapsulating the cells in the 500 µm collagen layer rather than seeding them on surfaces prior to collagen casting was also studied in this configuration with a control study on TCPS. Cell metabolic activity and viability were analyzed at day 7. Cells were encapsulated within collagen by adding cell suspensions to the 1× α-MEM component during gel preparation.

5.3.6 Elevated Fiber-Hydrogel Configurations

To decouple the potential effect of a supported substrate on cell behavior, an elevated configuration was developed using fibers on PDMS rings (Figure 5.3). Fiber rings were flipped and 100 µL of collagen was cast on the bottom side of fibers and allowed to gel at 37 °C for 5 min. Rings were then flipped back and cells were seeded directly on the fiber surface (Figure 5.3a). To study cell infiltration and morphology in the different phases, cells were seeded within a 500 µm collagen phase (Figure 5.3b) by adding cell suspensions to the 1× α-MEM component in gel

preparation. Fiber-hydrogel composites were flipped upside down for microscopic observations and image collection.

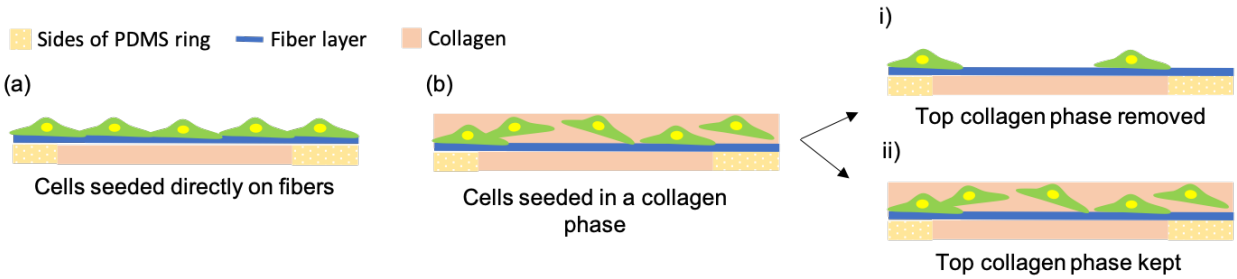

Figure 5.3: Illustrations of the different approaches taken to examine cell behavior in elevated fiber-hydrogel configurations.

5.3.7 Cell Metabolic Activity

For cell studies, samples were incubated in culture media, the media was changed every 3 or 4 days and samples were collected for analysis after 7 days. Cell metabolic activity was analyzed on the various fiber-hydrogel composite configurations using an alamarBlue cell viability assay kit (ThermoFisher Scientific, Grand Island, NY) which detects metabolically active cells. Fifty microliters of alamarBlue reagent was added per well sample and incubated at 37 °C for 3 h. Fluorescence values were then measured at 570 nm excitation and 585 nm emission using a SpectraMax M2 plate reader (Molecular devices, Sunnyvale, CA).

5.3.8 Cell Viability Analysis

A live/dead cytotoxicity kit (Biotium, Hayward, CA) was used to evaluate cell viability of cells seeded within the different fiber-hydrogel composite configurations after 7 days of cell

culture. Media was removed from the wells and the composites were washed twice with PBS. Composites were then incubated in 2 μM calcein-AM and 4 μM ethidium homodimer I in PBS at 37 °C for 30 min. Composites were then rinsed with PBS. To probe the morphologies of cells within the collagen phase and those in contact with the fibers (Figure 5.3bi & ii), the collagen phase atop the fiber layer was either left intact or removed. Composites was then inverted and fluorescence images were collected with an inverted Leica DM IL microscope (Leica Microsystems, Buffalo Grove, IL) using a blue band-pass filter to indicate live cells and a green band-pass filter to identify dead cells.

5.3.9 Cell Number Analysis

Cell numbers within the different fiber-hydrogel composites were quantified with a Quanti-iT PicoGreen kit (Invitrogen, Grand Island, NY) after 7 days of culture. Composites were washed twice with PBS and the cells lysed in 0.2% Triton-X100 for three freeze-thaw cycles along with thorough mixing. Quanti-iT PicoGreen dsDNA reagent was mixed with samples in a 1:1 volume ratio following manufacturer's protocol. Mixtures were then incubated for 5 min at room temperature before fluorescence was measured at 480 nm excitation and 520 nm emission with a SpectraMax M2 plate reader. Fluorescence data was converted to DNA quantity using a series of prepared standards and cell numbers calculated using a previously determined conversion factor of 8 pg DNA per cell.

5.3.10 Statistical Analysis

Experiments were carried out in triplicate and quantitative results were analyzed by one-way analysis of variance ANOVA using StatPlus (AnalystSoft, Walnut, CA). Results are reported

as mean ± standard error of the mean (SEM) with $p \leq 0.05$ considered statistically significant.

5.4 Results

5.4.1 Studies on Supported Fiber-Hydrogel Configurations

Cell studies on fiber-hydrogel composites were carried out to determine the effect of combining the two phases on cell behavior. Supported and elevated configurations model different design portions required to form the three-dimensional composite shown in Figure 5.1. Cellular metabolic activity on supported composite scaffolds was measured to confirm that collagen does not hinder cell viability. Cells on collagen-coated fibers and those beneath a thin (500 μm) collagen layer had similar metabolic activity as cells on TCPS. As shown in Figure 5.4, alamarBlue fluorescence demonstrates lower metabolic activity for cells beneath the thicker (1500 μm) collagen layer.

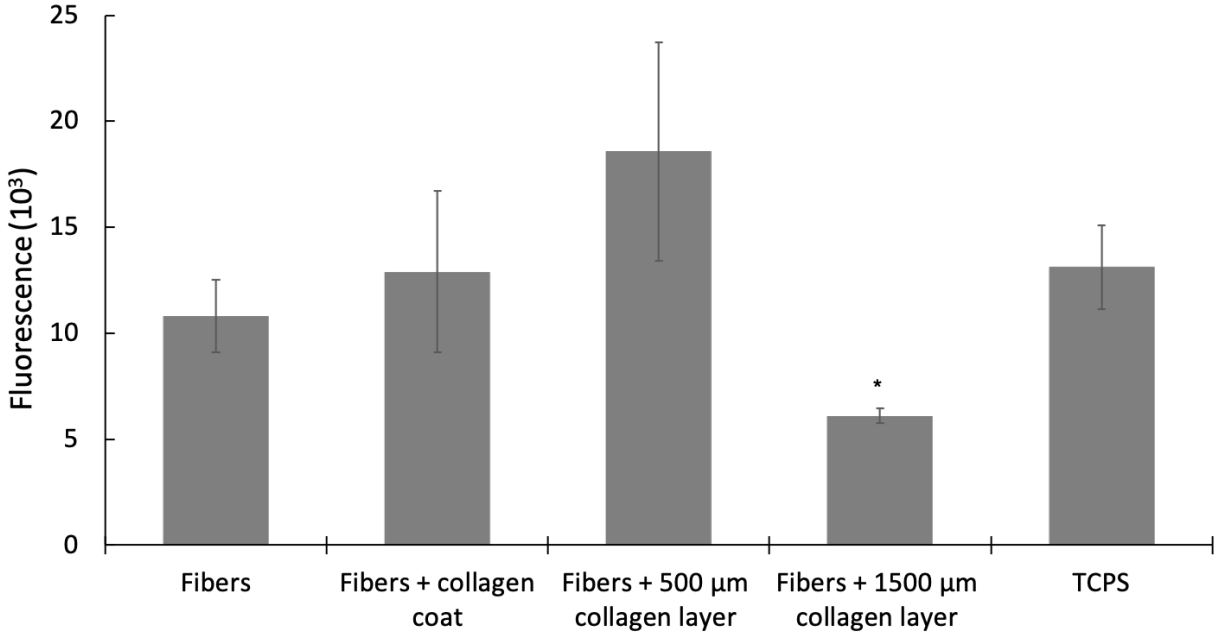

Figure 5.4: Metabolic activity for MSCs as measured by alamarBlue fluorescence at 7 days on PCL-Hep fibers with (a) no collagen, (b) a collagen coat, (c) a 500 µm collagen layer and (d) a 1500 µm collagen layer, with TCPS as the control. Bars correspond to the SEM for $n = 3$ samples. *Denotes statistical significance ($p < 0.05$) relative to TCPS.

Because MSCs seeded on fibers with a 1500 µm collagen layer exhibited a lower metabolic activity, this group was eliminated in subsequent studies. Live/dead staining studies carried out at day 7 show that MSCs remain viable and many attach to the fibers, as indicated by their elongated morphology (Figure 5.5). Further, MSCs on fibers with a collagen coat or beneath the 500 µm collagen layer were able to spread and exhibit morphologies similar to those on bare fibers. Likewise, cell numbers of the different configurations measured at day 7 were similar to those growing on TCPS (Figure 5.6).

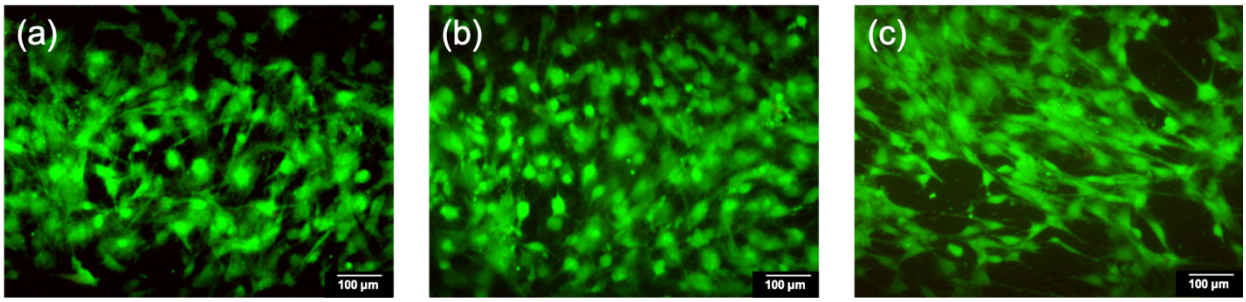

Figure 5.5: Live/dead staining of MSCs seeded on PCL-Hep fibers at day 7. (a) Cells on bare fibers, (b) cells on fibers with a collagen coat, and (c) cells beneath a thin (500 µm) collagen layer. Scale bars correspond to 100 µm.

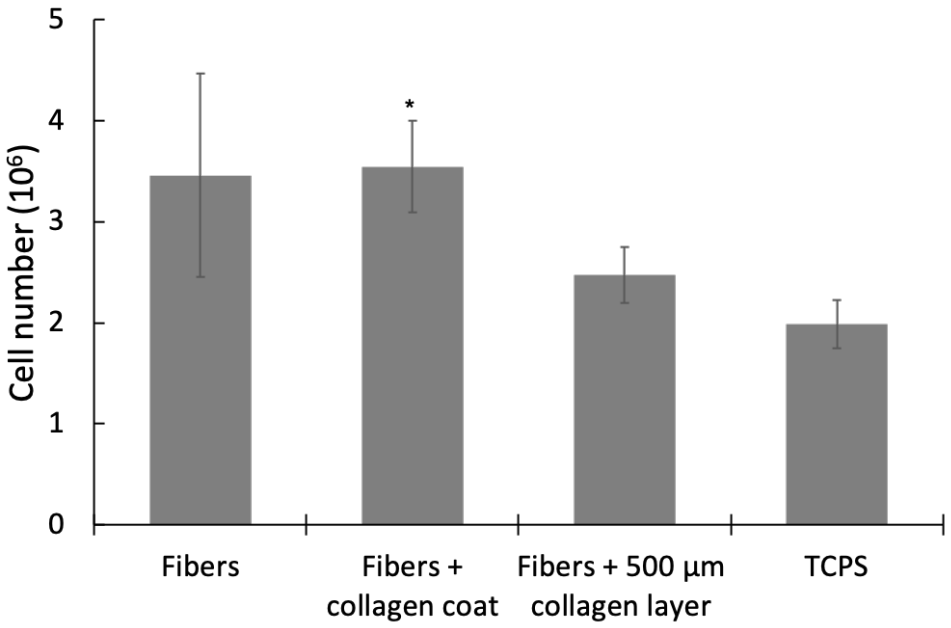

Figure 5.6: Cell numbers for MSCs seeded on PCL-Hep fibers at day 7 with (a) no collagen, (b) a collagen coat and (c) a 500 µm collagen layer with TCPS as the control. Bars correspond to the SEM for $n = 3$ samples. *Denotes statistical significance ($p < 0.05$) relative to TCPS.

A fiber-hydrogel composite could potentially be cellularized either by casting cells suspended in collagen over a fiber mesh or by seeding cells onto the surface of the composite. The control study of collagen cast on TCPS to compare the two involved performing metabolic and live/dead staining assays. AlamarBlue fluorescence values were statistically similar with 12600 ± 1040 and 14500 ± 760 cells for collagen embedding and surface seeding, respectively. Furthermore, live/dead staining of cells within a 500 μm collagen layer cast on TCPS (Figure 5.7a) shows that cells remain viable and exhibit a morphology similar to that of cells directly seeded on TCPS (Figure 5.7c). Nonetheless, some cells within the thicker outer edges of the 500 μm collagen layer cast on TCPS (Figure 5.7b) remain rounded within the collagen phase.

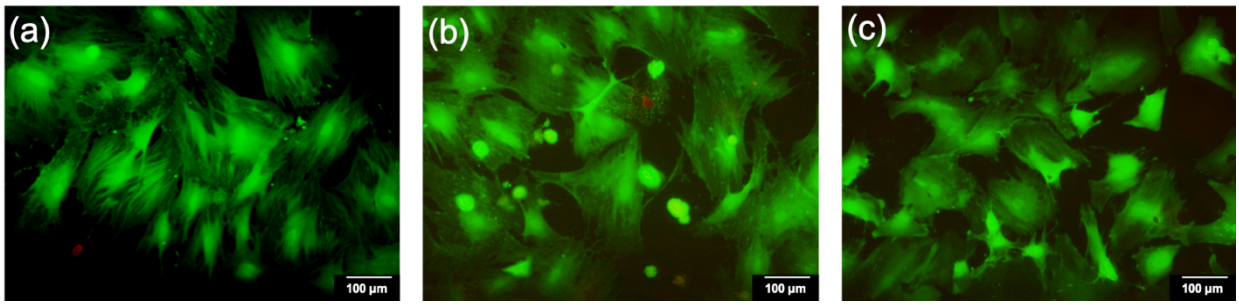

Figure 5.7: Live/dead staining of MSCs (a) embedded within a 500 μm collagen layer and (b) embedded within the thicker outer edges of a 500 μm collagen layer cast on TCPS, and (c) seeded on TCPS control at day 7. Scale bars correspond to 100 μm.

5.4.2 Studies on Elevated Fiber-Hydrogel Configurations

Elevated composite configurations modeling a portion of a three-dimensional rolled scaffold (Figure 5.1b) were fabricated to analyze cell morphologies and viability within the fiber-hydrogel composite. Cell staining studies show the different morphologies of cells present in each

of the fiber and collagen constituents. With the absence of a collagen layer on top of fibers, cells attach to fibers and spread in the same direction as fiber orientation (Figure 5.8a). Configurations with the presence of a collagen layer on top of the fibers demonstrate that cells either spread or remain rounded depending on whether they are near the fiber surface or within the collagen layer, respectively. Upon removing the collagen layer (Figure 5.3b-i), cells were observed on the fiber layer and they oriented with the fibers (Figure 5.8e). Configurations that kept the collagen layer (Figure 5.3 b-ii), show that some cells spread with fiber directions while others remain rounded up (Figure 5.8c). Cells on fibers were not seen in fluorescence staining (Figure 5.8f) and cells within the collagen were out of focus.

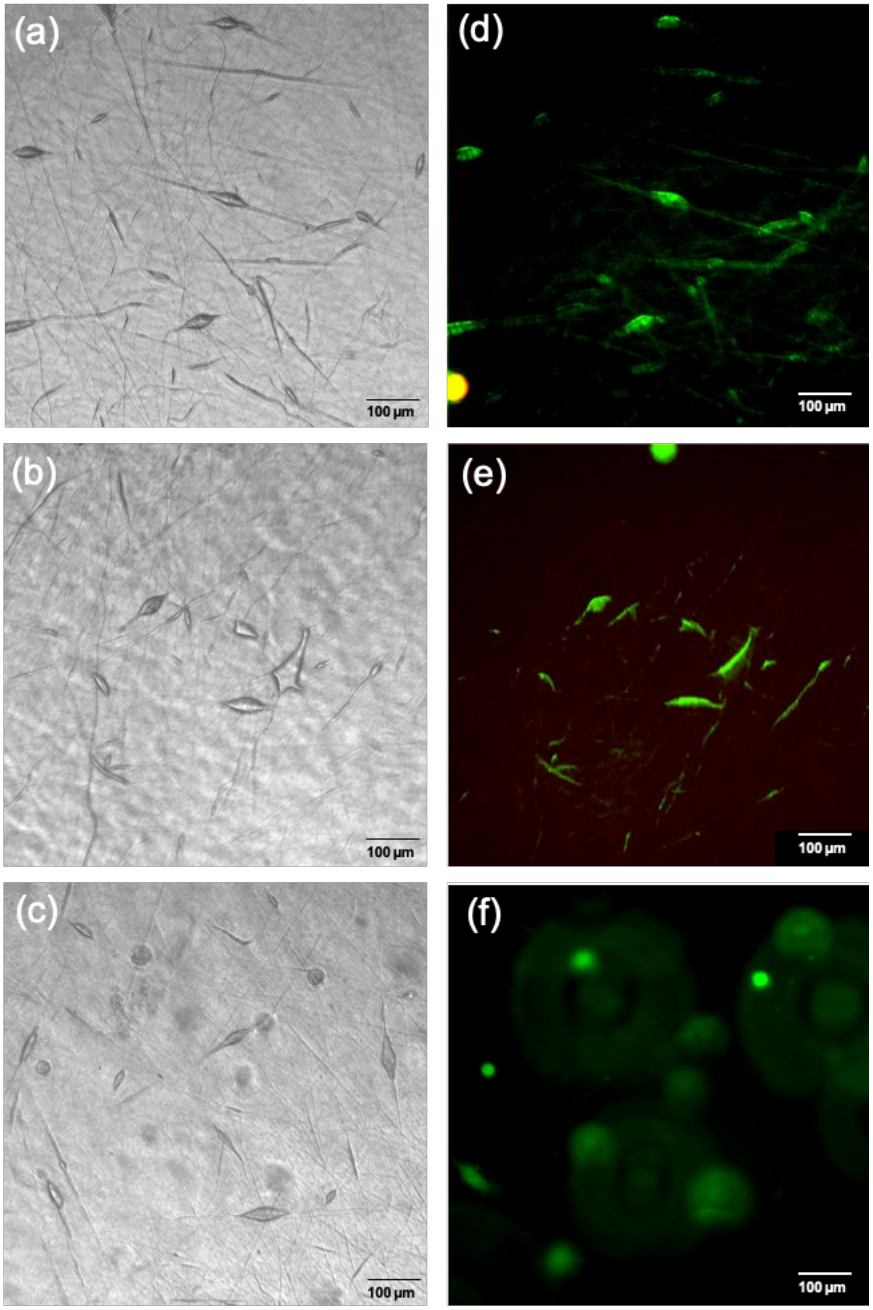

Figure 5.8: (a-c) Light microscope and (d-f) live/dead staining fluorescence of elevated fiber-hydrogel configurations at day 7 with MSCs (a,d) directly seeded on the fibers, or seeded within a 500 µm top collagen layer with the collagen phase (b,e) removed or (c,f) kept. Scale bars correspond to 100 µm.

5.5 Discussion

An ideal tissue engineered ACL graft requires significant cellular infiltration for graft remodeling into functional ligament tissue. Small pore sizes in electrospun fiber scaffolds tend to interfere with cell infiltration. In this study, PCL-Hep fibers were combined with collagen hydrogel to examine how different approaches to constructing fiber-hydrogel composites affect cell behavior. Among different approaches considered, seeding cells onto fibers coated with collagen or onto bare fibers beneath a thin (500 μm) layer of collagen permitted cells to orient with the fibers, and to exhibit metabolic activities and be of numbers similar to cells on a PCL-Hep fiber meshes and on TCPS. Furthermore, encapsulating cells in a 500 μm collagen layer rather than directly seeding them on surfaces also permitted cell-surface interaction. Thicker collagen layers, on the other hand, result in lower metabolic activities. For cells embedded within the collagen and cast over the fibers, the rounding of many cells present within the collagen phase, particularly those further away from the fibers, was observed. However, a number of cells seeded within a collagen layer confine to the fiber layer rather than remain within the collagen phase.

In an attempt to increase cell infiltration in electrospun fibers, multiple effort has been made. For example, to produce larger pores in electrospun poly(L-lactide) Wright *et al*. utilized sodium chloride crystals during electrospinning which were then leached out leaving pore sizes that were around tenfold larger than fibers in the absence of the crystals [217]. Similarly, a study by Baker *et al*. exploited poly(ethylene oxide) as a sacrificial component by co-electrospinning it with PCL followed by washing it off [8]. This technique of including sacrificial components has been widely used by various other researchers with different materials to increase porosity [218-220]. Although this approach increases pore sizes, improves cellular infiltration and does not affect cell proliferation, the mechanical strength of the fibrous scaffolds is reduced due to the resulting

lower fiber density. This could be detrimental to many tissue engineering applications since mechanical properties govern prevailing environments for cell growth. For instance, softer scaffolds for ACL regeneration might not successfully guide MSCs to differentiate into ligament tissue.

Our approach to overcome limitations of cellular infiltration in electrospun fibers is through the addition of a collagen phase to the fibers. That is, we combined the two phases to form a composite environment that benefits from the mechanical integrity of the ECM mimicking electrospun fibers as well as the three-dimensional ECM-like microenvironment provided by the collagen gel. The combination of electrospun fibers and a hydrogel phase has been previously explored for both ligament and tendon regeneration. For example, Kim *et al.* prepared composites by injecting an alginate hydrogel into rolled mats of electrospun PCL-silk fibronin fibers [118]. Analysis of these composites showed that the structure permitted even cell distribution throughout the composite as well as high cell viability and proliferation. Separately, Yang *et al.* fabricated PCL-methacrylated gelatin composite sheets by electrospinning both phases simultaneously [221]. Then, multiple sheets were stacked and reinforced with additional crosslinked gelatin. Cells within this construct were able to align along the fiber orientations and develop a tendon ligament phenotype when signaling molecules were added.

In our study, we introduced collagen to the fibrous layer using various approaches in supported and elevated fiber composite configurations. When incorporated as a coat or a thin (500 μm) layer, we found that collagen does not hinder cell response and that cellular activity in its presence is not different from the activity of cells on TCPS (Figures 5.4-5.6). However, we observed that the addition of collagen as a thicker (1500 μm) layer results in reduced metabolic activity (Figure 5.4). This could possibly be due to lower oxygen or alamarBlue reagent

availability as a consequence of molecular diffusion through the thicker collagen layer [222]. Nonetheless, live/dead staining of MSCs embedded within a 500 μm collagen layer (Figure 5.7) in the control study on TCPS shows that the morphologies of cells present within the thicker edge regions (as collagen adheres to the sides of wells) are rounded and could introduce difficulties in cells present in a fiber-hydrogel configuration of a collagen layer thicker than 500 μm. The difference in cell morphology between cells embedded in collagen and those on TCPS is possibly due to the difference in mechanical properties of the surface-collagen interface – where cells spread – in comparison to the softer collagen gel phase. Although metabolic activity, live/dead staining and cell number studies prove that the simple coating of fibers with collagen is also supportive of cell viability, the *in vitro* design consisting of a 500 μm collagen layer cast over a fiber layer was utilized to model the fiber-hydrogel composite (Figure 5.1) in elevated fiber-hydrogel configuration studies. This direction was chosen to permit possibilities of incorporating biomolecules as well as cells in the collagen layer for future continuation studies. Furthermore, being more representative of three-dimensional scaffolds, the presence of a collagen layer can help provide a more clinically relevant scaffold dimension for cell housing [217].

This work studies the formation of elevated composites that are representative of a three-dimensional rolled scaffold. The presence of two successive collagen regions surrounding a fiber layer allow better analysis of cell movement in a thicker and more clinically relevant structure. The two elevated fiber-hydrogel configurations encompassing cells within the collagen layer (Figure 5.3 b-i & ii) indicate that cells close to the fibers can sense the fiber layer beneath them and orient themselves in the direction of fibers (Figure 5.8 b,c,e) as do cells directly seeded on the fibers (Figure 5.8 a,d). On the other hand, cells deep within the collagen phase (rather than near the fiber-collagen interface) are rounded. This is possibly due to the low stiffness of collagen gels

that impairs the cells ability to spread and exert contractile forces [223]. The rounding of cells demonstrates that the cell spreading on fibers observed in Figure 5.5 a-b with the supported fiber-hydrogel configurations is not merely due to the stiffness of underlying glass substrate since cells are also able to spread on the fibers with the softer collagen bottom layer in elevated configurations. Nonetheless, the increased rounding of cells within the collagen phase in elevated configurations (Figure 5.8c) in comparison to cells on polystyrene surfaces (Figure 5.7a) demonstrates that cells better sense and respond to the stiffer underlying surfaces and/or the difference in morphology of the fibers and polystyrene surfaces [126, 224]. Regardless, Figure 5.8 shows that MSCs were detected both on the fibers and within the hydrogel phase of the composite, indicating that the cells remained distributed throughout the composite while remaining viable.

This study demonstrates that the use of a thinner collagen phase and a stiffer underlying substrate enhance cell metabolic activity (assuming that diffusion rate of alamarBlue reagent is not lowered with the thicker gel layer) and spreading in fiber-hydrogel materials. This study focused on how the construction of the composite affects cell viability, proliferation and morphology during the formation of three-dimensional composites. However, we note that a time lapse study of cell migration is important to understand the movement of cells within the phases and between them, and is thus a more detailed follow up study for this work. Additionally, a variety of other factors can affect cell behavior in the composites. First among them is the presence of biochemicals, such as growth and differentiation factors. Hence, the presentation of growth factors within fiber-hydrogel composites is another next logical investigation. Particularly, the addition of bone morphogenic protein-2 adsorption nanoparticles (such as those described in Chapter 4) to develop three-dimensional model scaffolds with the capacity to induce osteoblastic differentiation

can be evaluated. This will further explain the change in cell fate regulation and tissue formation upon incorporating an additional dimension compared to a two-dimensional fibrous environment.

5.6 Conclusions

Various fiber-hydrogel composite models mainly comprised of a thin collagen layer cast over fibers were fabricated. All composites formed serve as biological frameworks supportive of cell attachment and viability. However, thicker collagen layers appeared to suppress cell metabolic activity. Cells could either be seeded directly on fiber layers or embedded within the collagen layer. When embedded, thicker collagen layers and softer underlying substrates decreased cell spreading. The variety of composite models reflect the flexibility intrinsic to fabricating three-dimensional scaffolds for ligament regeneration, and demonstrate that cell response can depend on scaffold structure.

Chapter 6: Summary and Future Recommendations

6.1 Summary

The overall objective of this work was to develop strategies for the formation of the bone regenerating portion of a tissue engineered anterior cruciate ligament (ACL) substitute scaffold to facilitate integration when ultimately implanted *in vivo*. To achieve this, I first examined techniques to enhance bone formation and then approaches to improve cell infiltration. Specifically, this work involved 1) guiding osteoblastic differentiation through the direct presentation of trophic factors, 2) developing bone signaling nanoparticles that can be incorporated into biomaterials or their components, and 3) advancing assembly approaches for the fabrication of three-dimensional fiber-hydrogel composites.

Fabrication of materials that induce mesenchymal stem cells (MSCs) towards a bone phenotype was a shared goal in the first two projects (Chapter 3 and Chapter 4). The work of these two chapters exert efforts towards developing properly designed delivery systems that can be administered locally via surgery and can localize bone morphogenic protein (BMP)-2 only at the target repair site. For our objective, this corresponds to the region where tissue engineered ACL substitutes are anchored to adjacent native bone tunnels. For the first project, the scaffold serves as both the mechanical support and the vehicle for delivering BMP-2, while in the second a nanoparticle delivery system is formulated to be subsequently combined with the scaffold.

Chapter 3 involved electrospinning polycaprolactone (PCL) blended with different concentrations of heparin to produce fibrous meshes of altered fiber diameters, hydrophilicities, number of reactive groups, and mechanical properties. BMP-2 was then presented on the meshes through adsorption or covalent conjugation and MSCs were seeded on the different meshes for up to 28 days in the absence of any osteogenic supplement. The strategies of incorporating heparin in

PCL fibers and covalent conjugation both increased BMP-2 surface concentration. MSCs were viable on all meshes but expressed higher osteogenic differentiation markers on surfaces covalently conjugated with BMP-2. This study demonstrated that 5.1 ± 1.6 ng/cm^2 BMP-2 was sufficient to promote osteoblastic differentiation when covalently conjugated to the surface of biomaterials. However, the immobilization efficiency of BMP-2 was no more than 8%, necessitating alternative strategies that utilize BMP-2 more efficiently. This led to the alternative strategies discussed in Chapter 4.

Chapter 4 focused on producing an osteogenic protein delivery system. Central to doing so was the development of a technique to incorporate high amounts of BMP-2 into delivery vehicles that can release them at appropriates rates. Towards accomplishing this, three techniques were employed to incorporate BMP-2 with nanoparticle carriers: adsorption, encapsulation and covalent conjugation. The incorporation efficiencies of all three techniques were high, ranging from 92% to 98%. The release kinetic profiles varied widely, with a negligible release for encapsulation, a burst release followed by almost none for conjugation, and a continuous release for adsorption. Regardless of incorporation technique, MSCs cultured with BMP-2 incorporated nanoparticles were viable and proliferative. The dissimilar release profiles affected osteoblastic differentiation, where BMP-2 adsorbed to particles resulted in higher differentiation potential of MSCs as compared to particles that encapsulated BMP-2 or presented conjugated BMP-2.

Chapter 5 concerned aspects associated with the fabrication of three-dimensional porous fiber-hydrogel composites to fuse multiple meshes together through the introduction of a space-filling collagen hydrogel phase to a fiber layer. This included the addition of collagen to either a supported or an elevated fibrous mesh configuration, as a coat over the fibers or as a layer of different thicknesses. MSCs were seeded on the fibers prior to the addition of collagen or were

embedded within the collagen phase. MSCs seeded within a thin collagen layer or over collagen coated fibers proliferated, sensed underlying substrates and spread in the direction of fiber orientation. However, those with the thicker layers appeared to be less proliferative while cells embedded within a collagen phase and remained in it were of rounded morphologies. Additionally, cells seeded within a collagen layer over polystyrene surfaces were more spread than those within a collagen layer over elevated fibers. This difference in cell behavior may be due to the softer collagen phase in comparison to the stiffer polystyrene surfaces that cells can better sense. Together, these findings suggest that small changes in the structure and production methods of a composite can appreciably impact cell response. Consequently, this can affect ACL tissue regeneration when translated into a three-dimensional cylindrical composite.

6.2 Future Recommendations

The results of this work present advances in the fabrication of biomaterial scaffolds that can improve cell behavior and therefore tissue formation, which is the fundamental goal of such scaffold materials. A large portion of the work described is focused on developing material production methods that stimulate osteogenic regeneration (Chapters 3 and 4) while the other is focused on forming composite materials with an added dimension for tissue growth (Chapter 5). Together, the findings of this work can be further progressed for the development of an entire graft integrating ACL structure by 1) implanting BMP-2-conjugated PCL-heparin fibers in to a bone defect model, 2) extending growth factor incorporation methods to spatially modify different fiber regions for ligament regeneration (in addition to bone integration), and 3) constructing composite fiber-hydrogel scaffolds in anatomical dimensions. In the following three sections, each of these potential projects are described.

6.2.1 Bone Defect Model

The translation of *in vitro* findings to *in vivo* application can often be challenging due to the different levels of complexities associated with each. In a similar manner, the experimental findings of each can be significantly different, sometimes even contradicting each other [225-227]. It is, thus, important to move forward with the outcomes of the osteogenic fibrous meshes by implanting the BMP-2 conjugated PCL-heparin electrospun meshes [179] *in vivo*. Electrospun fibrous meshes of different shapes have been previously implanted for the repair of bone tissue [228-230]. Among them are electrospun fibers altered in the form of a simple mesh, discs or agglomerated freeze-dried electrospun fibers that were demonstrated to restore bone in rat cranial defects and to contribute to endochondral bone formation.

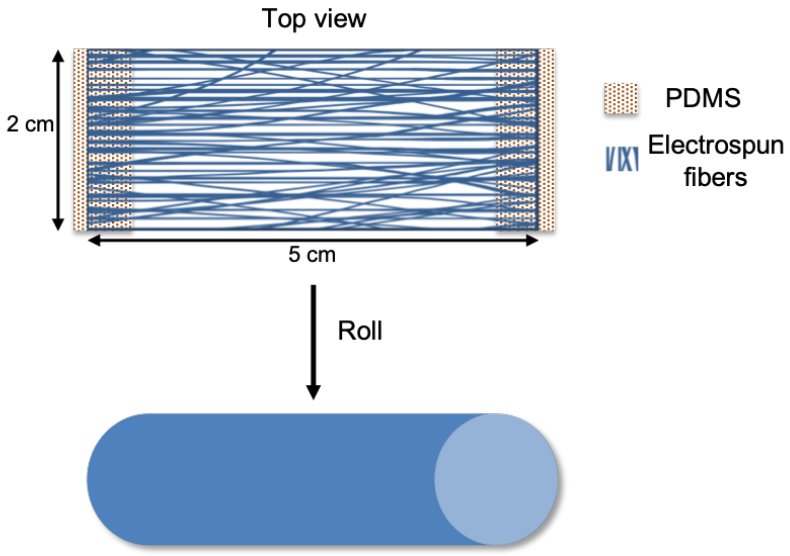

Figure 6.1: Design and preparation of an implantable scaffold for a bone defect model.

The intended design for an implantable scaffold for femur defect regeneration will be prepared. A rectangular fibrous mesh (5 cm × 2 cm) will be electrospun on elevated 2 mm thick polydimethylsiloxane strips (Figure 6.1a). Fibrous meshes of various orientations (aligned and

several degrees of random fibers) will be prepared by varying the rotation speed (250-2500 rpm) of the electrospinning collector. Different fiber alignments will be studied as fiber orientation greatly impacts cell orientation, cell growth and tissue formation [231]. BMP-2 will then be covalently conjugated to the meshes as previously described [179]. This thin modified fiber layer will then be rolled into a cylindrical structure 1 cm in diameter. Control scaffolds will be fabricated in the same manner but in the absence of BMP-2. A bone defect model with similar dimensions to the fabricated cylindrical scaffolds in rat femur will then be created. Ethibond sutures will then be passed through the scaffolds and through the bone defects created [15]. Scaffolds will be tested for integration with these bone defects that mimic the bone tunnels typically prepared for ACL reconstruction using micro-computed tomography analysis and histological evaluation to determine the volume of new bone formed and the presence of osteogenic differentiation markers, respectively.

6.2.2 Complete Ligament Regeneration

The capacity to regenerate bone at the end regions of a tissue engineered ACL graft when secured to bone tunnels in essential for graft integration. Graft integration during soft tissue reconstruction surgeries, nonetheless, remains a significant challenge and efforts in tissue engineering have led to the development of various multi-phased biomaterial scaffold designs to account for the native gradient of the ACL. Such designs typically involve an array of cell types and biological cues and their development continues to be of strong interest. Although many of those studies provide advances to ligament-bone interface regeneration, no complete replication of the structure and function of the different regions has been brought about. For instance, the use of multi-phased scaffolds containing various cell types has been demonstrated to introduce cell

regulation, morbidity and cost challenges [232, 233], while the creation of many gradients on a small scale of tissue regions is found to be tricky. Further, a mere change in the morphology of fibrous meshes or the topography of scaffolds along the graft structure for ligament and bone regions has been shown to help with the mechanical fixation of soft tissue yet had no effect on gene expression within the different regions [234, 235].

Consequently, the proposed simplistic approach aiming to engineer a complete ligament with bone-forming ends that could fit into the native bone tunnels is centered on the use of a single model cell population and the incorporation of a variety of molecular signals to guide cell differentiation into a range of different phenotypes. This approach is motivated by the body's ability to smoothly transmit forces between different tissue types, as well as its ability to heal a bone regenerating material with native bone (as it would in natural bone-bone healing). More specifically, the focus will be on fabricating ligament tissue using a homogenous fiber base and treating the bone tunnels housing the end of the native ACL within the femur and tibia as broken bones that heal with the bone forming region of the fabricated graft. This will be accomplished by using different trophic factors in the middle and end regions of the ligament scaffold.

A first set of studies would involve fabricating ligament forming scaffolds from electrospun PCL-heparin fibers [179] with tuned fiber alignment [69] covalently conjugated with fibroblast growth factor (FGF)-2 [80, 236]. FGF-2 has the ability to bind to heparin in addition to its ability to signal ligament tissue regeneration [237]. The potential of the scaffolds to support ligament formation will be studied through analyzing its ability to enhance the expression of ligamentous markers (eg., tenomodulin, decorin and scleraxis). The next set of studies would involve the use of a customized divider to present each region of a single homogenous contiguous fiber base with its respective trophic factors (Figure 6.2) to guide MSC differentiation down

corresponding cell lineages within each region. It is anticipated that having a single contiguous base fiber structure for the middle and end regions of the graft (Figure 6.2a) will ensure a mechanically robust scaffold that is capable of transmitting tensile loads [28]. This is in contrast to having a non-continuous fiber structure for each of the bone and ligament regions (Figure 6.2b) which would then need to be bond together and would result in an overall weaker scaffold. Further, the spatial functionalization (using ligamentous and osteogenic signaling molecules in each corresponding region) will guide the development of the proper phenotypes for tissue regeneration. Thus, this potentially provides a transformative method to regenerate a complete ligament that accounts for soft tissue-bone integration.

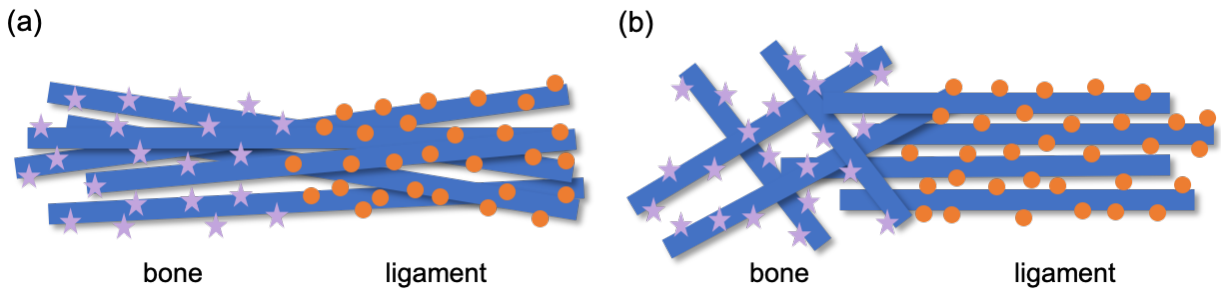

Figure 6.2: Spatial signaling molecule functionalization of a bone to ligament scaffold using (a) a continuous and (b) a non-continuous fiber base. Blue segments correspond to electrospun fibers. Orange circles and purple stars represent ligament and bone trophic factors, respectively.

6.2.3 Ligament-Mimetic Construct

Fiber-hydrogel composites can benefit from the mechanical properties of electrospun fibers and the favorable three-dimensional microenvironment of hydrogels only when properly fabricated. Hence, it is key to make sure that advantages of each phase are obtained. The use of

scaffolds only based on a hydrogel phase for the regeneration of tissue is often complicated as specific extracellular matrix (ECM) microarchitectures can be hard to mimic in comparison to fibers [118]. Further, hydrogels on their own are mechanically weak and thus extremely inappropriate for the formation of hard tissue. Another issue with the use of hydrogel-based scaffolds is the contraction of gels that results in the separation of hydrogels into layers [238, 239]. Hence, the inclusion of fibers with the hydrogels to overcome these issues and their presence as the base structure is essential. Fiber-hydrogel composites have been previously designed in dimensions close to those of ligaments [118, 120, 121]. These designs include the injection of cellular hydrogels in the inner core of a cylindrical fiber mat or the layering of multiple fiber-hydrogel rectangular sheets after cell seeding [118, 221].

The following proposed set of studies could be carried out to determine whether the fiber-hydrogel models developed in Chapter 5 are ideal for the formation of a ligament-mimetic structure, particularly the casting of a 500 μm collagen layer over a thin elevated rectangular fiber sheet. In a first set of studies, collagen could be added to a 3 cm × 5 cm electrospun fiber sheet followed by rolling into a cylindrical scaffold (Figure 6.3a) with the guidance of a stainless-steel wire, and the second adding the collagen to several 3 cm × 1 cm fiber sheets followed by layering the sheets (Figure 6.3b). Mechanical testing of the constructs will then be carried out by investigating the tensile properties of single layers, rolled constructs and multilayered ones. Constructs will be secured to the clamps of a material testing system (MTS) and subjected to a displacement rate of 0.3 mm/s using a 50 N load cell. The disintegration of the two phases within successive layers will then be studied.

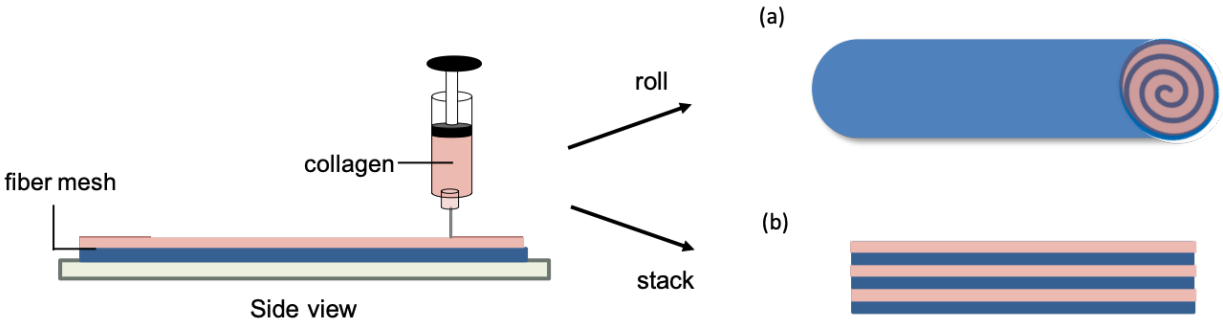

Figure 6.3: Three-dimensional fiber-hydrogel composites formed (a) by rolling a single fiber sheet cast with a collagen layer or (b) by stacking multiple sheets.

In the second set of studies, the ability of the constructs to enhance cell differentiation and ECM formation will be studied for both ligament and bone tissue. Here, cells will be seeded on BMP-2 or fibroblast growth factor (FGF)-2 (a ligamentous signaling molecule) covalently conjugated fibers prior to the addition of collagen. A 1 mm thick specimen construct will then be cut across the different constructs' length and the ability of each of the growth factors to guide tissue formation will be studied by analyzing the expression of specific gene profiles associated with each tissue using polymerase chain reaction technique.

6.3 Concluding Remarks

The focus of this work was to acquire strategies for the development of bone regenerating materials and the recapitulation of a three-dimensional microenvironment. Methods that increase the bioactivity and biocompatibility of materials used in tissue engineering to better promote tissue formation were developed. The efforts of this work demonstrate that both chemical and physical material functionalization can improve growth factor localization, subsequent cell differentiation

and tissue growth. Future studies will concentrate on advancing materials with the ability to guide the formation of ligament tissue and on combining ligament and bone constructs through the creation of a bioactive spatial gradient over a homogenous fiber mesh. Together, these serve as progressions towards the formation of an ACL reconstruction substitute scaffold that enables proper integration when ultimately implanted *in vivo.*

References

[1] T. Nau, A. Teuschl, Regeneration of the anterior cruciate ligament: Current strategies in tissue engineering, World J Orthop 6(1) (2015) 127-36.
[2] E. Hing, D.K. Cherry, D.A. Woodwell, National Ambulatory Medical Care Survey: 2004 summary, Adv Data (374) (2006) 1-33.
[3] D. Olvera, B.N. Sathy, S.F. Carroll, D.J. Kelly, Modulating microfibrillar alignment and growth factor stimulation to regulate mesenchymal stem cell differentiation, Acta Biomater 64 (2017) 148-160.
[4] A.H. Teuschl, S. Tangl, P. Heimel, U.Y. Schwarze, X. Monforte, H. Redl, T. Nau, Osteointegration of a Novel Silk Fiber-Based ACL Scaffold by Formation of a Ligament-Bone Interface, Am J Sports Med 47(3) (2019) 620-627.
[5] C.J. Bishop, J. Kim, J.J. Green, Biomolecule delivery to engineer the cellular microenvironment for regenerative medicine, Annals of biomedical engineering 42(7) (2014) 1557-1572.
[6] M. Tallawi, E. Rosellini, N. Barbani, M.G. Cascone, R. Rai, G. Saint-Pierre, A.R. Boccaccini, Strategies for the chemical and biological functionalization of scaffolds for cardiac tissue engineering: a review, Journal of the Royal Society Interface 12(108) (2015) 20150254.
[7] Y. Hou, J. Hu, H. Park, M. Lee, Chitosan-based nanoparticles as a sustained protein release carrier for tissue engineering applications, Journal of Biomedical Materials Research Part A 100(4) (2012) 939-947.
[8] B.M. Baker, A.O. Gee, R.B. Metter, A.S. Nathan, R.A. Marklein, J.A. Burdick, R.L. Mauck, The potential to improve cell infiltration in composite fiber-aligned electrospun scaffolds by the selective removal of sacrificial fibers, Biomaterials 29(15) (2008) 2348-2358.
[9] Y. Zhang, H. Ouyang, C.T. Lim, S. Ramakrishna, Z.M. Huang, Electrospinning of gelatin fibers and gelatin/PCL composite fibrous scaffolds, Journal of Biomedical Materials Research Part B: Applied Biomaterials: An Official Journal of The Society for Biomaterials, The Japanese Society for Biomaterials, and The Australian Society for Biomaterials and the Korean Society for Biomaterials 72(1) (2005) 156-165.
[10] J. Nam, Y. Huang, S. Agarwal, J. Lannutti, Improved cellular infiltration in electrospun fiber via engineered porosity, Tissue Eng 13(9) (2007) 2249-57.
[11] J. Wu, Y. Hong, Enhancing cell infiltration of electrospun fibrous scaffolds in tissue regeneration, Bioactive materials 1(1) (2016) 56-64.
[12] A.K. Ekaputra, G.D. Prestwich, S.M. Cool, D.W. Hutmacher, Combining electrospun scaffolds with electrosprayed hydrogels leads to three-dimensional cellularization of hybrid constructs, Biomacromolecules 9(8) (2008) 2097-2103.
[13] D.L. Bunker, V. Ilie, V. Ilie, S. Nicklin, Tendon to bone healing and its implications for surgery, Muscles Ligaments Tendons J 4(3) (2014) 343-50.
[14] K.S. Leung, L. Qin, L.K. Fu, C.W. Chan, A comparative study of bone to bone repair and bone to tendon healing in patella-patellar tendon complex in rabbits, Clin Biomech (Bristol, Avon) 17(8) (2002) 594-602.
[15] Y. Kawakami, K. Takayama, T. Matsumoto, Y. Tang, B. Wang, Y. Mifune, J.H. Cummins, R.J. Warth, R. Kuroda, M. Kurosaka, F.H. Fu, J. Huard, Anterior Cruciate Ligament-Derived Stem Cells Transduced With BMP2 Accelerate Graft-Bone Integration After ACL Reconstruction, Am J Sports Med 45(3) (2017) 584-597.

[16] E.B. Hunziker, L. Enggist, A. Kuffer, D. Buser, Y. Liu, Osseointegration: the slow delivery of BMP-2 enhances osteoinductivity, Bone 51(1) (2012) 98-106.
[17] A.S. Herford, P.J. Boyne, Reconstruction of mandibular continuity defects with bone morphogenetic protein-2 (rhBMP-2), Journal of Oral and Maxillofacial Surgery 66(4) (2008) 616-624.
[18] S. Zhong, Y. Zhang, C.T. Lim, Fabrication of large pores in electrospun nanofibrous scaffolds for cellular infiltration: a review, Tissue Engineering Part B: Reviews 18(2) (2012) 77-87.
[19] G. Milano, P.D. Mulas, F. Ziranu, L. Deriu, C. Fabbriciani, Comparison of femoral fixation methods for anterior cruciate ligament reconstruction with patellar tendon graft: a mechanical analysis in porcine knees, Knee Surg Sports Traumatol Arthrosc 15(6) (2007) 733-8.
[20] J. He, W. Zhang, Y. Liu, X. Li, D. Li, Z. Jin, Design and fabrication of biomimetic multiphased scaffolds for ligament-to-bone fixation, Mater Sci Eng C Mater Biol Appl 50 (2015) 12-8.
[21] P. Mahapatra, S. Horriat, B.S. Anand, Anterior cruciate ligament repair - past, present and future, J Exp Orthop 5(1) (2018) 20.
[22] N.L. Leong, F.A. Petrigliano, D.R. McAllister, Current tissue engineering strategies in anterior cruciate ligament reconstruction, J Biomed Mater Res A 102(5) (2014) 1614-24.
[23] N. Davarinos, B.J. O'Neill, W. Curtin, A Brief History of Anterior Cruciate Ligament Reconstruction, Advances in Orthopedic Surgery 2014 (2014).
[24] C. Legnani, A. Ventura, C. Terzaghi, E. Borgo, W. Albisetti, Anterior cruciate ligament reconstruction with synthetic grafts. A review of literature, Int Orthop 34(4) (2010) 465-71.
[25] M.I. Olmos, B. Sonnery-Cottet, J. Barth, How to Succeed in Arthroscopic Anterior Cruciate Ligament Primary Repair? Step-by-Step Technique, Arthrosc Tech 8(1) (2019) e37-e46.
[26] W. Satora, A. Krolikowska, A. Czamara, P. Reichert, Synthetic grafts in the treatment of ruptured anterior cruciate ligament of the knee joint, Polim Med 47(1) (2017) 55-59.
[27] T. Chen, J. Jiang, S. Chen, Status and headway of the clinical application of artificial ligaments, Asia Pac J Sports Med Arthrosc Rehabil Technol 2(1) (2015) 15-26.
[28] K. Markatos, M.K. Kaseta, S.N. Lallos, D.S. Korres, N. Efstathopoulos, The anatomy of the ACL and its importance in ACL reconstruction, Eur J Orthop Surg Traumatol 23(7) (2013) 747-52.
[29] K.L. Moffat, W.H. Sun, P.E. Pena, N.O. Chahine, S.B. Doty, G.A. Ateshian, C.T. Hung, H.H. Lu, Characterization of the structure-function relationship at the ligament-to-bone interface, Proc Natl Acad Sci U S A 105(23) (2008) 7947-52.
[30] D. Lu, C. Yang, Z. Zhang, M. Xiao, Enhanced tendon-bone healing with acidic fibroblast growth factor delivered in collagen in a rabbit anterior cruciate ligament reconstruction model, J Orthop Surg Res 13(1) (2018) 301.
[31] I.E. Wang, S. Mitroo, F.H. Chen, H.H. Lu, S.B. Doty, Age-dependent changes in matrix composition and organization at the ligament-to-bone insertion, J Orthop Res 24(8) (2006) 1745-55.
[32] H. Tsukada, Y. Ishibashi, E. Tsuda, T. Kusumi, T. Kohno, S. Toh, The actual tendon-bone interface strength in a rabbit model, Arthroscopy 26(3) (2010) 366-74.
[33] V.B. Duthon, C. Barea, S. Abrassart, J.H. Fasel, D. Fritschy, J. Menetrey, Anatomy of the anterior cruciate ligament, Knee Surg Sports Traumatol Arthrosc 14(3) (2006) 204-13.

[34] H. Pauly, D. Kelly, K. Popat, J. Easley, R. Palmer, T.L. Haut Donahue, Mechanical properties of a hierarchical electrospun scaffold for ovine anterior cruciate ligament replacement, J Orthop Res 37(2) (2019) 421-430.
[35] B.R. Bach, Jr., M.E. Levy, J. Bojchuk, S. Tradonsky, C.A. Bush-Joseph, N.H. Khan, Single-incision endoscopic anterior cruciate ligament reconstruction using patellar tendon autograft. Minimum two-year follow-up evaluation, Am J Sports Med 26(1) (1998) 30-40.
[36] M. Marieswaran, I. Jain, B. Garg, V. Sharma, D. Kalyanasundaram, A Review on Biomechanics of Anterior Cruciate Ligament and Materials for Reconstruction, Appl Bionics Biomech 2018 (2018) 4657824.
[37] R.v. Zyl, A.-N.v. Schoor, P.d. Toit, E. Louw, Clinical anatomy of the anterior cruciate ligament and pre-operative prediction of ligament length, SA Orthopaedic Journal 15(4) (2016).
[38] C. Vaquette, P.T. Sudheesh Kumar, E.B. Petcu, S. Ivanovski, Combining electrospinning and cell sheet technology for the development of a multiscale tissue engineered ligament construct (TELC), J Biomed Mater Res B Appl Biomater 106(1) (2018) 399-409.
[39] D. Qu, S.D. Subramony, A.L. Boskey, N. Pleshko, S.B. Doty, H.H. Lu, Compositional mapping of the mature anterior cruciate ligament-to-bone insertion, J Orthop Res 35(11) (2017) 2513-2523.
[40] S.F. Tellado, E.R. Balmayor, M. Van Griensven, Strategies to engineer tendon/ligament-to-bone interface: Biomaterials, cells and growth factors, Advanced drug delivery reviews 94 (2015) 126-140.
[41] I. Calejo, R. Costa-Almeida, M.E. Gomes, Cellular complexity at the interface: Challenges in enthesis tissue engineering, Cell Biology and Translational Medicine, Volume 5: Stem Cells: Translational Science to Therapy (2019) 71-90.
[42] C. Domnick, M.J. Raschke, M. Herbort, Biomechanics of the anterior cruciate ligament: Physiology, rupture and reconstruction techniques, World J Orthop 7(2) (2016) 82-93.
[43] J.W. Freeman, M.D. Woods, D.A. Cromer, E.C. Ekwueme, T. Andric, E.A. Atiemo, C.H. Bijoux, C.T. Laurencin, Evaluation of a hydrogel-fiber composite for ACL tissue engineering, J Biomech 44(4) (2011) 694-9.
[44] W. Petersen, B. Tillmann, Structure and vascularization of the cruciate ligaments of the human knee joint, Anat Embryol (Berl) 200(3) (1999) 325-34.
[45] M.A. Walters, M.C. Chambers, R. Karki, E. Knox, G. Levengood, S.F. El-Amin, Anterior Cruciate Ligament Tissue Engineering: A Review of Current Investigations, Journal of Nanotechnology and Materials Science (2016).
[46] A.L. Augustus D Mazzocca, Biologics in Orthopaedic Surgery, Elsevier Health Sciences 2018.
[47] H.M. Pauly, D.J. Kelly, K.C. Popat, N.A. Trujillo, N.J. Dunne, H.O. McCarthy, T.L. Haut Donahue, Mechanical properties and cellular response of novel electrospun nanofibers for ligament tissue engineering: Effects of orientation and geometry, J Mech Behav Biomed Mater 61 (2016) 258-270.
[48] J.O. Hollinger, An introduction to biomaterials, CRC press2011.
[49] C. Niyibizi, C. Sagarrigo Visconti, G. Gibson, K. Kavalkovich, Identification and immunolocalization of type X collagen at the ligament-bone interface, Biochem Biophys Res Commun 222(2) (1996) 584-9.
[50] M. Benjamin, J.R. Ralphs, Fibrocartilage in tendons and ligaments--an adaptation to compressive load, J Anat 193 (Pt 4) (1998) 481-94.

[51] J.P. Spalazzi, A.L. Boskey, N. Pleshko, H.H. Lu, Quantitative mapping of matrix content and distribution across the ligament-to-bone insertion, PLoS One 8(9) (2013) e74349.
[52] L. Ren, P. Yang, Z. Wang, J. Zhang, C. Ding, P. Shang, Biomechanical and biophysical environment of bone from the macroscopic to the pericellular and molecular level, J Mech Behav Biomed Mater 50 (2015) 104-22.
[53] B. Clarke, Normal bone anatomy and physiology, Clin J Am Soc Nephrol 3 Suppl 3 (2008) S131-9.
[54] M.M. Cohen, Jr., The new bone biology: pathologic, molecular, and clinical correlates, Am J Med Genet A 140(23) (2006) 2646-706.
[55] H.I. Roach, Why does bone matrix contain non-collagenous proteins? The possible roles of osteocalcin, osteonectin, osteopontin and bone sialoprotein in bone mineralisation and resorption, Cell Biol Int 18(6) (1994) 617-28.
[56] J.W. Pugh, R.M. Rose, E.L. Radin, Elastic and viscoelastic properties of trabecular bone: dependence on structure, J Biomech 6(5) (1973) 475-85.
[57] M.R. Urist, Bone: formation by autoinduction, Science 150(3698) (1965) 893-9.
[58] J.S. Walsh, Normal bone physiology, remodelling and its hormonal regulation, Surgery (Oxford) 36(1) (2018) 1-6.
[59] D. Kanjilal, J.A. Cottrell, Bone Morphogenetic Proteins (BMPs) and Bone Regeneration, Methods Mol Biol 1891 (2019) 235-245.
[60] G. Wang, K. Siggers, S. Zhang, H. Jiang, Z. Xu, R.F. Zernicke, J. Matyas, H. Uludag, Preparation of BMP-2 containing bovine serum albumin (BSA) nanoparticles stabilized by polymer coating, Pharm Res 25(12) (2008) 2896-909.
[61] Y. Li, H. Song, S. Xiong, T. Tian, T. Liu, Y. Sun, Chitosan-stablized bovine serum albumin nanoparticles having ability to control the release of NELL-1 protein, Int J Biol Macromol 109 (2018) 672-680.
[62] L.-S. Liu, S.-Q. Liu, S.Y. Ng, M. Froix, T. Ohno, J. Heller, Controlled release of interleukin-2 for tumour immunotherapy using alginate/chitosan porous microspheres, Journal of Controlled release 43(1) (1997) 65-74.
[63] S. Mathews, S.A. Mathew, P.K. Gupta, R. Bhonde, S. Totey, Glycosaminoglycans enhance osteoblast differentiation of bone marrow derived human mesenchymal stem cells, J Tissue Eng Regen Med 8(2) (2014) 143-52.
[64] A. Di Martino, L. Liverani, A. Rainer, G. Salvatore, M. Trombetta, V. Denaro, Electrospun scaffolds for bone tissue engineering, Musculoskelet Surg 95(2) (2011) 69-80.
[65] A.L. Butcher, G.S. Offeddu, M.L. Oyen, Nanofibrous hydrogel composites as mechanically robust tissue engineering scaffolds, Trends Biotechnol 32(11) (2014) 564-570.
[66] G. Jin, R. He, B. Sha, W. Li, H. Qing, R. Teng, F. Xu, Electrospun three-dimensional aligned nanofibrous scaffolds for tissue engineering, Mater Sci Eng C Mater Biol Appl 92 (2018) 995-1005.
[67] Y. Ikada, Challenges in tissue engineering, J R Soc Interface 3(10) (2006) 589-601.
[68] F.A. Petrigliano, G.A. Arom, A.N. Nazemi, M.G. Yeranosian, B.M. Wu, D.R. McAllister, In vivo evaluation of electrospun polycaprolactone graft for anterior cruciate ligament engineering, Tissue Eng Part A 21(7-8) (2015) 1228-36.
[69] S. Samavedi, P. Vaidya, P. Gaddam, A.R. Whittington, A.S. Goldstein, Electrospun meshes possessing region-wise differences in fiber orientation, diameter, chemistry and mechanical properties for engineering bone-ligament-bone tissues, Biotechnol Bioeng 111(12) (2014) 2549-59.

[70] P.S. Thayer, S.S. Verbridge, L.A. Dahlgren, S. Kakar, S.A. Guelcher, A.S. Goldstein, Fiber/collagen composites for ligament tissue engineering: influence of elastic moduli of sparse aligned fibers on mesenchymal stem cells, J Biomed Mater Res A 104(8) (2016) 1894-901.
[71] A.C. Gurlek, B. Sevinc, E. Bayrak, C. Erisken, Synthesis and characterization of polycaprolactone for anterior cruciate ligament regeneration, Mater Sci Eng C Mater Biol Appl 71 (2017) 820-826.
[72] H.M. Pauly, B.N. Sathy, D. Olvera, H.O. McCarthy, D.J. Kelly, K.C. Popat, N.J. Dunne, T.L. Haut Donahue, Hierarchically Structured Electrospun Scaffolds with Chemically Conjugated Growth Factor for Ligament Tissue Engineering, Tissue Eng Part A 23(15-16) (2017) 823-836.
[73] M.S. Carvalho, J.C. Silva, R.N. Udangawa, J.M.S. Cabral, F.C. Ferreira, C.L. da Silva, R.J. Linhardt, D. Vashishth, Co-culture cell-derived extracellular matrix loaded electrospun microfibrous scaffolds for bone tissue engineering, Mater Sci Eng C Mater Biol Appl 99 (2019) 479-490.
[74] Z. Lin, X. Zhao, S. Chenad, C. Du, Osteogenic and tenogenic induction of hBMSCs by an integrated nanofibrous scaffold with chemical and structural mimicry of the bone–ligament connection, Journal of Materials Chemistry B (5) (2017) 1015-1027.
[75] P. Gentile, K. McColgan-Bannon, N.C. Gianone, F. Sefat, K. Dalgarno, A.M. Ferreira, Biosynthetic PCL-graft-collagen bulk material for tissue engineering applications, Materials 10(7) (2017) 693.
[76] M. Silva, F.N. Ferreira, N.M. Alves, M.C. Paiva, Biodegradable polymer nanocomposites for ligament/tendon tissue engineering, Journal of Nanobiotechnology 18(1) (2020) 23.
[77] H.J. Sung, C. Meredith, C. Johnson, Z.S. Galis, The effect of scaffold degradation rate on three-dimensional cell growth and angiogenesis, Biomaterials 25(26) (2004) 5735-42.
[78] F.J. O'Brien, Biomaterials & scaffolds for tissue engineering, Materials Today 14(3) (2011) 88-95.
[79] R. van Dijkhuizen-Radersma, L. Moroni, A. van Apeldoorn, Z. Zhang, D. Grijpma, Degradable polymers for tissue engineering, Tissue engineering, Elsevier2008, pp. 193-221.
[80] P. Vavken, M.M. Murray, Tissue Engineering of Ligaments and Tendons, in: F. B. (Ed.) The ACL Handbook, Springer, New York, NY, 2013.
[81] R. Yoshida, M.M. Murray, Scaffolds and Biologic Additives for ACL Surgery, The ACL Handbook, Springer, New York, NY, 2013.
[82] Z. Ge, F. Yang, J.C. Goh, S. Ramakrishna, E.H. Lee, Biomaterials and scaffolds for ligament tissue engineering, J Biomed Mater Res A 77(3) (2006) 639-52.
[83] N.K. Dubey, W.-P. Deng, Polymeric gels for cartilage tissue engineering, Polymeric Gels, Elsevier2018, pp. 505-525.
[84] A. Teuschl, P. Heimel, S. Nurnberger, M. van Griensven, H. Redl, T. Nau, A Novel Silk Fiber-Based Scaffold for Regeneration of the Anterior Cruciate Ligament: Histological Results From a Study in Sheep, Am J Sports Med 44(6) (2016) 1547-57.
[85] G.H. Altman, R.L. Horan, H.H. Lu, J. Moreau, I. Martin, J.C. Richmond, D.L. Kaplan, Silk matrix for tissue engineered anterior cruciate ligaments, Biomaterials 23(20) (2002) 4131-41.
[86] J.K. Hong, S.V. Madihally, Three-dimensional scaffold of electrosprayed fibers with large pore size for tissue regeneration, Acta Biomater 6(12) (2010) 4734-42.
[87] N.L. Leong, F.A. Petrigliano, D.R. McAllister, Current tissue engineering strategies in anterior cruciate ligament reconstruction, Journal of biomedical materials research Part A 102(5) (2014) 1614-1624.

[88] S. Hankemeier, M. van Griensven, M. Ezechieli, T. Barkhausen, M. Austin, M. Jagodzinski, R. Meller, U. Bosch, C. Krettek, J. Zeichen, Tissue engineering of tendons and ligaments by human bone marrow stromal cells in a liquid fibrin matrix in immunodeficient rats: results of a histologic study, Arch Orthop Trauma Surg 127(9) (2007) 815-21.
[89] S. Naahidi, M. Jafari, M. Logan, Y. Wang, Y. Yuan, H. Bae, B. Dixon, P. Chen, Biocompatibility of hydrogel-based scaffolds for tissue engineering applications, Biotechnol Adv 35(5) (2017) 530-544.
[90] X. Yang, Y. Li, W. He, Q. Huang, R. Zhang, Q. Feng, Hydroxyapatite/collagen coating on PLGA electrospun fibers for osteogenic differentiation of bone marrow mesenchymal stem cells, J Biomed Mater Res A 106(11) (2018) 2863-2870.
[91] R. Dimitriou, E. Jones, D. McGonagle, P.V. Giannoudis, Bone regeneration: current concepts and future directions, BMC Med 9 (2011) 66.
[92] D. Gan, M. Liu, T. Xu, K. Wang, H. Tan, X. Lu, Chitosan/biphasic calcium phosphate scaffolds functionalized with BMP-2-encapsulated nanoparticles and RGD for bone regeneration, J Biomed Mater Res A 106(10) (2018) 2613-2624.
[93] S.Y. Chew, Y. Wen, Y. Dzenis, K.W. Leong, The role of electrospinning in the emerging field of nanomedicine, Curr Pharm Des 12(36) (2006) 4751-70.
[94] N. Bhardwaj, S.C. Kundu, Electrospinning: a fascinating fiber fabrication technique, Biotechnol Adv 28(3) (2010) 325-47.
[95] W.E. Teo, S. Ramakrishna, A review on electrospinning design and nanofibre assemblies, Nanotechnology 17(14) (2006) R89-R106.
[96] K. Ye, H. Kuang, Z. You, Y. Morsi, X. Mo, Electrospun Nanofibers for Tissue Engineering with Drug Loading and Release, Pharmaceutics 11(4) (2019).
[97] G.C. Ingavle, J.K. Leach, Advancements in electrospinning of polymeric nanofibrous scaffolds for tissue engineering, Tissue Eng Part B Rev 20(4) (2014) 277-93.
[98] N.G. Rim, C.S. Shin, H. Shin, Current approaches to electrospun nanofibers for tissue engineering, Biomed Mater 8(1) (2013) 014102.
[99] R. Dorati, A. DeTrizio, T. Modena, B. Conti, F. Benazzo, G. Gastaldi, I. Genta, Biodegradable Scaffolds for Bone Regeneration Combined with Drug-Delivery Systems in Osteomyelitis Therapy, Pharmaceuticals (Basel) 10(4) (2017).
[100] N.J. Schaub, C. Le Beux, J. Miao, R.J. Linhardt, J.G. Alauzun, D. Laurencin, R.J. Gilbert, The Effect of Surface Modification of Aligned Poly-L-Lactic Acid Electrospun Fibers on Fiber Degradation and Neurite Extension, PLoS One 10(9) (2015) e0136780.
[101] C. Liu, H.M. Wong, K.W.K. Yeung, S.C. Tjong, Novel Electrospun Polylactic Acid Nanocomposite Fiber Mats with Hybrid Graphene Oxide and Nanohydroxyapatite Reinforcements Having Enhanced Biocompatibility, Polymers (Basel) 8(8) (2016).
[102] T.A. Telemeco, C. Ayres, G.L. Bowlin, G.E. Wnek, E.D. Boland, N. Cohen, C.M. Baumgarten, J. Mathews, D.G. Simpson, Regulation of cellular infiltration into tissue engineering scaffolds composed of submicron diameter fibrils produced by electrospinning, Acta Biomater 1(4) (2005) 377-85.
[103] Q.L. Loh, C. Choong, Three-dimensional scaffolds for tissue engineering applications: role of porosity and pore size, Tissue Eng Part B Rev 19(6) (2013) 485-502.
[104] N. Kasoju, D. Kubies, M.M. Kumorek, J. Kriz, E. Fabryova, L. Machova, J. Kovarova, F. Rypacek, Dip TIPS as a facile and versatile method for fabrication of polymer foams with controlled shape, size and pore architecture for bioengineering applications, PLoS One 9(9) (2014) e108792.

[105] M. Persson, P.P. Lehenkari, L. Berglin, S. Turunen, M.A.J. Finnila, J. Risteli, M. Skrifvars, J. Tuukkanen, Osteogenic Differentiation of Human Mesenchymal Stem cells in a 3D Woven Scaffold, Sci Rep 8(1) (2018) 10457.
[106] P. Nezhad-Mokhtari, M. Ghorbani, L. Roshangar, J.S. Rad, A review on the construction of hydrogel scaffolds by various chemically techniques for tissue engineering, European Polymer Journal (2019).
[107] V.K. Thakur, M.K. Thakur, M.R. Kessler, Handbook of Composites From Renewable Materials, Polymeric Composites, John Wiley & Sons2017.
[108] Y. Fang, B. Wang, Y. Zhao, Z. Xiao, J. Li, Y. Cui, S. Han, J. Wei, B. Chen, J. Han, Q. Meng, X. Hou, J. Luo, J. Dai, Z. Jing, Collagen scaffold microenvironments modulate cell lineage commitment for differentiation of bone marrow cells into regulatory dendritic cells, Sci Rep 7 (2017) 42049.
[109] I. El Bialy, W. Jiskoot, M. Reza Nejadnik, Formulation, Delivery and Stability of Bone Morphogenetic Proteins for Effective Bone Regeneration, Pharm Res 34(6) (2017) 1152-1170.
[110] B.B. Nguyen, R.A. Moriarty, T. Kamalitdinov, J.M. Etheridge, J.P. Fisher, Collagen hydrogel scaffold promotes mesenchymal stem cell and endothelial cell coculture for bone tissue engineering, J Biomed Mater Res A 105(4) (2017) 1123-1131.
[111] S.R. Caliari, J.A. Burdick, A practical guide to hydrogels for cell culture, Nat Methods 13(5) (2016) 405-14.
[112] I.M. El-Sherbiny, M.H. Yacoub, Hydrogel scaffolds for tissue engineering: Progress and challenges, Glob Cardiol Sci Pract 2013(3) (2013) 316-42.
[113] L. Cao, J.A. Werkmeister, J. Wang, V. Glattauer, K.M. McLean, C. Liu, Bone regeneration using photocrosslinked hydrogel incorporating rhBMP-2 loaded 2-N, 6-O-sulfated chitosan nanoparticles, Biomaterials 35(9) (2014) 2730-42.
[114] C.D. Spicer, Hydrogel scaffolds for tissue engineering: the importance of polymer choice, Polymer Chemistry (2020).
[115] M. Pensalfini, A.E. Ehret, S. Studeli, D. Marino, A. Kaech, E. Reichmann, E. Mazza, Factors affecting the mechanical behavior of collagen hydrogels for skin tissue engineering, J Mech Behav Biomed Mater 69 (2017) 85-97.
[116] M.P. Lutolf, J.L. Lauer-Fields, H.G. Schmoekel, A.T. Metters, F.E. Weber, G.B. Fields, J.A. Hubbell, Synthetic matrix metalloproteinase-sensitive hydrogels for the conduction of tissue regeneration: engineering cell-invasion characteristics, Proc Natl Acad Sci U S A 100(9) (2003) 5413-8.
[117] M.G. Drozdova, D.S. Zaytseva-Zotova, R.A. Akasov, A.S. Golunova, A.A. Artyukhov, O.O. Udartseva, E.R. Andreeva, D.E. Lisovyy, M.I. Shtilman, E.A. Markvicheva, Macroporous modified poly (vinyl alcohol) hydrogels with charged groups for tissue engineering: Preparation and in vitro evaluation, Mater Sci Eng C Mater Biol Appl 75 (2017) 1075-1082.
[118] J.H. Kim, Y.J. Choi, H.G. Yi, J.H. Wang, D.W. Cho, Y.H. Jeong, A cell-laden hybrid fiber/hydrogel composite for ligament regeneration with improved cell delivery and infiltration, Biomed Mater 12(5) (2017) 055010.
[119] J. Elisseeff, C. Puleo, F. Yang, B. Sharma, Advances in skeletal tissue engineering with hydrogels, Orthod Craniofac Res 8(3) (2005) 150-61.
[120] S. Xu, L. Deng, J. Zhang, L. Yin, A. Dong, Composites of electrospun-fibers and hydrogels: A potential solution to current challenges in biological and biomedical field, J Biomed Mater Res B Appl Biomater 104(3) (2016) 640-56.

[121] R.E. McMahon, X. Qu, A.C. Jimenez-Vergara, C.A. Bashur, S.A. Guelcher, A.S. Goldstein, M.S. Hahn, Hydrogel-electrospun mesh composites for coronary artery bypass grafts, Tissue Eng Part C Methods 17(4) (2011) 451-61.
[122] G. Subramanian, C. Bialorucki, E. Yildirim-Ayan, Nanofibrous yet injectable polycaprolactone-collagen bone tissue scaffold with osteoprogenitor cells and controlled release of bone morphogenetic protein-2, Mater Sci Eng C Mater Biol Appl 51 (2015) 16-27.
[123] S. Deepthi, K. Jeevitha, M.N. Sundaram, K.P. Chennazhi, R. Jayakumar, Chitosan–hyaluronic acid hydrogel coated poly(caprolactone) multiscale bilayer scaffold for ligament regeneration, Chemical Engineering Journal 260 (2015) 478-485.
[124] Y.M. Kolambkar, K.M. Dupont, J.D. Boerckel, N. Huebsch, D.J. Mooney, D.W. Hutmacher, R.E. Guldberg, An alginate-based hybrid system for growth factor delivery in the functional repair of large bone defects, Biomaterials 32(1) (2011) 65-74.
[125] A. De Mori, M. Pena Fernandez, G. Blunn, G. Tozzi, M. Roldo, 3D Printing and Electrospinning of Composite Hydrogels for Cartilage and Bone Tissue Engineering, Polymers (Basel) 10(3) (2018).
[126] B.P. Chan, K.W. Leong, Scaffolding in tissue engineering: general approaches and tissue-specific considerations, Eur Spine J 17 Suppl 4 (2008) 467-79.
[127] C.J. Kowalczewski, J.M. Saul, Biomaterials for the delivery of growth factors and other therapeutic agents in tissue engineering approaches to bone regeneration, Frontiers in pharmacology 9 (2018) 513.
[128] R. Dimitriou, P.V. Giannoudis, Discovery and development of BMPs, Injury 36 Suppl 3 (2005) S28-33.
[129] L. Grgurevic, M. Pecina, S. Vukicevic, Marshall R. Urist and the discovery of bone morphogenetic proteins, Int Orthop 41(5) (2017) 1065-1069.
[130] O.A. Arosarena, F.E. Del Carpio-Cano, R.A. Dela Cadena, M.C. Rico, E. Nwodim, F.F. Safadi, Comparison of bone morphogenetic protein-2 and osteoactivin for mesenchymal cell differentiation: effects of bolus and continuous administration, J Cell Physiol 226(11) (2011) 2943-52.
[131] X. Zhao, Y. Han, J. Li, B. Cai, H. Gao, W. Feng, S. Li, J. Liu, D. Li, BMP-2 immobilized PLGA/hydroxyapatite fibrous scaffold via polydopamine stimulates osteoblast growth, Materials Science and Engineering: C 78 (2017) 658-666.
[132] S. Andrews, A. Cheng, H. Stevens, M.T. Logun, R. Webb, E. Jordan, B. Xia, L. Karumbaiah, R.E. Guldberg, S. Stice, Chondroitin Sulfate Glycosaminoglycan Scaffolds for Cell and Recombinant Protein-Based Bone Regeneration, Stem cells translational medicine 8(6) (2019) 575-585.
[133] N.M. Wolfman, G. Hattersley, K. Cox, A.J. Celeste, R. Nelson, N. Yamaji, J.L. Dube, E. DiBlasio-Smith, J. Nove, J.J. Song, Ectopic induction of tendon and ligament in rats by growth and differentiation factors 5, 6, and 7, members of the TGF-beta gene family, The Journal of clinical investigation 100(2) (1997) 321-330.
[134] E. Farng, A.R. Urdaneta, D. Barba, S. Esmende, D.R. McAllister, The effects of GDF-5 and uniaxial strain on mesenchymal stem cells in 3-D culture, Clinical orthopaedics and related research 466(8) (2008) 1930-1937.
[135] M. Rickert, M. Jung, M. Adiyaman, W. Richter, H.G. Simank, A growth and differentiation factor-5 (GDF-5)-coated suture stimulates tendon healing in an Achilles tendon model in rats, Growth Factors 19(2) (2001) 115-126.

[136] M.M. Murray, M. Spector, The migration of cells from the ruptured human anterior cruciate ligament into collagen-glycosaminoglycan regeneration templates in vitro, Biomaterials 22(17) (2001) 2393-402.
[137] H. Fan, H. Liu, E.J. Wong, S.L. Toh, J.C. Goh, In vivo study of anterior cruciate ligament regeneration using mesenchymal stem cells and silk scaffold, Biomaterials 29(23) (2008) 3324-37.
[138] Z. Ge, J.C.H. Goh, E.H. Lee, Selection of cell source for ligament tissue engineering, Cell transplantation 14(8) (2005) 573-583.
[139] J. Chen, G.H. Altman, V. Karageorgiou, R. Horan, A. Collette, V. Volloch, T. Colabro, D.L. Kaplan, Human bone marrow stromal cell and ligament fibroblast responses on RGD-modified silk fibers, Journal of Biomedical Materials Research Part A: An Official Journal of The Society for Biomaterials, The Japanese Society for Biomaterials, and The Australian Society for Biomaterials and the Korean Society for Biomaterials 67(2) (2003) 559-570.
[140] Z. Liu, Y. Li, Y. Ren, Y. Jin, J. Yang, S. Wang, X. Zhu, H. Xiong, G. Zou, Y. Liu, Enhancement of in vitro proliferation and bioactivity of human anterior cruciate ligament fibroblasts using an in situ tissue isolation method and basic fibroblast growth factor culture conditions: A pilot analysis, Medicine 98(22) (2019).
[141] F. Van Eijk, D.B. Saris, J. Riesle, W.J. Willems, C.A. Van Blitterswijk, A.J. Verbout, W.J. Dhert, Tissue engineering of ligaments: a comparison of bone marrow stromal cells, anterior cruciate ligament, and skin fibroblasts as cell source, Tissue Eng 10(5-6) (2004) 893-903.
[142] M. Brittberg, Cellular and Acellular Approaches for Cartilage Repair: A Philosophical Analysis, Cartilage 6(2 Suppl) (2015) 4S-12S.
[143] P. de Mille, J. Osmak, Performance: Bridging the Gap After ACL Surgery, Curr Rev Musculoskelet Med 10(3) (2017) 297-306.
[144] N.A. Mall, P.N. Chalmers, M. Moric, M.J. Tanaka, B.J. Cole, B.R. Bach, Jr., G.A. Paletta, Jr., Incidence and trends of anterior cruciate ligament reconstruction in the United States, Am J Sports Med 42(10) (2014) 2363-70.
[145] J.P. Spalazzi, S.B. Doty, K.L. Moffat, W.N. Levine, H.H. Lu, Development of controlled matrix heterogeneity on a triphasic scaffold for orthopedic interface tissue engineering, Tissue Eng 12(12) (2006) 3497-508.
[146] P. Bhattacharjee, D. Naskar, T.K. Maiti, D. Bhattacharya, S.C. Kundu, Investigating the potential of combined growth factors delivery, from non-mulberry silk fibroin grafted poly(ε-caprolactone)/hydroxyapatite nanofibrous scaffold, in bone tissue engineering, Applied Materials Today 5 (2016) 52-67.
[147] T.M. De Witte, L.E. Fratila-Apachitei, A.A. Zadpoor, N.A. Peppas, Bone tissue engineering via growth factor delivery: from scaffolds to complex matrices, Regen Biomater 5(4) (2018) 197-211.
[148] M. Beederman, J.D. Lamplot, G. Nan, J. Wang, X. Liu, L. Yin, R. Li, W. Shui, H. Zhang, S.H. Kim, W. Zhang, J. Zhang, Y. Kong, S. Denduluri, M.R. Rogers, A. Pratt, R.C. Haydon, H.H. Luu, J. Angeles, L.L. Shi, T.C. He, BMP signaling in mesenchymal stem cell differentiation and bone formation, J Biomed Sci Eng 6(8A) (2013) 32-52.
[149] N.S. Gandhi, R.L. Mancera, Prediction of heparin binding sites in bone morphogenetic proteins (BMPs), Biochim Biophys Acta 1824(12) (2012) 1374-81.
[150] S. Liu, Y. Liu, L. Jiang, Z. Li, S. Lee, C. Liu, J. Wang, J. Zhang, Recombinant human BMP-2 accelerates the migration of bone marrow mesenchymal stem cells via the CDC42/PAK1/LIMK1 pathway in vitro and in vivo, Biomater Sci 7(1) (2018) 362-372.

[151] S.A. Rodeo, K. Suzuki, X.-h. Deng, J. Wozney, R.F. Warren, Use of Recombinant Human Bone Morphogenetic Protein-2 to Enhance Tendon Healing in a Bone Tunnel, American Journal of Sports Medicine 27(4) (1999) 476-488.
[152] C. Li, C. Vepari, H.J. Jin, H.J. Kim, D.L. Kaplan, Electrospun silk-BMP-2 scaffolds for bone tissue engineering, Biomaterials 27(16) (2006) 3115-24.
[153] P. Gentile, K. McColgan-Bannon, N.C. Gianone, F. Sefat, K. Dalgarno, A.M. Ferreira, Biosynthetic PCL-graft-Collagen Bulk Material for Tissue Engineering Applications, Materials (Basel) 10(7) (2017) 693.
[154] J. Zhang, J. Wang, Y. Wei, C. Gao, X. Chen, W. Kong, D. Kong, Q. Zhao, ECM-mimetic heparin glycosamioglycan-functionalized surface favors constructing functional vascular smooth muscle tissue in vitro, Colloids Surf B Biointerfaces 146 (2016) 280-8.
[155] N.S. Gandhi, R.L. Mancera, The structure of glycosaminoglycans and their interactions with proteins, Chem Biol Drug Des 72(6) (2008) 455-82.
[156] U. Uciechowska-Kaczmarzyk, S. Babik, F. Zsila, K.K. Bojarski, T. Beke-Somfai, S.A. Samsonov, Molecular dynamics-based model of VEGF-A and its heparin interactions, J Mol Graph Model 82 (2018) 157-166.
[157] S. Kang, J.S. Yoon, J.Y. Lee, H.-J. Kim, K. Park, S.E. Kim, Long-term local PDGF delivery using porous microspheres modified with heparin for tendon healing of rotator cuff tendinitis in a rabbit model, Carbohydrate Polymers 209 (2019) 372-381.
[158] S. Samavedi, S.A. Guelcher, A.S. Goldstein, A.R. Whittington, Response of bone marrow stromal cells to graded co-electrospun scaffolds and its implications for engineering the ligament-bone interface, Biomaterials 33(31) (2012) 7727-35.
[159] B.G. Keselowsky, D.M. Collard, A.J. Garcia, Surface chemistry modulates fibronectin conformation and directs integrin binding and specificity to control cell adhesion, J Biomed Mater Res A 66(2) (2003) 247-59.
[160] L. Cao, Y. Yu, J. Wang, J.A. Werkmeister, K.M. McLean, C. Liu, 2-N, 6-O-sulfated chitosan-assisted BMP-2 immobilization of PCL scaffolds for enhanced osteoinduction, Mater Sci Eng C Mater Biol Appl 74 (2017) 298-306.
[161] L. Jia, M.P. Prabhakaran, X. Qin, D. Kai, S. Ramakrishna, Biocompatibility evaluation of protein-incorporated electrospun polyurethane-based scaffolds with smooth muscle cells for vascular tissue engineering, Journal of Materials Science 48(15) (2013) 5113-5124.
[162] K. Kim, Y.K. Luu, C. Chang, D. Fang, B.S. Hsiao, B. Chu, M. Hadjiargyrou, Incorporation and controlled release of a hydrophilic antibiotic using poly(lactide-co-glycolide)-based electrospun nanofibrous scaffolds, J Control Release 98(1) (2004) 47-56.
[163] Z. Xinhua, K. Kwangsok, F. Dufei, R. Shaofeng, S.H. Benjamin, C. Benjamin, Structure and process relationship of electrospun bioabsorbable nanofiber membranes, Polymer 43(16) (2002) 4403-4412.
[164] A.J. Engler, S. Sen, H.L. Sweeney, D.E. Discher, Matrix elasticity directs stem cell lineage specification., Cell 126 (2006) 677-689.
[165] J. Nam, J. Johnson, J.J. Lannutti, S. Agarwal, Modulation of embryonic mesenchymal progenitor cell differentiation via control over pure mechanical modulus in electrospun nanofibers, Acta Biomaterialia 7(4) (2011) 1516-1524.
[166] F. Song, D. Jiang, T. Wang, Y. Wang, F. Chen, G. Xu, Y. Kang, Y. Zhang, Mechanical Loading Improves Tendon-Bone Healing in a Rabbit Anterior Cruciate Ligament Reconstruction Model by Promoting Proliferation and Matrix Formation of Mesenchymal Stem Cells and Tendon Cells, Cell Physiol Biochem 41(3) (2017) 875-889.

[167] R. Budiraharjo, K.G. Neoh, E.T. Kang, Enhancing bioactivity of chitosan film for osteogenesis and wound healing by covalent immobilization of BMP-2 or FGF-2, J Biomater Sci Polym Ed 24(6) (2013) 645-62.
[168] V. Karageorgiou, L. Meinel, S. Hofmann, A. Malhotra, V. Volloch, D. Kaplan, Bone morphogenetic protein-2 decorated silk fibroin films induce osteogenic differentiation of human bone marrow stromal cells, J Biomed Mater Res A 71(3) (2004) 528-37.
[169] S.B. Brown, J.A. Hornyak, R.R. Jungels, Y.Y. Shah, E.G. Yarmola, K.D. Allen, B. Sharma, Characterization of Post-Traumatic Osteoarthritis in Rats Following Anterior Cruciate Ligament Rupture by Non-Invasive Knee Injury (NIKI), Journal of Orthopaedic Research® (2019).
[170] X. Zhang, X.-H. Deng, Z. Song, B. Croen, C.B. Carballo, Z. Album, Y. Zhang, R. Bhandari, S.A. Rodeo, Matrix Metalloproteinase Inhibition With Doxycycline Affects the Progression of Posttraumatic Osteoarthritis After Anterior Cruciate Ligament Rupture: Evaluation in a New Nonsurgical Murine ACL Rupture Model, The American journal of sports medicine 48(1) (2020) 143-152.
[171] J.D. Kosy, J.R. Phillips, A. Edordu, R. Pankhania, P.J. Schranz, V. Mandalia, Failure to return to preinjury activity level after hamstring anterior cruciate ligament reconstruction: Factors involved and considerations in goal setting, Indian journal of orthopaedics 53(6) (2019) 714.
[172] A.G. Gagliardi, P.M. Carry, H.B. Parikh, J.C. Albright, Outcomes of Quadriceps Tendon With Patellar Bone Block Anterior Cruciate Ligament Reconstruction in Adolescent Patients With a Minimum 2-Year Follow-up, The American journal of sports medicine 48(1) (2020) 93-98.
[173] R.A. Duerr, K.D. Garvey, J. Ackermann, E.G. Matzkin, Influence of graft diameter on patient reported outcomes after hamstring autograft anterior cruciate ligament reconstruction, Orthopedic reviews 11(3) (2019).
[174] S.H. Park, Y.-J. Choi, S.W. Moon, B.H. Lee, J.-H. Shim, D.-W. Cho, J.H. Wang, Three-dimensional bio-printed scaffold sleeves with mesenchymal stem cells for enhancement of tendon-to-bone healing in anterior cruciate ligament reconstruction using soft-tissue tendon graft, Arthroscopy: The Journal of Arthroscopic & Related Surgery 34(1) (2018) 166-179.
[175] M.Y. Soon, A. Hassan, J.H. Hui, J.C. Goh, E. Lee, An analysis of soft tissue allograft anterior cruciate ligament reconstruction in a rabbit model: a short-term study of the use of mesenchymal stem cells to enhance tendon osteointegration, The American journal of sports medicine 35(6) (2007) 962-971.
[176] R.N. Wang, J. Green, Z. Wang, Y. Deng, M. Qiao, M. Peabody, Q. Zhang, J. Ye, Z. Yan, S. Denduluri, Bone Morphogenetic Protein (BMP) signaling in development and human diseases, Genes & diseases 1(1) (2014) 87-105.
[177] S.A. Rodeo, K. Suzuki, X.-h. Deng, J. Wozney, R.F. Warren, Use of recombinant human bone morphogenetic protein-2 to enhance tendon healing in a bone tunnel, The American journal of sports medicine 27(4) (1999) 476-488.
[178] M. Kanatani, T. Sugimoto, H. Kaji, T. Kobayashi, K. Nishiyama, M. Fukase, M. Kumegawa, K. Chihara, Stimulatory effect of bone morphogenetic protein-2 on osteoclast-like cell formation and bone-resorbing activity, J Bone Miner Res 10(11) (1995) 1681-90.
[179] D. Gadalla, A.S. Goldstein, Improving the Osteogenicity of PCL Fiber Substrates by Surface-Immobilization of Bone Morphogenic Protein-2, Ann Biomed Eng 48(3) (2020) 1006-1015.

[180] R.H. Li, J.M. Wozney, Delivering on the promise of bone morphogenetic proteins, Trends in biotechnology 19(7) (2001) 255-265.
[181] V. Luginbuehl, L. Meinel, H.P. Merkle, B. Gander, Localized delivery of growth factors for bone repair, European Journal of Pharmaceutics and Biopharmaceutics 58(2) (2004) 197-208.
[182] R.S. Leena, M. Vairamani, N. Selvamurugan, Alginate/Gelatin scaffolds incorporated with Silibinin-loaded Chitosan nanoparticles for bone formation in vitro, Colloids Surf B Biointerfaces 158 (2017) 308-318.
[183] A.T. Raiche, D.A. Puleo, Cell responses to BMP-2 and IGF-I released with different time-dependent profiles, J Biomed Mater Res A 69(2) (2004) 342-50.
[184] F. Bastami, Z. Paknejad, M. Jafari, M. Salehi, M. Rezai Rad, A. Khojasteh, Fabrication of a three-dimensional beta-tricalcium-phosphate/gelatin containing chitosan-based nanoparticles for sustained release of bone morphogenetic protein-2: Implication for bone tissue engineering, Mater Sci Eng C Mater Biol Appl 72 (2017) 481-491.
[185] Q. Gan, T. Wang, Chitosan nanoparticle as protein delivery carrier—Systematic examination of fabrication conditions for efficient loading and release, Colloids and Surfaces B: Biointerfaces 59(1) (2007) 24-34.
[186] S. Sreekumar, F.M. Goycoolea, B.M. Moerschbacher, G.R. Rivera-Rodriguez, Parameters influencing the size of chitosan-TPP nano-and microparticles, Scientific reports 8(1) (2018) 1-11.
[187] I. Ortega-Oller, M. Padial-Molina, P. Galindo-Moreno, F. O'Valle, A.B. Jódar-Reyes, J.M. Peula-García, Bone regeneration from PLGA micro-nanoparticles, BioMed research international 2015 (2015).
[188] P. Calvo, C. Remunan-Lopez, J.L. Vila-Jato, M. Alonso, Novel hydrophilic chitosan-polyethylene oxide nanoparticles as protein carriers, Journal of Applied Polymer Science 63(1) (1997) 125-132.
[189] M. Ekdahl, J.H.-C. Wang, M. Ronga, F.H. Fu, Graft healing in anterior cruciate ligament reconstruction, Knee Surgery, Sports Traumatology, Arthroscopy 16(10) (2008) 935-947.
[190] H. Bangun, S. Tandiono, A. Arianto, Preparation and evaluation of chitosan-tripolyphosphate nanoparticles suspension as an antibacterial agent, Journal of Applied Pharmaceutical Science 8 (12) (2018) 147-156.
[191] R. Asasutjarit, C. Sorrachaitawatwong, N. Tipchuwong, S. Pouthai, Effect of Formulation Compositions on Particle Size and Zeta Potential of Diclofenac Sodium-Loaded Chitosan Nanoparticles International Journal of Pharmacological and Pharmaceutical Sciences 7 (2013).
[192] J. Antoniou, F. Liu, H. Majeed, J. Qi, WallaceYokoyama, F. Zhong, Physicochemical and morphological properties of size-controlled chitosan–tripolyphosphate nanoparticles, Colloids and Surfaces A: Physicochemical and Engineering Aspects 465 (2015) 137-146.
[193] C.M.R.L.G. Ciardelli, Chitosan nanoparticles as therapeutic protein nanocarriers: The effect of ph on particle formation and encapsulation efficiency, Plolymer Composites 34(9) (2013).
[194] Y. Huang, Y. Cai, Y. Lapitsky, Factors affecting the stability of chitosan/tripolyphosphate micro-and nanogels: resolving the opposing findings, Journal of Materials Chemistry B 3(29) (2015) 5957-5970.
[195] N. Poth, V. Seiffart, G. Gross, H. Menzel, W. Dempwolf, Biodegradable chitosan nanoparticle coatings on titanium for the delivery of BMP-2, Biomolecules 5(1) (2015) 3-19.

[196] L. Cao, J. Wang, J. Hou, W. Xing, C. Liu, Vascularization and bone regeneration in a critical sized defect using 2-N, 6-O-sulfated chitosan nanoparticles incorporating BMP-2, Biomaterials 35(2) (2014) 684-698.
[197] Q. Li, G. Zhou, X. Yu, T. Wang, Y. Xi, Z. Tang, Porous deproteinized bovine bone scaffold with three-dimensional localized drug delivery system using chitosan microspheres, Biomedical engineering online 14(1) (2015) 33.
[198] Y.J. Xia, H. Xia, L. Chen, Q.S. Ying, X. Yu, L.H. Li, J.H. Wang, Y. Zhang, Efficient delivery of recombinant human bone morphogenetic protein (rhBMP-2) with dextran sulfate-chitosan microspheres, Experimental and therapeutic medicine 15(4) (2018) 3265-3272.
[199] S. Shrestha, A. Diogenes, A. Kishen, Temporal-controlled release of bovine serum albumin from chitosan nanoparticles: effect on the regulation of alkaline phosphatase activity in stem cells from apical papilla, J Endod 40(9) (2014) 1349-54.
[200] M.L. Macdonald, R.E. Samuel, N.J. Shah, R.F. Padera, Y.M. Beben, P.T. Hammond, Tissue integration of growth factor-eluting layer-by-layer polyelectrolyte multilayer coated implants, Biomaterials 32(5) (2011) 1446-1453.
[201] R.C.F. Cheung, T.B. Ng, J.H. Wong, W.Y. Chan, Chitosan: an update on potential biomedical and pharmaceutical applications, Marine drugs 13(8) (2015) 5156-5186.
[202] Q. Wang, M. Wang, P. Li, K. Wang, L. Fang, F. Ren, G. Lu, X. Lu, The interaction of chitosan and BMP-2 tuned by deacetylation degree and pH value, Journal of Biomedical Materials Research Part A 107(4) (2019) 769-779.
[203] M.H. Hettiaratchi, L. Krishnan, T. Rouse, C. Chou, T.C. McDevitt, R.E. Guldberg, Heparin-mediated delivery of bone morphogenetic protein-2 improves spatial localization of bone regeneration, Science Advances 6(1) (2020) eaay1240.
[204] B. Wang, Y. Guo, X. Chen, C. Zeng, Q. Hu, W. Yin, W. Li, H. Xie, B. Zhang, X. Huang, Nanoparticle-modified chitosan-agarose-gelatin scaffold for sustained release of SDF-1 and BMP-2, International journal of nanomedicine 13 (2018) 7395.
[205] H. Zhang, F. Migneco, C.Y. Lin, S.J. Hollister, Chemically-conjugated bone morphogenetic protein-2 on three-dimensional polycaprolactone scaffolds stimulates osteogenic activity in bone marrow stromal cells, Tissue Eng Part A 16(11) (2010) 3441-8.
[206] Q. Tan, H. Tang, J. Hu, Y. Hu, X. Zhou, Y. Tao, Z. Wu, Controlled release of chitosan/heparin nanoparticle-delivered VEGF enhances regeneration of decellularized tissue-engineered scaffolds, International journal of nanomedicine 6 (2011) 929.
[207] T. Nessler, L. Denney, J. Sampley, ACL injury prevention: what does research tell us?, Current reviews in musculoskeletal medicine 10(3) (2017) 281-288.
[208] S.-L. Kan, Z.-F. Yuan, G.-Z. Ning, B. Yang, H.-L. Li, J.-C. Sun, S.-Q. Feng, Autograft versus allograft in anterior cruciate ligament reconstruction: a meta-analysis with trial sequential analysis, Medicine 95(38) (2016).
[209] A. Sensini, L. Cristofolini, Biofabrication of electrospun scaffolds for the regeneration of tendons and ligaments, Materials 11(10) (2018) 1963.
[210] M. Sadat-Shojai, M.-T. Khorasani, A. Jamshidi, A new strategy for fabrication of bone scaffolds using electrospun nano-HAp/PHB fibers and protein hydrogels, Chemical Engineering Journal 289 (2016) 38-47.
[211] A. Bianco, E.D. Federico, I. Moscatelli, A. Camaioni, I. Armentano, L. Campagnolo, M. Dottori, J.M. Kenny, G. Siracusa, G. Gusmano, Electrospun poly(ε-caprolactone)/Ca-deficient hydroxyapatite nanohybrids: Microstructure, mechanical properties and cell response by murine embryonic stem cells, Materials Science and Engineering: C 29(6) (2009) 2063-2071.

[212] Y. Hong, A. Huber, K. Takanari, N.J. Amoroso, R. Hashizume, S.F. Badylak, W.R. Wagner, Mechanical properties and in vivo behavior of a biodegradable synthetic polymer microfiber–extracellular matrix hydrogel biohybrid scaffold, Biomaterials 32(13) (2011) 3387-3394.
[213] A.K. Ekaputra, G.D. Prestwich, S.M. Cool, D.W. Hutmacher, The three-dimensional vascularization of growth factor-releasing hybrid scaffold of poly (ε-caprolactone)/collagen fibers and hyaluronic acid hydrogel, Biomaterials 32(32) (2011) 8108-8117.
[214] Y.-H. Tsou, J. Khoneisser, P.-C. Huang, X. Xu, Hydrogel as a bioactive material to regulate stem cell fate, Bioactive materials 1(1) (2016) 39-55.
[215] M.W. Tibbitt, K.S. Anseth, Hydrogels as extracellular matrix mimics for 3D cell culture, Biotechnology and bioengineering 103(4) (2009) 655-663.
[216] M.B. Bornstein, Reconstituted rattail collagen used as substrate for tissue cultures on coverslips in Maximow slides and roller tubes, Lab Invest 7(2) (1958) 134-7.
[217] L. Wright, T. Andric, J. Freeman, Utilizing NaCl to increase the porosity of electrospun materials, Materials Science and Engineering: C 31(1) (2011) 30-36.
[218] L. Lu, S.J. Peter, M.D. Lyman, H.-L. Lai, S.M. Leite, J.A. Tamada, J.P. Vacanti, R. Langer, A.G. Mikos, In vitro degradation of porous poly (L-lactic acid) foams, Biomaterials 21(15) (2000) 1595-1605.
[219] S.B. Lee, Y.H. Kim, M.S. Chong, S.H. Hong, Y.M. Lee, Study of gelatin-containing artificial skin V: fabrication of gelatin scaffolds using a salt-leaching method, Biomaterials 26(14) (2005) 1961-1968.
[220] J.M. Ameer, A.K. PR, N. Kasoju, Strategies to tune electrospun scaffold porosity for effective cell response in tissue engineering, Journal of functional biomaterials 10(3) (2019) 30.
[221] G. Yang, H. Lin, B.B. Rothrauff, S. Yu, R.S. Tuan, Multilayered polycaprolactone/gelatin fiber-hydrogel composite for tendon tissue engineering, Acta biomaterialia 35 (2016) 68-76.
[222] K.M. Park, S. Gerecht, Hypoxia-inducible hydrogels, Nat Commun 5 (2014) 4075.
[223] Y.-K. Wang, Y.-H. Wang, C.-Z. Wang, J.-M. Sung, W.-T. Chiu, S.-H. Lin, Y.-H. Chang, M.-J. Tang, Rigidity of collagen fibrils controls collagen gel-induced down-regulation of focal adhesion complex proteins mediated by α2β1 integrin, Journal of Biological Chemistry 278(24) (2003) 21886-21892.
[224] D.E. Discher, P. Janmey, Y.-l. Wang, Tissue cells feel and respond to the stiffness of their substrate, Science 310(5751) (2005) 1139-1143.
[225] M. Nickien, A. Heuijerjans, K. Ito, C.C. van Donkelaar, Comparison between in vitro and in vivo cartilage overloading studies based on a systematic literature review, Journal of Orthopaedic Research® 36(8) (2018) 2076-2086.
[226] N. Gotlieb, E. Rosenne, P. Matzner, L. Shaashua, L. Sorski, S. Ben-Eliyahu, The misleading nature of in vitro and ex vivo findings in studying the impact of stress hormones on NK cell cytotoxicity, Brain, behavior, and immunity 45 (2015) 277-286.
[227] G. Walden, X. Liao, S. Donell, M.J. Raxworthy, G.P. Riley, A. Saeed, A clinical, biological, and biomaterials perspective into tendon injuries and regeneration, Tissue Engineering Part B: Reviews 23(1) (2017) 44-58.
[228] E. Pişkin, İ.A. İşoğlu, N. Bölgen, İ. Vargel, S. Griffiths, T. Çavuşoğlu, P. Korkusuz, E. Güzel, S. Cartmell, In vivo performance of simvastatin-loaded electrospun spiral-wound polycaprolactone scaffolds in reconstruction of cranial bone defects in the rat model, Journal of Biomedical Materials Research Part A: An Official Journal of the Society for Biomaterials, The

Japanese Society for Biomaterials, and The Australian Society for Biomaterials and the Korean Society for Biomaterials 90(4) (2009) 1137-1151.
[229] J. Wu, L. Cao, Y. Liu, A. Zheng, D. Jiao, D. Zeng, X. Wang, D.L. Kaplan, X. Jiang, Functionalization of silk fibroin electrospun scaffolds via BMSC affinity peptide grafting through oxidative self-polymerization of dopamine for bone regeneration, ACS applied materials & interfaces 11(9) (2019) 8878-8895.
[230] T. Xu, J.M. Miszuk, Y. Zhao, H. Sun, H. Fong, Electrospun polycaprolactone 3D nanofibrous scaffold with interconnected and hierarchically structured pores for bone tissue engineering, Advanced healthcare materials 4(15) (2015) 2238-2246.
[231] R. Murugan, S. Ramakrishna, Design strategies of tissue engineering scaffolds with controlled fiber orientation, Tissue engineering 13(8) (2007) 1845-1866.
[232] J.P. Spalazzi, E. Dagher, S.B. Doty, X.E. Guo, S.A. Rodeo, H.H. Lu, In vivo evaluation of a multiphased scaffold designed for orthopaedic interface tissue engineering and soft tissue-to-bone integration, Journal of Biomedical Materials Research Part A: An Official Journal of The Society for Biomaterials, The Japanese Society for Biomaterials, and The Australian Society for Biomaterials and the Korean Society for Biomaterials 86(1) (2008) 1-12.
[233] H. Li, J. Fan, L. Sun, X. Liu, P. Cheng, H. Fan, Functional regeneration of ligament-bone interface using a triphasic silk-based graft, Biomaterials 106 (2016) 180-192.
[234] J.A. Cooper, H.H. Lu, F.K. Ko, J.W. Freeman, C.T. Laurencin, Fiber-based tissue-engineered scaffold for ligament replacement: design considerations and in vitro evaluation, Biomaterials 26(13) (2005) 1523-1532.
[235] S. Font Tellado, W. Bonani, E.R. Balmayor, P. Foehr, A. Motta, C. Migliaresi, M. van Griensven, Fabrication and characterization of biphasic silk fibroin scaffolds for tendon/ligament-to-bone tissue engineering, Tissue Engineering Part A 23(15-16) (2017) 859-872.
[236] Y.-R. Yun, J.E. Won, E. Jeon, S. Lee, W. Kang, H. Jo, J.-H. Jang, U.S. Shin, H.-W. Kim, Fibroblast growth factors: biology, function, and application for tissue regeneration, Journal of tissue engineering 1(1) (2010) 218142.
[237] H.-C. Yu, F.-M. Huang, S.-S. Lee, C.-C. Yu, Y.-C. Chang, Effects of fibroblast growth factor-2 on cell proliferation of cementoblasts, Journal of Dental Sciences 11(4) (2016) 463-467.
[238] E. Harris, Y. Liu, G. Cunniffe, D. Morrissey, S. Carroll, K. Mulhall, D.J. Kelly, Biofabrication of soft tissue templates for engineering the bone–ligament interface, Biotechnology and bioengineering 114(10) (2017) 2400-2411.
[239] J.Z. Paxton, K. Donnelly, R.P. Keatch, K. Baar, Engineering the bone–ligament interface using polyethylene glycol diacrylate incorporated with hydroxyapatite, Tissue engineering part A 15(6) (2009) 1201-1209.